Formation and Structure of Acid Soap Crystals through in-situ Neutralisation in the Environments of Surfactant

By

Qi Wang

Submitted in accordance with the requirements for the degree of

DOCTOR OF PHILOSOPHY

(Chemical Engineering)

The University of Leeds

School of Chemical and Process Engineering

December 2019

Acknowledgement

I would like to thank my supervisor Dr. Xiaojun Lai and Prof. Andrew Bayly for their support and guidance throughout my PhD. I would like to thank my industrial supervisor Eric Robles and Hossam Tantawy for their support in Newcastle.

I would also like to thank my friends, colleagues in crystallisation group at Leeds for their help and support. I would like to thank my colleagues in Procter & Gamble Newcastle Innovation Centre. I would like to particularly thank Paul Lapham, Brandon Stone, Laure Oakley and Georgina Luxton for their help, advice and support during my studies in Newcastle. I would like to thank Procter & Gamble for providing the funding.

Finally, I would like to thank my family for supporting me through my studies.

Abstract

Non-ionic surfactants are important co-surfactant in detergent products to enhance the detergency in hard water. And the alcohol ethoxylates are the most common non-ionic surfactants used in consumer products. However, the liquid-like surfactant can cause unwanted aggregation of washing powder. In order to accelerate the solidification of non-ionic surfactant, the acid-soaps were chosen as gelator to form crystal networks in the mixtures to encapsulate the liquid-like non-ionic surfactant.

Acid-soaps are the co-crystals formed by fatty acids and their metallic salts stoichiometrically. Although the acid-soaps were extensively studied over decades, the stoichiometric ratios are still unclear. In this project, the crystal structure of stearate acid-soap with series neutralisation ratio were determined by powder X-ray diffraction. The thermodynamic properties were determined by differential scanning calorimetry and the binary phase diagram of the stearic acid and sodium stearate system was generated. The phase behaviour during heating process was observed by small angle X-ray scattering (SAXS) and wide angle X-ray scattering. The phase transitions associate with the endo/exo-thermal peaks in DSC were assigned. The results indicated that the stoichiometric ratios of stearate acid-soaps are 2:1 and 1:1, which is contradict with the previous publications that the acid: soap ratios are 3:2, 1:1, 2:3, 2:5 and 1:5. The SAXS/WAXS with temperature stage results indicated that the acid-soaps with high acid ratio can transform to the form with low acid ratio, and the polymorphs were also observed. The morphologies of acid-soaps were observed by scanning electron microscopy.

The studies on the influences of the surfactants on the acid-soaps formation were carried out with non-ionic surfactants (alcohol ethoxylates) and cationic surfactants (alcohol ethoxylate sulfonates). The characteristic peaks associate with acid-soaps were observed in the mixtures. The d-spacings of the crystals formed in the mixtures of alcohol ethoxylate sulfonates and stearic acid were complex, which is because the AES has tendency to form acid-soap. The influences of perfume on the liquid crystal of AES and the crystals of stearic acid/acid-soaps were also studied.

Table of Contents

List of figures

List of tables

Chapter 1 Introduction

The scientific background and current research in this field is outlined along with the research aims and objectives.

1.1 Research background

The surfactants, also known as surface-active agents, are compounds that contain hydrophobic and hydrophilic groups, which provides them amphiphilic property to adjust the surface tension. This property plays important roles in versatile chemical products like pharmaceuticals, laundry detergents, and wetting agent.[1] The market surveys indicated that the surfactant manufacture represents the largest chemical process industries[2], the value of the global surfactants market was USD 31.15 billion in 2018, and the consumption will rise to USD 43.03 billion by 2026.[3] As the strict increasing requirement of environment, the surfactants based on natural products attract more interests these years because of the excellent biodegradation property. The natural-based surfactants are typically synthesised from sugars[4], sterols[5] and fatty acids[6]. Soaps are the metal salts of fatty acids[7], and they are the most common natural based surfactant.

One of the most important applications of surfactants is laundry detergent, and the global market in 2019 was valued at around USD 117 billion.[8] The most common forms of laundry detergents are powder, liquid and cake. Although some new products like powder tablets and liquid detergent pouches appeared in the last decade, the regular washing powder continues to constitute the largest market share in both volume and value.[9] Also, the washing powders prefer to use surfactants with longer hydrophobic tails, whose detergency is better than the surfactants used in liquid detergents. Hence, washing powders are still important to study. The formulations of detergent powders are complex that can consist of over 20 ingredients. These ingredients can be divided into four categories: surfactants, builders, bleaching agents and auxiliary agents.[10] The typical builders used in washing powder are sodium carbonate, sodium sulphate and zeolite. These ingredients are constituting around 50wt% of total washing powder. The bleaching agents are used for removing protein-based or starch-based stains, which the surfactants have limited detergency. The washing powders contain some other ingredients to improve the customers' satisfaction, such as perfumes and softener. The surfactants in washing powder are active components and typically compositional formulated, the surfactants with different chain lengths and saturation degrees are added to the products. For example, the linear alkyl benzene sulphate (LAS) is the primary surfactant in commercial detergent powders, and the previous

studies indicated that the LAS could be significantly affected by the counterions. Hence, the non-ionic surfactant (NI), alcohol ethoxylates, which is not sensitive to the counterions, are added to the washing powders to improve the detergency in hard water.[11]

The non-ionic surfactant used in this project is liquid at room temperature. It is not possible to add a large amount of non-ionic surfactant to washing powders as it can cause caking of the washing powder. The compositional formulation provides scope for solidifying the liquid compounds by compounding with gelators such as polymers and fatty acid/acid-soaps. These gelators can trap the liquid ingredients in the networks formed by long molecules or crystals. The manufacturing conditions require that the better flowability at high temperature and quick solidification at a lower temperature during the spray process. Hence, the fatty acid and sodium hydroxide were chosen as gelator to solidify the liquid compounds in washing powder because of the appropriate melting and crystallising temperature. Although previous studies done by P&G indicated that the addition of gelators could improve the anti-caking property of washing powder, the principles are still unclear. Hence, it is necessary to investigate the crystallisation process of fatty acid in the environment of surfactants.

It was reported that the structures and their physical properties of neutralised or partially neutralised fatty acids in water are influenced by the neutralisation ratio between the acids and counter ions.[12] The intermediate phase between fully neutralised fatty acids and un-neutralised fatty acids is called acid-soaps.[13] The acid-soaps was first reported by Chevreul in 1823[14], and the systematic research on it was from Ekwall and McBain in 1920s[15-17]. After that, the acid-soaps becomes a hot topic because of the importance in both academic and industrial fields. It can be found in many consumer products like superfatted soap bars, facial cleaners and cosmetics.[18] In recent years, the acid-soaps becomes popular in food industries as gelators. The crystal network formed by acid-soaps can trap the liquid oil in the cells, which can structure the liquid oil into solid-state.[19] In the academic field, the strong hydrogen bonds between the carboxylic acid group and carboxylate group attract lots of attention, and the development of X-ray diffraction and Infrared radiation lead two significant jumps in the 1950s and 1990s.[20-22] Plenty of literature about acid-soaps' crystal structure, acid/soap ratio and binary/ternary phase diagrams were published.[13, 22, 23]

The simulation of the interaction between palmitic acid and sodium palmitate was reported by Lynch et al..[24] Although loads of research in the acid-soap formation were published, the types and thermodynamic relations between acid-soap crystals are still ambiguity.[22] Understanding and modifying the crystallisation process of acid-soaps is better to control the solidification of the liquid compounds.

The surfactants have hydrophobic tails and hydrophilic head groups. The polar hydrophilic head groups have electrostatic interactions with surrounding molecules, whilst the hydrophobic tails have van de Waals interaction.[25] Little information in the literature of the acid-soaps structure in surfactants environments can be found. The liquid compounds in washing powders can act as solvents, which may dissolve the acid-soaps/fatty acids. Hence, it is important to understand the interactions between the environments and acid-soaps and the crystallisation behaviour of acid-soaps. The stearic acid, alcohol ethoxylates and alcohol ethoxylate sulphates were selected for study because of the wildly use in consumer products.

As the smell of part of the ingredients (alkaline, e.g.) in washing powders is awful, perfumes are added to the washing powder to provide a fresh scent and covering the odour, which can improve customers satisfaction. However, another industrial problem is that the perfume loss during manufacturing is significant. In order to reduce the perfume loss, the AES with partially neutralised stearic acid was applied to the system. The purpose is restricting the movement of perfume molecules by dispersing the perfume between the bilayers of AES liquid crystal. As the AES and AES/perfume mixtures are liquid-like materials, the partially neutralised stearic acid was used for modifying the physical properties. Hence, it is necessary to investigate the influence of perfume on crystal structures of surfactants and acid-soaps/fatty acids. The understanding of crystallisation behaviours and crystal structures of these compounds is better to modify the formulas and control the properties of the product.

1.2 Aims

The aims for this project are understanding the types of acid-soaps and the thermodynamic relationships of acid-soap crystals, the influence of surfactants on the crystallisation behaviour of acid-soaps. This will be illustrated through the following objective:

1. Stearate acid-soaps: as the stoichiometric ratios and crystal structures of stearate acid-soaps are still unclear, and these information are important for the following sections, the following aspects will be investigated:
    - The stoichiometric ratios.
    - The crystal structures of the acid-soaps with different soap content.
    - The phase transformations between these acid-soaps as function of temperature.
    - The morphologies of the acid-soaps.
2. The influence of surfactants (AES and AE7) on the crystallisation of acid-soaps:
    - Determining the crystal structures of acid-soaps formed in the environment of surfactants.
    - Investigating the phase transformation of acid-soaps in the environment of surfactant.
    - Observing the morphologies of acid-soaps in the environment of surfactant.
3. The influence of perfumes on the crystal structures of AES and acid-soaps. This problem will be answered by:
    - Determining the crystal structure of AES and acid-soaps in the environment of perfume.
    - Investigating the phase transitions of AES and acid-soaps, and comparing with the samples without perfume.
    - Observing the morphologies of the mixtures by Cryo-SEM to confirm the conclusions from SAXS/WAXS patterns.

1.3 Delivery plan

The objectives will be realised through combinations of different experimental actives:

• The stearate acid-soaps will be prepared by dissolving different amount stearic acid and sodium stearate in de-ionized water and produce the acid-soap crystals through evaporation. Characterising the crystals by P-XRD at room temperature to determine the stoichiometry ratios of acid-soaps. Investigating the thermodynamic transitions of acid-soap crystals by SAXS/WAXS with

temperature stage and DSC. The morphologies of the crystals were observed by SEM and polarized microscopy.

• The influence of NI and AES on the crystallisation behaviour will be investigated through observing the crystal structures of acid-soaps in the mixtures of stearate acid-soaps and NI with various ratios. The crystal structures of acid-soaps will be characterised by SAXS/WAXS with temperature stage. The morphologies and dispersion of the crystals will be screened by SEM and polarized microscopy.

• The influence of perfumes on the crystallisation behaviour will be AES and stearic acid/acid-soaps will be investigated separately, AES/HSt, AES/perfume, HSt/perfume and AES/HSt/perfume. The crystal structures of AES and HSt will be characterised by SAXS/WAXS and the morphologies will be observed by cryo-SEM and polarized microscopy.

1.4 Thesis plan

This thesis contains 8 chapters:

Chapter 1 Introduction: an introduction of the research background and the thesis aims and objectives were presented.

Chapter 2 Crystallisation theory: literature review of the fundamentals of crystallisation.

Chapter 3 Acid-soaps and surfactants: literature review of the fundamentals of the surfactant structures and the phase transitions, provides a view of the acid-soaps structures and crystallisation behaviours of carboxylic acids.

Chapter 4 Materials and methods: description of the materials and experimental set ups within this project.

Chapter 5 Characterisation of the stearate acid-soaps: presents the results of the stearate acid-soaps at room temperature and the thermodynamic transformation of the crystals during heating ramp.

Chapter 6 Acid-soaps in surfactants: presents the results of stearate acid-soaps in NI and AES surfactants and probes the crystallisation behaviours of surfactants and acid-soaps.

Chapter 7 The influence of perfumes on AES/HSt mixtures: presents the results of AES/perfume, HSt/perfume and AES/HSt/perfume mixtures and probe the influence of the perfume on the crystallisation behaviours of surfactants and fatty acids/acid-soaps.

Chapter 8 Conclusions and future work: summarises the conclusions and describe the future works.

2 Chapter 2 Crystallisation theory, X-ray diffraction and washing powder manufacturing

A review of the fundamental theories of the crystallisation. Together with a review of X-ray diffraction and Small/Wide angle scattering theories. The typical formula and manufacturing process of washing powder also been discussed in this chapter.

2.1 Introduction.

Crystallisation is the process of aggregation of atoms or molecules and forms highly organised solid structures known as crystals.[26] The crystallisation starts from nucleation, following with the crystal growth. The basic theory of the nucleation is known as classic nucleation theory (CNT), which describes the nucleation process as the cluster formation in supersaturated solutions.[27] Moreover, the recent researches disagree with this theory and raised the two-step theory, which is the solute formed liquid-like clusters first and followed with the nucleus formation.[28, 29] This chapter starts with the basic concepts of crystallography and crystal structures. Followed by the crystallisation process includes the nucleation and crystal growth.

2.2 Crystal and crystallography.

A crystal is defined as an anisotropic, homogeneous body consisting of a three-dimensional periodic ordering of atoms, ions or molecules.[30] The simplest description of a crystal is lattice, which is a three-dimensional ordering points. The space lattice defined by three vectors $\underset{a}{\rightarrow}$, $\underset{b}{\rightarrow}$ and $\underset{c}{\rightarrow}$ (figure 2-1). The unit cell is the minimum cell in the space lattice and it can be described by three translation vectors, $\left|\underset{a}{\rightarrow}\right| = a$, $\left|\underset{b}{\rightarrow}\right| = b$ and $\left|\underset{c}{\rightarrow}\right| = c$, and three inter-axial lattice angles $\underset{a}{\rightarrow} \wedge \underset{b}{\rightarrow} = \gamma$, $\underset{a}{\rightarrow} \wedge \underset{c}{\rightarrow} = \beta$ and $\underset{b}{\rightarrow} \wedge \underset{c}{\rightarrow} = \alpha$.[30]

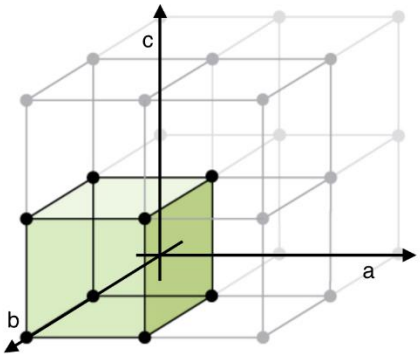

Figure 2-1 The crystal lattice and unit cell.

The crystals can be divided into seven systems based on the three translation vectors and three inter-axial lattice angles as listed in table 2-1. And this system is called seven crystal system.[31]

Table 2-1 The seven crystal system.

System	Axial length	Axial angles
Regular (Cubic)	$a = b = c$	$\alpha = \beta = \gamma = 90^{\circ}$
Tetragonal	$a = b \neq c$	$\alpha = \beta = \gamma = 90^{\circ}$
Orthorhombic	$a \neq b \neq c$	$\alpha = \beta = \gamma = 90^{\circ}$
Monoclinic	$a \neq b \neq c$	$\alpha = \beta = 90^{\circ} \neq \gamma$
Triclinic	$a \neq b \neq c$	$\alpha \neq \beta \neq \gamma \neq 90^{\circ}$
Trigonal	$a = b = c$	$\alpha = \beta = \gamma \neq 90^{\circ}$
Hexagonal	$a = b \neq c$	$\alpha = \beta = 90^{\circ}, \gamma = 120^{\circ}$

The unit cells are required to fill the three-dimensional space with minimum free energy, and because of the geometrical restriction of lattices, Bravais indicated that there are only 14 possible lattices (table2-2) in seven crystal systems, which is known as Bravais lattices.[31]

Table 2-2 The 14 Bravais lattices

System	Lattice
Regular	Cube
	Body-centred cube
	Face-centred cube
Tetragonal	Square prism
	Body-centred square prism
Orthorhombic	Rectangular prism
	Body-centred rectangular prism
	Rhombic prism
	Body-centred rhombic prism
Monoclinic	Monoclinic parallelepiped
	Clinorhombic prism
Triclinic	Triclinic parallelepiped
Trigonal	Rhombohedron
Hexagonal	Hexagonal prism

2.3 Miller indices

As the physical and chemical properties of the materials are affected by the crystal structures, it is important to define the faces of the crystals. Also, the planes of the crystals are important for analysing the XRD patterns. Miller indices are a group of three indices h, k and l to describe the crystal faces. The three lattice vectors a, b and

c are shown in figure 2-2[30]. If the lattice plane intersecting the axes at point m00, 0n0 and 00p, the hkl can be written as:

$$h = \frac{a}{m}$$

$$k = \frac{b}{n}$$

$$l = \frac{c}{p}$$

$$\frac{a}{m} : \frac{b}{n} : \frac{c}{p} = h : k : l$$

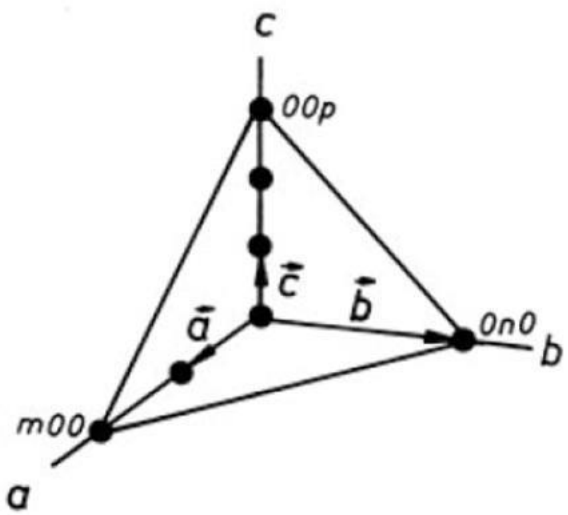

Figure 2-2 The intersections of lattice plane on the axes[30]

If the intercepts are negative, a minus sign needs to be placed above the number. For instance, the lattice plane intercepts with axes at m=-2, n=1 and p=3. And the reciprocals are -1/2, 1 and 1/3. By multiplying with common number 6, the hkl are given as (3 6 2).

2.4 Crystal polymorphism

Polymorphism is a given compound has more than on molecules arrangement in the crystals, and the different polymorphs may have different physicochemical

properties.[32] Because of the different arrangements of molecules, especially the molecules on the surface, the interactions with the surrounding materials varies. And these interactions like hydrogen bonding with solvent can change the stability and solubility of the compound.[33]

The polymorphs can transform between each other under certain conditions like temperature and solvent because the crystals tend to form the most stable form. The polymorphs are known as thermodynamically related if the stabilities of the polymorphs are temperature dependent, which means that one polymorph is more stable in specific temperature range and it can transform to other polymorphs at a certain temperature. If the stability of one polymorph is always the most stable on at all temperatures, these polymorphs are monotropic related.[34] However, Ostwald indicated that the compounds often form the nearest metastable polymorph rather than the most stable form. The metastable form remains stable for a while and transformed to most stable form eventually. This phenomenon is known as "Ostwald rule".

2.5 Solubility and Supersaturation

The solution is the solute dissolved in the solvent to form a homogeneous solution. And the maximum amount of the solute that can be dissolved in the solvent at a given temperature and form homogeneous and saturated solution is the solubility. The saturation state is a thermodynamic equilibrium state, which means the dissolution rate equals to the deposition rate of the solute.[31, 35] In the ideal solution, the interactions between solute and solvent are equal to the interactions between solute and solute. Hence, the solubility can be predicted from the van't Hoff equation:

$$\ln(x) = \frac{\Delta H_f}{R}\left(\frac{1}{T_f} - \frac{1}{T}\right)$$

Where, x is the mole fraction of solute in the solution, ΔH_f is the molal enthalpy of fusion of the solute, R is the gas constant, T_f is the melting point of solute and T is the temperature of the solution. The $\ln(x)$ has linear relationship with the $\frac{1}{T}$ as the equation can be converted to:

$$\ln(x) = -\frac{\Delta H_f}{RT} + \frac{\Delta S_f}{T}$$

Where $\Delta S_f = {}^{\Delta H_f}\!/_{T_f}$. The solubility measured in the real system often varies from the ideal system, which is because of the interactions between solute and solvent are different from the interactions between solute and solute. If the interactions between solute and solvent are stronger than the interactions between solute and solute, the solubility is higher than the ideal. In contrast, if the interactions between solute and solvent are weaker than the interactions between solute and solute, the solubility is smaller than the ideal.

The supersaturation is a metastable state that the solution contains more solute than solubility. A typical solubility-supersolubility diagram is shown in figure 2-3[31]. The supersolubility is the concentration at which the crystals are first detected at a given temperature. The supersolubility are circumstances dependent such as the cooling rate and crystallisation conditions.[36] In other words, the differences between supersolubility and solubility temperature, which is the term of metastable zone width (MSZW), are circumstance dependent.

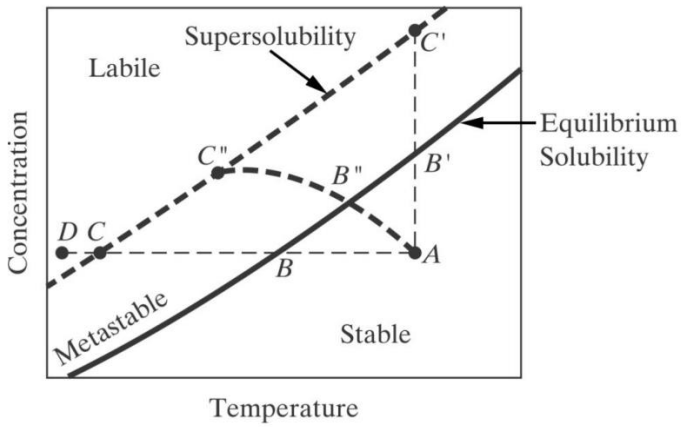

Figure 2-3 The solubility-supersolubility diagram.

The supersaturation is the driving force for crystallisation. The supersaturation can be achieved by decreasing temperature to lower the solubility (line ABC in figure 2-3). If the solubility is not sensitive to the temperature, the supersaturation can be achieved by removing the solvent (line AB'C' in figure 2-3). And the most effective method is combining these two methods, as the line AB"C" in figure 2-3.

The supersaturation ratio, S, is defined by the concentrations:

$$S = \frac{c}{c^*}$$

$$\Delta \mathrm{c} = \mathrm{c} - c^*$$

$$\sigma = \frac{\Delta c}{c^*} = \frac{c - c^*}{c^*} = S - 1$$

Where, c is the concentration of the solution, c^* is the concentration of saturated solution, Δc is the value of supersaturation, and σ is the relative supersaturation.

The concentration of the solution can also be represented by the mole fraction, y. And the relationship between c and y is:

$$\Delta c = \rho y - \rho^* y^*$$

Where, ρ is the molar density of supersaturated solution, ρ^* is the molar density of saturated solution and y^* is the mole fraction of saturated solution. And typically, the density can be considered as constant, therefore:

$$\Delta c = \rho \Delta y$$

$$S = \frac{y}{y^*}$$

$$\sigma = \frac{\Delta y}{y^*} = \frac{y - y^*}{y^*} = S - 1$$

Secondly, change the temperature at a given concentration:

$$\Delta T = T - T^*$$

Where, T is the temperature of the supersaturated solution (K) and T^* is the temperature of saturated solution (K). And the relationship between ΔT and Δc is:

$$\Delta c = \left(\frac{d\, c^*}{dT}\right) \Delta T$$

Finally, although the supersaturation is treated as the driving force of crystallisation, but the fundamental force is the difference of chemical potential between supersaturation solution and crystal state[31]:

$$\Delta\mu = \mu_s - \mu_c$$

Where the μ_s is the chemical potential of solute in solution and the $\mu_c$is the chemical potential of the substance in crystal state.

The chemical potential contains internal chemical potential and external chemical potential, which is temperature related term:

$$\mu = \mu_{int} + \mu_{ext} = \mu_{int} + RTln\ a$$

Where R is the gas constant, T is absolute temperature and a is the activity.

Hence,

$$\frac{\Delta\mu}{RT} = ln\frac{a}{a^*} = ln\ S$$

Where a^* is the saturated solution's activity and S is the fundamental supersaturation.

$$S = \exp\left(\frac{\Delta\mu}{RT}\right)$$

The crystallisation cannot proceed spontaneously in metastable zone, but the crystals will form with the present of crystal seeds. If the supersaturation increased and entered the labile zone, the crystallisation is spontaneously and inevitable.

2.6 Nucleation

Nucleation is the first step of the crystallisation process. It is the formation of small aggregations like clusters and nuclei from a homogeneous solution. Nucleation is a complex process and can be influenced by agitation, mechanical shock, friction, etc..[35] The nucleation can be classified as primary nucleation and secondary nucleation. The nucleation without the presence of crystals is primary nucleation, whereas secondary nucleation is induced by crystals. The primary nucleation can be further divided into

two categories, homogeneous and heterogeneous nucleation. The nuclei formed spontaneously in homogeneous nucleation, whereas the nucleation is induced by foreign particles.

The formation of nuclei not only contains the coagulation of molecules and re-dissolve of nuclei, but also the arrangement of molecules needs to be fixed in the nuclei. And the nuclei formation process is like the bimolecular addition process[31]:

$$\mathrm{A} + \mathrm{A} \rightleftharpoons A_2$$

$$A_2 + \mathrm{A} \rightleftharpoons A_3$$

$$A_{n-1} + A \rightleftharpoons A_n \ (Critical\ cluster)$$

The A_n is the critical cluster, which means that the rate of molecules coagulate equal with the rate of redissolve. A phenomenon called Ostwald ripening was observed that the equilibrium state is not stable: if large nuclei appears, the small one will dissolve and the large one continues growing until the smaller nuclei disappears. This is because the large nuclei have small surface energy and the system trying to lower the energy by moving the molecules from small nuclei to large nuclei.[37]

The critical nucleus can be expressed by classic nucleation theory (CNT). The CNT is the simplest illustration of nucleation, which is based on the Gibbs' Free Energy, and has well illustrated by many books and reviews.[31, 38-40] The free energy change can be expressed by the equation below (assume the nucleus is a sphere and the radius is r):

$$\Delta \mathrm{G} = \Delta G_S + \Delta G_V = 4\pi r^2 \gamma + \frac{4}{3}\pi r^3 \Delta G_v$$

Where, $\Delta \mathrm{G}$ is the overall excess free energy, ΔG_S is the surface excess free energy, ΔG_V is the volume excess free energy, γ is the interfacial tension and ΔG_v is the free energy change per unit volume. Figure 2-4 shows how the free energy changes of the three components: $\Delta \mathrm{G}$, ΔG_S and ΔG_V.

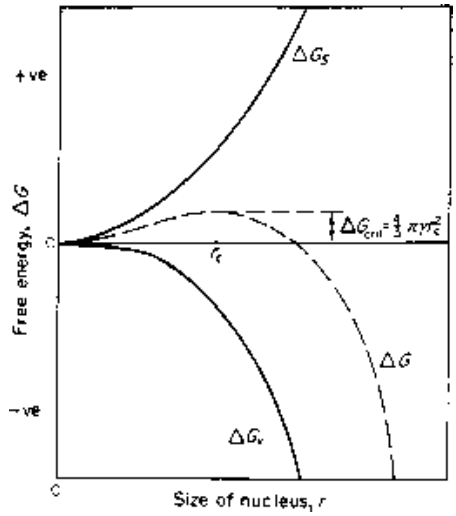

Figure 2-4The free energy diagram for nucleation. [29]

The maximum point of the ΔG is the critical point, ΔG_{crit}, and the corresponding radius r_{crit} is the critical radius. If the radius of nucleus is smaller than r_{crit}, the dissolve will occur to reduce the free energy. Once the radius exceeds the r_{crit}, the nucleus will grow as the decrease of free energy. At the critical point, the slope of the curve of ΔG equals:

$$\frac{d\Delta \mathrm{G}}{dr} = 8\pi r\gamma + 4\pi r^2 \Delta G_v = 0$$

Therefore,

$$r_{crit} = \frac{-2\gamma}{\Delta G_v}$$

And the critical free energy can be expressed by the r_{crit}:

$$\Delta G_{crit} = \frac{16\pi\gamma^3}{3(\Delta G_v)^2} = \frac{4\pi\gamma r_{crit}^2}{3}$$

In order to derive the nucleation rate, the Gibbs-Thomason relationship need to be introduced:

$$\ln S = \frac{2\gamma v}{kTr}$$

Where, S is the degree of supersaturation, v is the molecular volume and k is Boltzmann constant.

$$-\Delta G_v = \frac{2\gamma}{r} = \frac{kT \ln S}{v}$$

$$\Delta G_{crit} = \frac{16\pi\gamma^3 v^2}{3(kT \ln S)^2}$$

And then, the nucleation rate can be expressed as:

$$\mathrm{J} = K_J \exp\left(-\frac{\Delta G}{kT}\right) = K_J \exp\left[-\frac{16\pi\gamma^3 v^2}{3k^3T^3(\ln S)^2}\right]$$

From this equation, there are three variables can affect the nucleation rate: the interface tension, the temperature and the degree of supersaturation.[31] And fig. 2-5[41, 42] shows how these variables affects the nucleation rate. This equation also suitable for heterogeneous nucleation by replacing the interfacial tension γ with effective interfacial tension, γ_{eff}.[31]

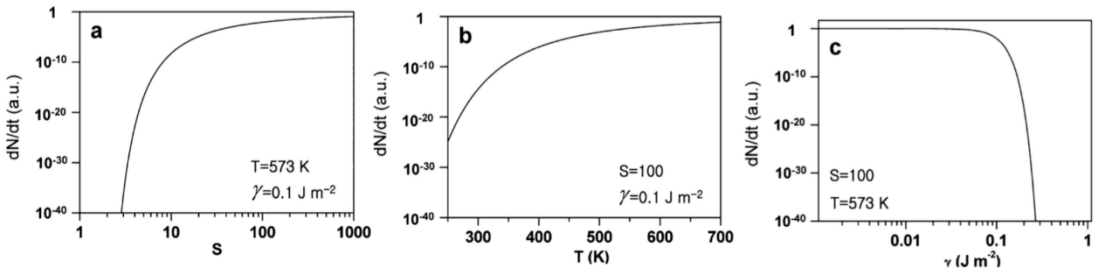

Figure 2-5 Nucleation rate as a function of a) supersaturation, b) temperature, and c) interfacial tension.

Secondary nucleation has different mechanism with primary nucleation and typically occurs by adding crystal seeds into supersaturate solution. The primary nucleation cannot occur in the metastable zone, whereas the secondary nucleation is easier than primary nucleation and can form nuclei at lower supersaturation. The mechanisms of secondary nucleation were well studied, such as initial breeding, needle breeding, friction, and contact.[43, 44]

The two-step nucleation is a modern approach that the molecules form disordered liquid-like clusters and then the molecules re-arrange and form nuclei.[45] Comparing with classic nucleation theory (CNT), the CNT assumed that the molecules formed nuclei directly through biomolecules additions process, whereas the two-step models indicated that the molecules formed the liquid-like clusters first and the nuclei formed within the clusters.[46] The two-step nucleation was first reported by Wolde and Frankel[47] and the computational simulations suggested the formation of the disordered liquid-like clusters. The experimental observation of the two-step nucleation are particularly focusing on the large molecules like proteins and polymers, which is because of these materials take longer time to rearrange into ordered stable structure.

2.7 Crystal growth

Following with the formation of nuclei, the crystal growth process begins in the supersaturated solutions. The crystal growth process is environmental dependent, the temperature, supersaturation degree, impurities have influence on the crystal growth. The internal factors like intermolecular interactions and crystal defects also have influence on the crystal growth. The crystal growth process can be split into three major steps:

- Transport the molecules to the boundary layer between crystal surfaces and solution.
- Adsorb the molecules onto the crystal surfaces and migrate the molecules to energetically favourable sites.
- Binding the molecules into the sites.

The adsorption layer theories were first introduced by Volmer in 1939. Volmer indicated that the crystal growth process is a discontinuous process: the molecules or atoms are not integrated into the lattice once they reach the surface of crystal but form a loosely absorbed layer and the molecules or atoms can move around the surface of crystal. The molecules or atoms will integrate into the lattice in positions with the greatest attractive forces. Once the layer is completed, a two-dimensional nucleation process occurs on the surface of crystal before the crystal growth can continue. The derivation of the free energy and critical nucleus size uses the same method with 3-dimensional nucleation.

$$\Delta G = a\gamma + v\Delta G_v$$

Where, a is the area of the nucleus and v is the volume of the nucleus.

Assume that the nucleus is a circular disc with a radius r and height h. Then:

$$\Delta G = 2\pi rh\gamma + \pi r^2 h\Delta G_v$$

And the critical point is the maximum value of ΔG,

$$\frac{d\Delta G}{dr} = 2\pi h\gamma + 2\pi rh\Delta G_v = 0$$

Therefore,

$$r_{crit} = -\frac{\gamma}{\Delta G_v}$$

$$\Delta G_{crit} = -\frac{\pi h\gamma^2}{\Delta G_v} \text{ or } \Delta G_{crit} = \frac{\pi h\gamma^2 v}{kT \ln S}$$

And the nucleation rate can be expressed as,

$$J' = K_J \exp\left(-\frac{\Delta G_{crit}}{kT}\right) \text{or } J' = K_J \exp\left[-\frac{\pi h\gamma^2 v}{k^2 T^2 \ln S}\right]$$

Comparing the 2-D nucleation and 3-D nucleation,

$$\frac{J}{J'} = \frac{16\gamma v}{3hkT \ln S}$$

Which means that the 2-D nucleation still need the supersaturation or supercooling, but the degree of supersaturation/supercooling is lower than 3-D nucleation.

The Kossel's model is shown in figure 2-6[48, 49] and an assumption has made that the growth units are cubic and each face has one bond.

The main positions of crystal growing are at kink site, step site and terrace site. The growing unit integrates at the kink site can form 3 bonds and the surface energy does

not change. When the crystal growth occurs at step site, the unit can form 2 bonds and there are two new faces are formed. When comes to the terrace site, only one bond is formed and four new faces appear. Hence, the kink site is the easiest point for crystal growing: kink > step > terrace.

As the crystal growth process can be affected by the properties of nuclei surface, several other models have been set up: screw dislocation (BCF), birth and spread (B&S), and tough interface (RIG). The BCF model is used for the crystals with screw dislocation on crystal surface. The B&S model requires the process start as 2-D nucleation. And the RIG model is for the crystal with a rough surface.

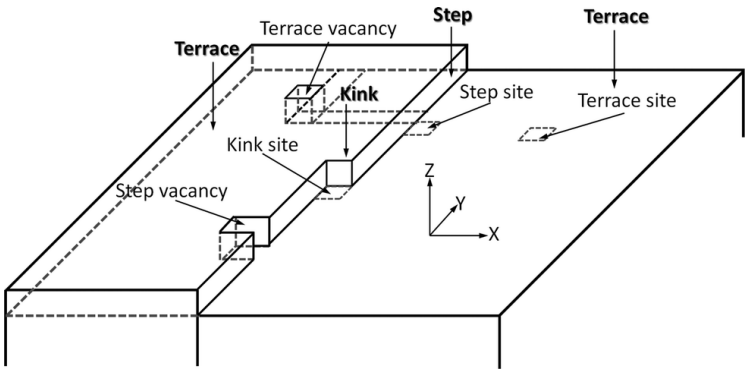

Figure 2-6 Schematic diagram of the Kossel's model

2.8 X-rays and diffraction

The X-rays electromagnetic radiations, which is similar with visible light, but the wavelengths are much shorter. The electromagnetic spectrum shown in figure 2-7[50] is divided into seven regions by wavelength. The wavelength of X-rays ranges from 0.01nm to 10nm. The X-rays are produced by decelerating the electrically charged particles rapidly. The energy conducted to the anode can accelerate the electrons, ions and nuclei. Only 1% of the total energy is emitted as X-ray, and the rest of the energy is lost as heat.

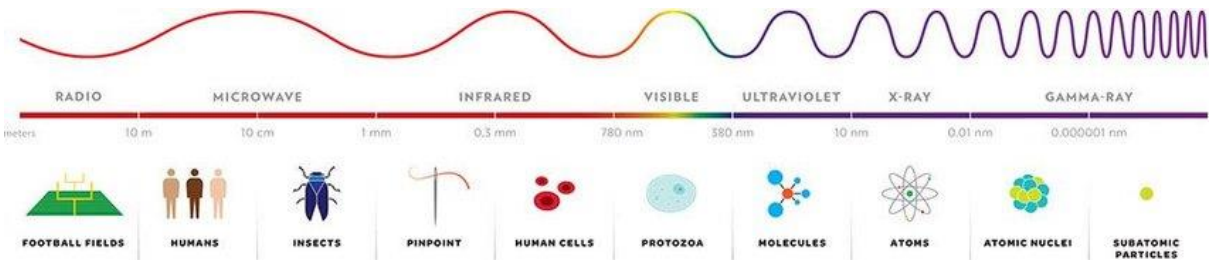

Figure 2-7 Electromagnetic spectrum.[49]

The relationship between the energy and accelerated electrons can be explained by the following equation:

$$E = eV = 1/2\ mv^2$$

Where V is the accelerating voltage applied to the electrodes, e is the charge of an electron, m is the mass of electron and v is the velocity of the accelerated electron. The accelerated electrons transmit the energy to photon energy:

$$E_{photon} = \frac{hc}{\lambda}$$

Where, h is Plank's constant, c is the speed of light and λ is the wavelength. According to these two equations, the X-ray spectrum is depending on the anode materials and accelerating voltage.

There are three types of laboratory X-ray tubes: Crookes tube (cold cathode tube), Coolidge tube (hot cathode tube) and Rotating anode tube. The wildly used X-ray tube is the Coolidge tube and the set-up is shown in figure 2-8[51]. The cathode in the X-ray tube is used for thermal emission of electrons. The high voltage, U_a, is used for generating an external electrical field to accelerate the electrons and the typically accelerating voltage ranges from 30kV to 50kV. The radiations are generated when the electrons decelerated by the metal anode. The unit used in X-ray measurement is angstrom (Å), which is equal to ^{10}-10m. The wavelength of X-rays ranges from 0.5Å to 2.5Å, and it depends on the materials of the anode. Typically, the materials of the anode are Cu or Mo, and the wavelengths are 1.541Å or 1.790Å, respectively.

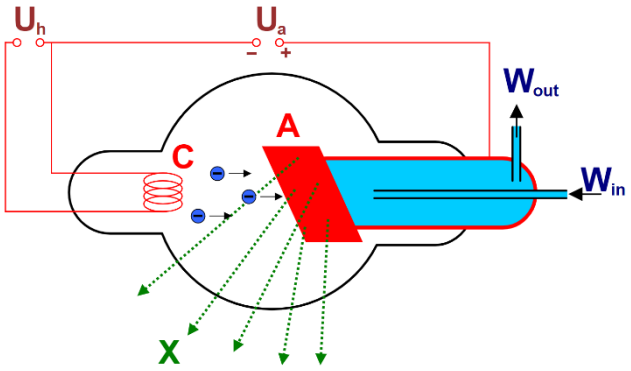

Figure 2-8 General Coolidge tube.[50] C, cathode. A, anode. U_h, heater voltage. U_a, accelerating voltage. W, cooling water. X, X-rays.

2.8.1 Braggs Law and X-ray diffraction

XRD is an analytical technique used for the determination of crystal structure. As shown in figure 2-9[52], the atoms/repeating units arranged on planes in crystal and the interlayer spacing, d, is constant. Assuming the incident angle is θ and the wavelength of X-rays is λ. The X-ray beam can scatter to all directions once it interacts with the atoms. However, only part of the scattered X-rays can be detected because of the interference. The interference depends on the path difference:

The path difference between X-ray 1 and 1a shown in figure 2-9 is:

$$QK - PR = PK\cos\theta - PK\cos\theta = 0$$

Hence, these two incident X-rays are out of phase. The path difference between X-ray 1 and 2 can be calculated as:

$$ML + LN = d\sin\theta + d\sin\theta = 2d\ sin\ \theta$$

Hence, X-ray 1' and 2' are reinforcing each other. The specific path difference between two constructive interference is $2d\ sin\ \theta$. And this relationship is known as Bragg's Law:

$$n\lambda = 2d\sin\theta$$

$$d = \frac{n\lambda}{2\ sin\ \theta}$$

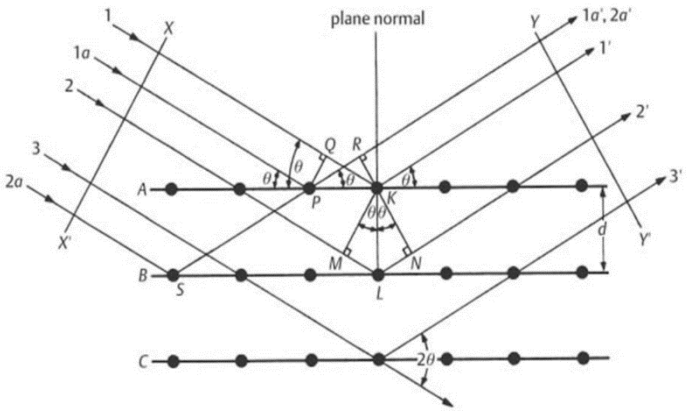

Figure 2-9 Diffraction of X-rays in crystal.[51]

2.8.2 Powder X-ray diffraction

The powder XRD is one of the most wildly used techniques of XRD to determine the crystal structures. Although the single crystal XRD is the most powerful technique for crystallography determination, the P-XRD still plays an important role in this filed because of the simplicity in the instrument and sample preparation. The P-XRD consists of a sample holder, X-ray tube and detector. Both reflection and transmission mode can be achieved by arranging the position of the three components.

As for the sample of P-XRD, the samples are ground to very fine powder. The tiny particles of crystals are randomly oriented with the incident X-rays, and all the planes in crystals are aligned to the beam. For instance, some of the particles will reflect the X-rays by (100) planes, whereas the (110) planes will align to the beam in other particles. Hence, the X-ray patterns of powder samples are reflections of every possible plane in the crystals. Except for the plane orientation, the planes can also rotate randomly. As the result of the rotation, the shape of the diffracted radiation is cone-shaped and different cone represents different hkl planes as shown in figure 2-10.[53]

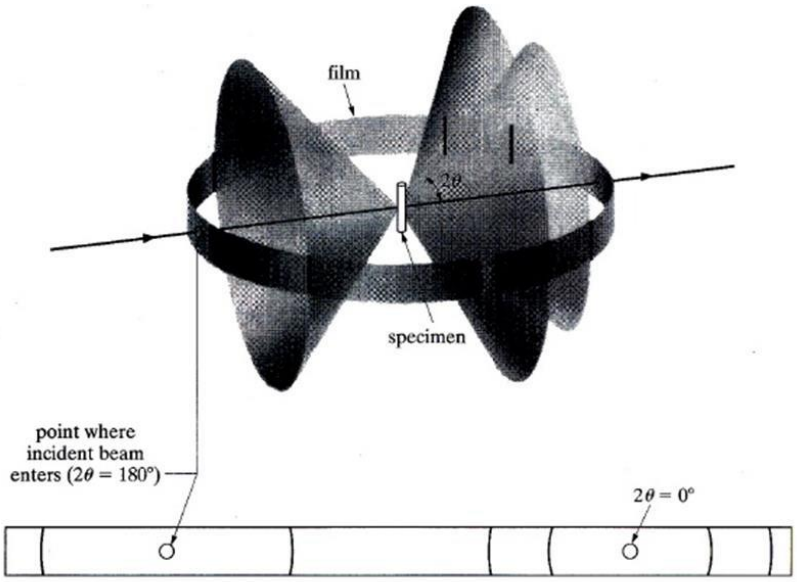

Figure 2-10 The Hull/Debye-Scherer method of powder-XRD[52].

There are two primary methods for powder XRD, Hull/Debye-Scherer method and Bragg – Brentano geometry. The Hull/Debye-Scherer method is the first developed powder diffractometer and the model is shown in figure 2-10. The samples are placed in the centre of the ring of film. The incident X-ray is perpendicular to the axis of the ring of film and the diffracted radiations can be recorded by the film. The diffracted angle θ can be calculated with the known radius and arc length. And then, the d-spacing can be calculated by the Bragg's Law with a known wavelength of incident radiation and θ. As shown in figure 2-11, the Bragg-Brentano diffractometer uses different geometry, θ/θ scan[54] and θ/2θ scan[55]. In Bragg-Brentano diffractometer, the diffracted radiations are collected by the detector and the resolution is determined by the width of receiving slit. Only a small portion of the diffracted radiations can be recorded per scan and the detector are moving on the diffractometer circle with a speed of several degrees per minute. The position of the samples in the θ/θ scan is fixed, the X-ray source and detector is moving simultaneously on the diffractometer circle in different directions, and the incident angle and reflect angle are same. Whereas in the θ/2θ scan, the position of X-ray source is fixed. The sample holder is rotating with a speed of θ per minute and the detector is moving on the diffractometer circle with a speed of 2θ per minute.

a

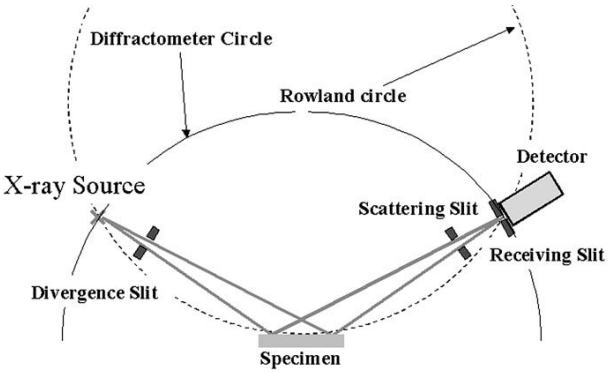

b

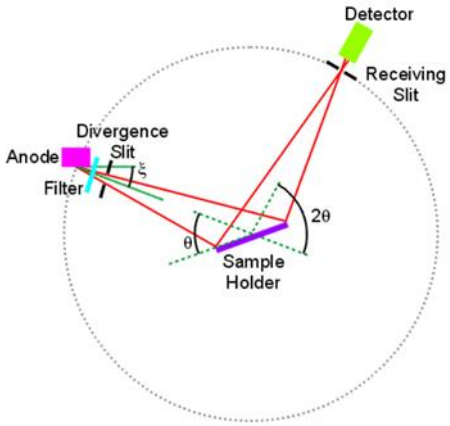

Figure 2-11 Two Bragg-Brentano diffractometer: θ/θ scan[53] (a) and θ/2θ scan[54] (b).

2.9 Small Angle X-ray Scattering (SAXS)

Small angle X-ray scattering is a non-destructive analytical method used for structure determination. The SAXS is similar to XRD, and the instrument contains the same components with XRD, which are X-ray source, sample holder and detector. The difference between SAXS and XRD is the scales, the SAXS is focusing on the structure of the samples at nano-scale, whereas the XRD is focusing on smaller scales. Hence, SAXS can be used for investigating the nano-scale structure such as pores and particles. As this project is studying the liquid crystals of surfactants, the SAXS is useful for studying the long range spacing of the molecules such as interlayer spacing (d-spacing). Besides the investigation on long range molecules arrangement, SAXS can also be used for studying the particular samples, such as the particle size and shape in solution. The principle of SAXS is same as the XRD and the scattering also follows the Bragg's Law. Hence, the particles with smaller size will scatter X-ray at larger 2θ. Hence, the particle sizes of 2 are larger than 1, as shown in figure 2-12[56].

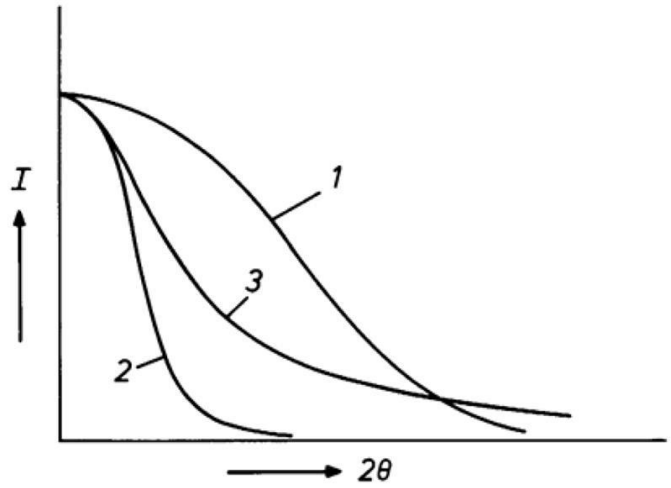

Figure 2-12 Scattering intensities of particles with different size[55].

2.9.1 SAXS patterns

The raw results collected by SAXS are 2-dimensional scattering patterns, which are the rings of scattered X-rays. The 1-dimensional scattering patterns with the function of I(q) are generated by integrating the 2-D patterns radially, where q is the momentum transfer:

$$q = \frac{4\pi \sin\theta}{\lambda}$$

Where, λ is the wavelength of X-ray, θ is the ½ of scattering angle. Hence, q is related to the scattering angle. The d-spacing can be calculated by comparison with Bragg's law:

$$d = \frac{\lambda}{2\sin\theta} = \frac{\lambda}{q\lambda/4\pi} = \frac{2\pi}{q}$$

As shown in figure 2-13[57], the 2D pattern is the raw results collected from SAXS, which is the rings of scattered X-rays. The 1D pattern with the function of intensity vs q is generated by radial integration.

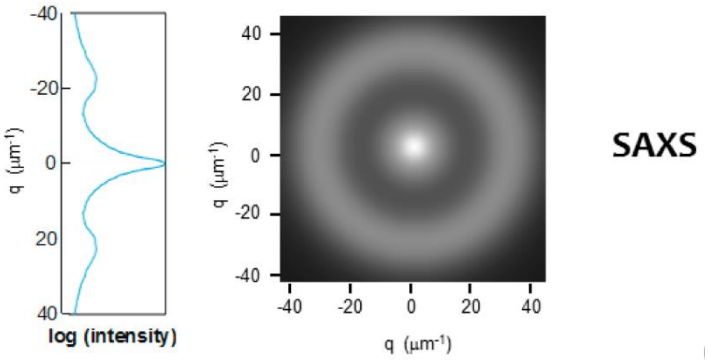

Figure 2-13 Integration the 2D scattering pattern to 1D profile[56].

2.9.2 Mono-disperse scattering

SAXS can be used for investigating the structure information of mono-disperse and poly-disperse system.[58] The mono-disperse system is the ideal system for SAXS, which is reduced the complexity of inter-particle interactions.[59] As the SAXS data of the mono-disperse system is from a single particle, it is ideal for size, shape and surface analysis.[60] Unlike XRD, where the diffraction provides clear information of crystal structure, the SAXS curves do not provide the information of size, shape and surface straightforward and need further analysis. The analysis is dependent on the theoretical model fitting and the simple model of a homogeneous spherical particle is derived below. Assuming the particles with the radius of R (figure 2-14) are mono-disperse, homogeneous, and no long range interactions.[61] The wave function is used for describing the scattering from a point in the particle:

$$\psi(q) = \exp(-iq.r)$$

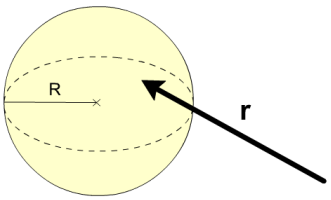

Figure 2-14 Spherical particle of radius R and position vector r.

Assuming the scattering length of a point in the particle is b, and the scattering length density of point j in the particle is b_j/V, where V is the volume of the particle over r. The scattering pattern obtained is the summation of the scattering length density of all the possible point:

$$\rho(r) = \sum \frac{b_j}{V}$$

The amplitude of the scattering can be obtained by combining with the wave function of the scattering from a point in the particle:

$$A(q) = \int \rho(r) \exp(-iq.r)$$

As the particle is assumed as a centrosymmetric sphere, which is free from orientation effects, the scattering amplitude becomes:

$$A(q) = 4\pi \int \rho(r) \frac{\sin(qr)}{qr} r^2 dr$$

By setting the limit to 0 to R, the equation becomes:

$$A(q) = \frac{4}{3}\pi R^3 \frac{3[\sin(qR) - qR\cos(qR)]}{(qR)^3}$$

The amplitude can be converted to intensity by the following equation:

$$I(q) = n\Delta\rho^2 V^2 \mid A(q) \mid^2$$

$$I(q) = I_0[3\frac{\sin(q.r) - q.r\cos(q.r)}{(q.r)^3}]^2$$

The scattering curve of solid sphere particles can be produced by this equation. Following this basis, the samples with different geometrical shape can be fitted with SAXS scattering patterns and the theoretical scattering curves are shown in figure 2-15[62].

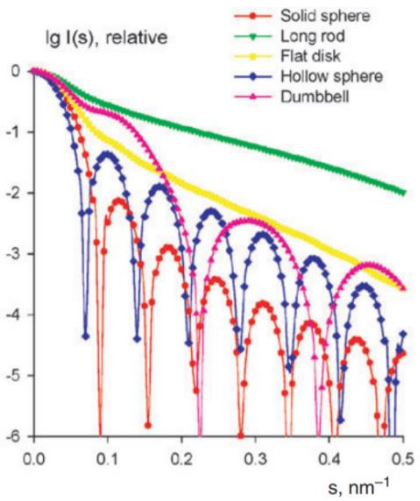

Figure 2-15 Theoretical scattering curves of samples with different geometrical shape[61].

2.10 Washing powder and manufacturing process

2.10.1 Washing powder formula

Washing powder is one of the most widely used consumer products and plays an important role in daily life. The detergency of the products depends on the formulations, which contains over 20 ingredients. These chemicals can be divided into nine groups. However, not all the products contain all these ingredients.[63]

Surfactants: The surfactants are active components in washing powder. With the washing action, the hydrophobic tails can penetrate into the soil, which can loosen and remove the soil from fabric. Then the soils can be emulsified or suspended in water before washing away. Typically, the main surfactant in washing powders is LAS.

Builders and fillers: The builders are the main ingredients in washing powder, typically contains over 50%. Except for lowering the cost, they can also soften water by binding the metallic ions water, dirt or textiles. Typically, the builders used in washing powders are sodium carbonate, sodium sulphate or zeolite. The builders can form insoluble compounds by ion exchange to reduce the ion concentration.

Enzymes: The stains and soils are complex, and protein-based stains and starch-based stains from food, grass or blood are common. The detergency of surfactants on

these stains is limited. Hence, the enzymes are added to washing powder to improve the detergency on these stains. The enzymes can break down the peptide bonds by enzymatic hydrolysis.

Polymers: In order to avoid the re-depositing of the soils on fabrics, polymers are added to the washing powder. They can capture the soils before washing away. Typically, P&G relies on swelling cellulosic polymers.[63]

Bleach: Some of the stains or soils have strong interactions with fabrics and surfactants/enzymes have limited detergency on them. The bleach can decolour the stains/soils by oxidising the chromophore compounds. There are two kinds of bleach used in washing powders: peroxide hypochlorite.

Softeners: The softeners are a kind of surfactants, which can deposit on the fabric and form a layer on it to reduce fabric friction. The reduction of friction helps to improve the appearance and feel of the fabrics.

Stabilisers: Some of the stabilisers can improve the stability of washing powders and prolong the shelf life, especially the enzymes and bleach.[64] In some regions, such as China, the subs level is an important mark of detergency. Hence, foam stabilisers are added to the washing powders.

Preservatives: Chemicals for protecting the washing powder from ageing.

Perfumes: Some of the surfactants, such as LAS and AES, have awful odours. In order to improve customer satisfaction, perfumes are added to washing powders to provide lovely scent to fabrics and cover the odours.[64]

2.10.2 Manufacturing process

The manufacturing process of washing powders has several stages and can be comprised as mixing, drying and densification.[64] Except for these processes, some thermal sensitive ingredients, such as perfumes and enzymes, are added to washing powder after spray drying process by spray-on process.[63] The typical washing powder manufacturing process is shown in figure 2-16, which can be divided into slurry preparation, pumping, atomization, drying, fining and finishing.

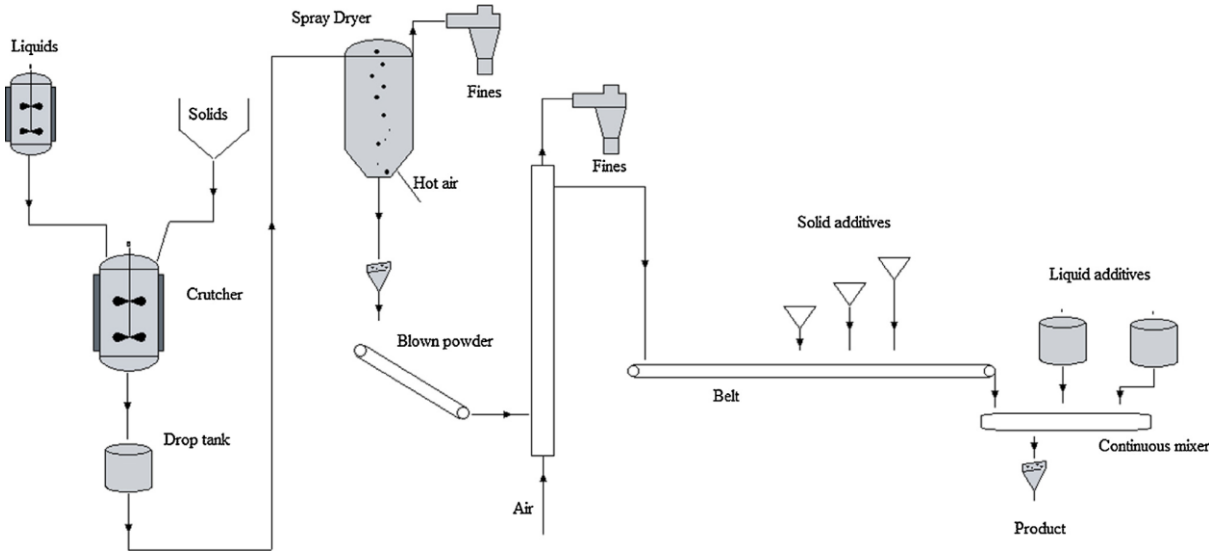

Figure 2-16 Washing powder manufacturing process.[64]

The first stage is preparing homogeneous slurry for the spray drying process. In this stage, the surfactants are mixed with solid samples such as sodium carbonate in Crutcher. And then the slurry will be transferred to drop tank for further process. Due to the low water/liquid content, lumps can be formed in the slurry, which may block the spray nozzle in the spray drying tower. Hence, the mixtures are filtered and disintegrated before being pumped to the spray drying tower. The most common method for removing water in the mixtures and preparing washing powders is the counter-current spray drying tower. And the inlet temperature can reach 300°C.[64] The powder properties, such as density and particle size distribution, can be controlled during this stage. Typically, the density of washing powder ranges from 250 to 550kg/m^3, and the particle sizes range from 400 to 500μm. It should be aware that the exhaust air needs to be filtered and the waste collected can reuse. The temperature at the base of the spray drying tower is around 70°C, which means that the powders need to be cooled down before adding temperature-sensitive ingredients, such as bleach and enzymes. The cooling could be done while transporting the powder to the next stage through airlift.

The final stage of washing powder manufacturing process is mixing all the ingredients to form a homogeneous mixture. These ingredients include spray-dried powder, enzymes, filler, perfumes, surfactant granules and other additives. Some liquid ingredients, such as perfumes and non-ionic surfactants, can be added to the product during this stage. However, this needs to be careful because the liquid ingredients can

over-wetting the dried powder and cause caking. Also, the liquid ingredients may build up on the drum wall. Hence, it not possible to add a large amount of non-ionic surfactant in the washing powders without solidifying the surfactant.

2.11 Summary

This chapter has introduced the fundamental concepts of the crystals, including crystallography and polymorphs, which provides basic knowledge for crystal formation of acid-soaps. The fundamental theories of nucleation and crystal growth provide base knowledge for understanding the influence of environments on the crystallisation process. As X-ray diffraction is the most important method for crystallography, the fundamental knowledge also been discussed in this chapter. The washing powder manufacturing process was also reviewed in this chapter, which provides base knowledge to understand industrial problems.

3 Chapter 3 Surfactants and the acid-soaps

Literature review of the fundamentals of the surfactant structures and the phase transitions, provides a view of the acid-soaps structures and crystallisation behaviours of carboxylic acids.

3.1 Introduction

The surfactants consist of hydrophobic and hydrophilic groups, and the typical molecule structure is shown in figure 3-1. The hydrophilic groups have electrostatic interactions with surrounding molecules, whereas the hydrophobic groups have interactions with non-polar molecules through van de Waals force. As this unique property, the surfactants are wildly used in versatile chemical products like pharmaceuticals, laundry detergents, and wetting agent.[1] This chapter will start with the basic theory of surfactants, such as structures and aggregations.

The most common surfactants used in consumer products are soaps, which are the metal salts of long chain fatty acids. The phase behaviours of soaps are complex because of the amphiphilic property. Furthermore, the phase behaviours are influenced by the alkyl chain length of fatty acids, the counterions and the saturation of alkyl chain. This chapter will review the researches on the crystallisation process and phase behaviours of fatty acid soaps/acid-soaps.

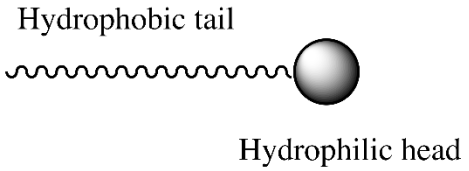

Figure 3-1 Typical molecule structure of the surfactants.

3.2 Surfactants

3.2.1 Structure

Surfactants are wildly used in consumer products such as pharmaceuticals[65], oil recovery[66, 67] and laundry products[68, 69]. The surfactants comprise a polar head group and a non-polar tail, which induces the amphiphilic properties. The hydrophobic tails of the surfactants can be hydrocarbon, fluorocarbon, short polymeric chains, or siloxane chains.[11] The size of the hydrophobic chains can be controlled to achieve the desired solubility in the solvent. Typically, the hydrocarbon chain length of the surfactants used in cleaning products ranges from 8 to 22. Based on the ionic properties of the head group, the surfactants can be classified as anionic surfactant, cationic surfactant, non-ionic surfactant and amphoteric surfactant.[68]

The anionic surfactants are the most common class of surfactants and over 70% of the surfactant consumptions are anionic surfactants. They consist of hydrophobic groups and anionic hydrophilic head groups, such as carboxylates, sulphate and sulfonates. The cationic surfactants comprise less than 10% worldwide surfactants consumption. However, this is not meaning the cationic surfactants are not important. The bacteriostatic properties were first reported in 1938, since then, these surfactants were wildly used in consumer products as antiseptic agents or fungicides. As the surface of hair is negatively charged, the cationic surfactants like Behentrimonium Chloride (BTAC) and Behenamidopropyl Dimethylamine (BAPDMA)[70] were wildly used in hair conditioners. The hydrophilic groups of the cationic surfactants form hydrogen bonding with the protein on the surface of hair. Therefore, the cationic surfactants protect the hair surface by forming new surface on the hair. The hydrophilic groups of non-ionic surfactants are neutrally charged. As the functional groups do not ionise in solution, the non-ionic surfactants are not sensitive to the counterions in solution, which improves the detergency of the surfactants in hard water.[11] The amphoteric surfactants contain amphoteric head groups and the ionic properties of the head groups are environmental dependent. The amphoteric properties give the amphoteric surfactants potential in the compositional formulation.

In order to correlate the surfactant molecule structures with the surface activities, the concept of hydrophile–lipophile balance (HLB) system was raised. The HLB method was first published by Griffin in 1949[71] and a more accurate method was published later[72, 73]. The HLB is the balance between the hydrophobic groups and hydrophilic groups in surfactants and it ranges from 0 to 20. The surfactants with high HLB values are water soluble and can be used as solubilising agents, detergents and emulsifier in oil-in-water emulsions. The surfactants with intermediate HLB values are water dispersible and can be used as wetting agents. The surfactants with low HLB values are oil soluble and can be used as emulsifier in water-in-oil emulsions.[11]

For the non-ionic surfactants, alcohol ethoxylates, the HLB can be calculated as:

$$HLB = \frac{E}{5}$$

Where E is the weight ratio of oxyethylene groups. The polyhydric alcohol fatty acid esters, the HLB can be calculated by the following formula,

$$HLB = 20\left(1 - \frac{S}{A}\right)$$

Where S is the saponification degree and A is the acid number of the fatty acid. An empirical equation was proposed by Griffin for the surfactants cannot be saponified,

$$HLB = \frac{E + P}{5}$$

Where P is the weight ratio of the hydrophobic groups.

The HLB method is wildly accepted experimental method for choosing surfactant system for given applications. The HLB value of the compositional formulated surfactants (HLB_m) can be calculated by:

$$HLB_m = \sum HLB_x \times f_x$$

Where HLB_x is the HLB value of the surfactant x and f_x is the weight ratio of the surfactant x in the system.

3.2.2 Phase behaviour

As described previously, surfactants consist of hydrophobic tails and hydrophilic head groups and this unique structure induces the complex phase behaviour. In the aqueous system, the hydrophobic groups tend to minimise the interactions with water, whereas the hydrophilic groups have tendency to maximise the interactions with water. As a result of this phenomenon, the surfactants have a strong tendency to aggregate on the interfaces between phases, such as liquid-oil and liquid-air, to reduce the free energy. If the concentration increased to a certain amount, the surfactants molecules fill all the interfaces, the hydrophobic effect drives them to aggregate and forms self-assembled structures as shown in figure 3-2.[11, 74] The self-assembled structures could be micelles, vesicles, liquid crystals and crystals.

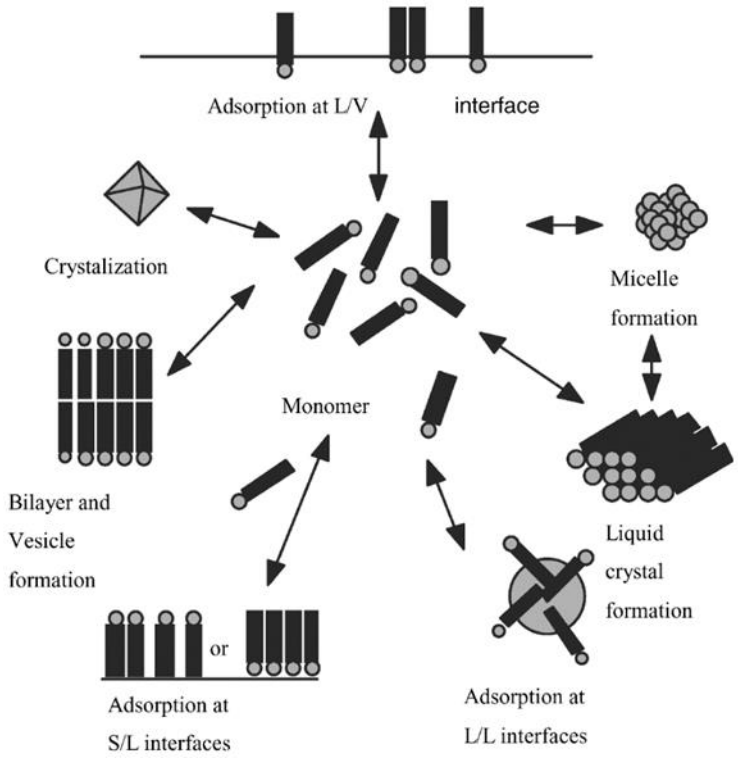

Figure 3-2 Adsorption of surfactants on the interfaces to reduce the free energy and surfactants aggregation.[22]

As illustrated in chapter 2, the crystallisation process occurred if the amount of solute exceeds the solubility at a given temperature. Although the aggregation occurred in the surfactant solutions, several mesophases appear before the formation of crystals. The possible mesophases of surfactants in aqueous solution are shown in figure 3-3. As the increasing amount of water, the surfactants transform from crystals/hydrated crystals to inverse hexagonal structure, followed by the inverse micelles. In these stages, the water is trapped in the centre of the hexagonal crystals or micelles. As the amount of water increasing further, the bi-continuous cubic phase appeared and the hydrophilic groups head toward outside. With the decreasing of the concentration of surfactants, the surfactants form hexagonal phase and micelles. Once the concentration decreases below the critical micelle concentration (CMC), which is the lowest concentration that micelles start to form, the surfactants appear as molecules solution.[11, 75]

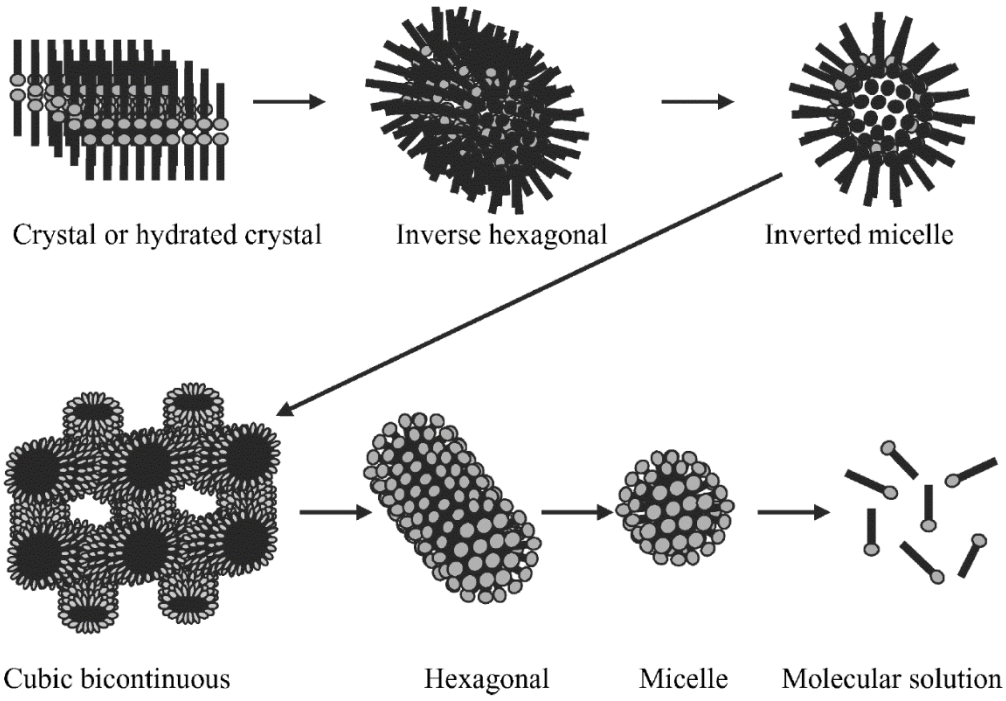

Figure 3-3 The mesophases of surfactants in solution with increasing amount of water.[22]

The solubility curve of surfactant and the critical micelle concentration curve is shown in figure 3-4, and the temperature of the intersect of these two curves is known as Krafft temperature or Krafft point. The solubility curve is below the CMC curve when the temperature is below the Krafft point, which indicated that the solubility of the surfactants is lower than the CMC and no micelles can be formed below Krafft temperature. When the temperature above the Krafft temperature, the concentration of surfactants increased above the CMC, and the micelles appeared in the solution. As the formation of the micelles, the concentration of free surfactant molecules do not change a lot and keeps at CMC, whereas the number of micelles increases with the increase of the total amount of surfactants in the solution.

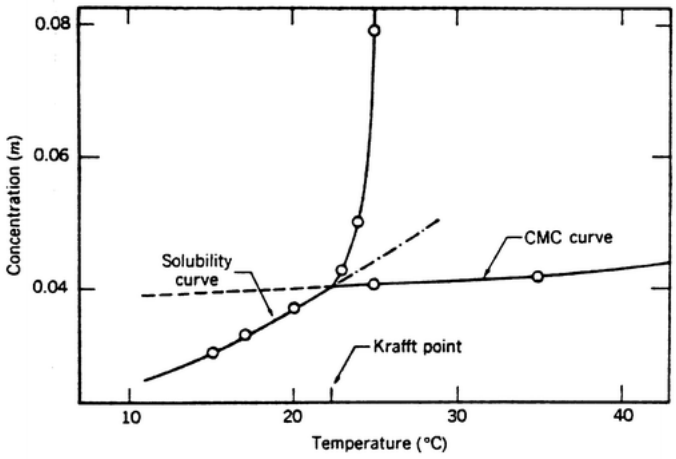

Figure 3-4 Temperature-concentration relationship.[58]

The molecular structures of the surfactant have significant influence on the micelle structures. And the aggregation structures can be predicted by packing parameter,

$$P = \frac{V}{a_o l_c}$$

Where V is the volume of hydrophobic groups, a_o is the area of cross-section of hydrophilic group and l_c is the hydrophobic chain length. As shown in figure 3-5, spherical micelles form if $P < 1/3$, worm-like micelles form if $1/3 < P < 1/2$, vesicles form if $1/2 < P < 1$, planar bilayers form if $P \sim 1$ and inverted micelles form if $P > 1$.[76]

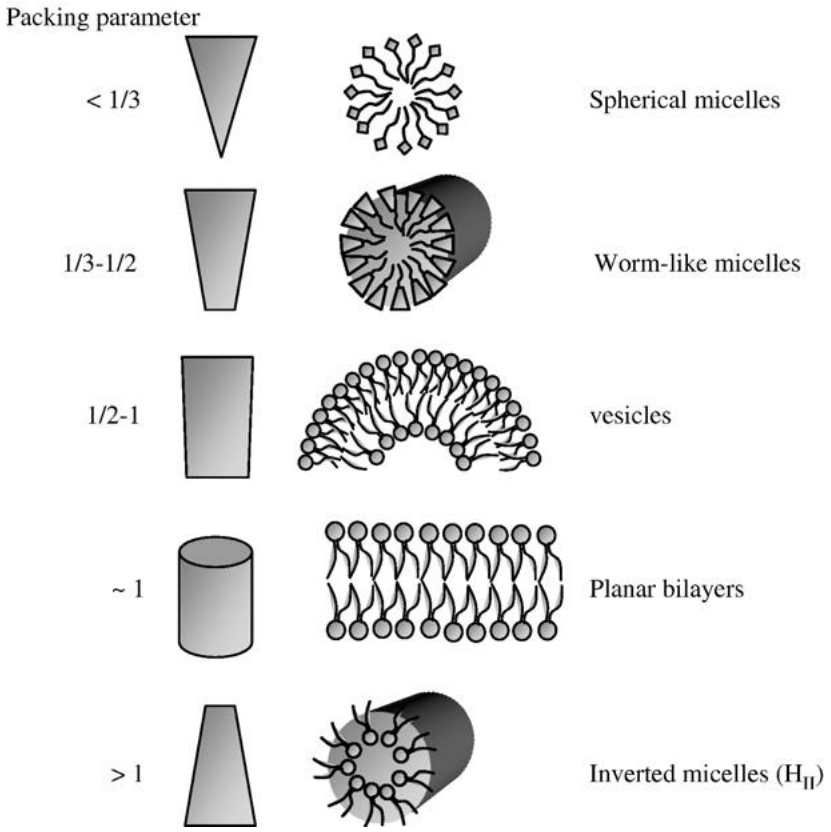

Figure 3-5 The relationship of surfactant aggregation structure with packing parameter.[59]

3.2.2.1 Micelles

As illustrated previously, when the temperature raised above the Krafft temperature, the micelles form in the solution. In order to minimise the free energy, the core-shell structure, micelles, formed in the solution, which is the hydrophilic groups formed a shell to prevent the interactions between solution and hydrophobic tails. The inverted micelles formed in the solutions with a low amount of water, as shown in figure 3-3, the water is trapped in the core and the hydrophobic tails face outside. This structure can also form in the solution with organic solvent.[77]

A. I. Rusanov indicated that the micelles have solid-liquid duality, which is the micelles have the ability to retain the shapes and the molecules in the micelles are mobile.[78] The motions of the molecules are restricted in the tangential direction. This property suggested that the micellization process is different from the nucleation process as the

nuclei are solids formed in supersaturated solutions. Numbers of publications on thermodynamic and kinetic of micellizations suggested that the micelles are equilibrium stage that the micelles have molecule exchange with the monomers in solution.[79-81] And this theory is the fundamental of computational simulation of micellization.

There are several types of micelles formed depending on internal and external effects, such as the chemical structure, surfactant concentration and counter-ions in solution. The formation of micelles follows the Gibbs free energy theory. The deformations of micelles are the process to minimise the free energy and the transitions could be spherical micelles to disk-like micelles, spherical micelles to prolate or oblate micelles.[77, 82, 83] Micelles are aggregations of surfactants molecules, and the mean value of the number of monomers in a micelle is called aggregation number. Because of the ionic strength of head groups, the aggregation number varies between surfactants, such as aggregation number of the non-ionic surfactants are typically 100 to 1000 and the ionic surfactants are 10 to 170.[84] The ionic strength of the solution also influences the micelles' structures as it can affect the headgroup size of surfactants.[85] Caroline Th'evenot verified this phenomenon that as the concentration of NaCl increases, the aggregation number of sodium dodecyl sulphate increases.[86]

As the increasing of surfactants concentration, the spherical, prolate, oblate and disk-like micelles can be elongated to form rod-like micelles. The aggregation number of rod-like micelles is hard to be predicted as there is no theoretical limit on the length.[11] The physical properties changed significantly if the rod-like micelles formed in the solution as the entanglement of the micelles can increase the viscosity and the size of the rod-like micelles are polydispersed.[11, 77]

3.2.2.2 Vesicles

The vesicles are hollow spherical aggregations of surfactants with bilayer structures as shown in figure 3-6[87]. The vesicles can be unilamellar, multilamellar or multivesicles. The size of vesicles ranges from less than 100nm to several micrometres. The vesicles are suitable for pharmaceutical or cosmetic delivery system as the active molecules

can be encapsulated in the hollow and the structure can maintain a relatively long time, typically several days to several months.[11, 88] The vesicles can be formed by the surfactants with packing parameter $1/2 < P < 1$, which is the surfactants contain two hydrophobic tails and one hydrophilic head group. And the most common method to produce the vesicles is mixing different surfactants with specific ratios.[87] The cryo-TEM images indicated that the unilamellar vesicles formed in the solution of cetyltrimethylammonium bromide (CTAB) with sodium salts of 5-methylsalicylic acid with a molar ratio of 1.1 and the vesicles transformed to spherical micelles upon shearing.[89]

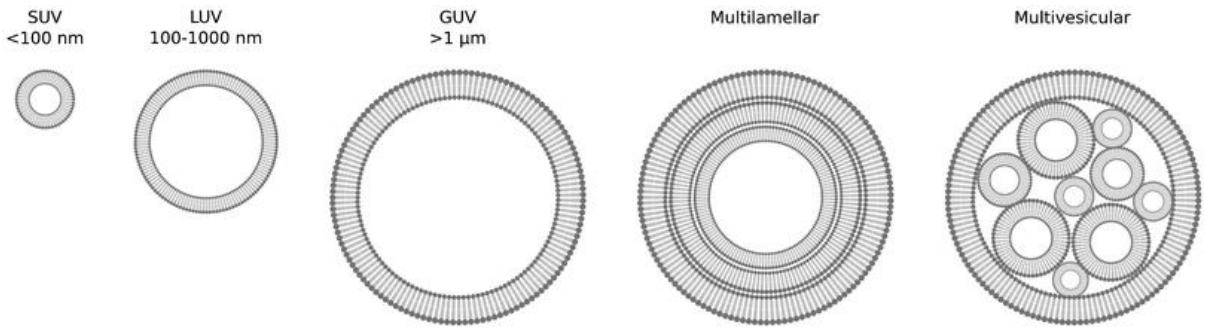

Figure 3-6 The typical vesicle structures. SUV, small unilamellar vesicle; LUV, large unilamelar vesicle; GUV, giant unilamelar vesicle.[70]

3.2.2.3 Liquid crystal

The liquid crystals formed by surfactants are also known as lyotropic liquid crystals (LLC). The liquid crystals of surfactants can be classified as cubic, hexagonal and lamellar as shown in figure 3-7[90]. And the cubic liquid crystals can be further classified as discontinuous and bicontinuous. With the increase of the concentration of the surfactants, the concentration of micelles (number of micelles) in solution increases. Once the concentration of micelles reached a critical point, the interactions between micelles embed the micelles in the cubic arrangement and form cubic liquid crystals. If the micelles are spherical or short rod-like micelles, the cubic liquid crystals would be discontinuous. Otherwise, the bicontinuous cubic liquid crystals would be formed in the solution.[91] The bicontinuous cubic liquid crystals are porous structure with water-filled channel.[92] Similar with the vesicle structures, the bicontinuous cubic phase also

has membrane structure. This structure provides the bicontinuous cubic phase abilities to encapsulate active compounds like pharmaceuticals and cosmetics in the channel and control the release rate.[90] A special cubic phase is called the sponge phase, which is formed by disk-like micelles. The structure of the sponge phase in similar with bicontinuous cubic phase but more highly disordered.[93, 94]

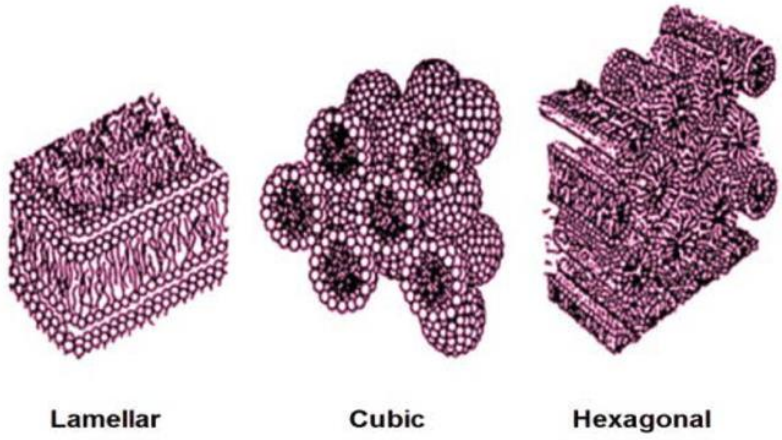

Figure 3-7 The three main types of lyotropic liquid crystals.[87]

The lamellar structure is bilayers of surfactant molecules separated by water layers. It can be classified as lamellar liquid crystals (L_α), lamellar gel networks and lamellar crystals depending on the concentration of surfactants. The water content in lamellar liquid crystals is the highest in these three phases. The interlayers spacing is depending on the water content in the system, the thickness of the water layer can range from 10Å to over 100Å.[95] Comparing with other two phases, the hydrophobic chains in lamellar liquid crystals are relatively disordered and the bilayers are flexible, and the layers could slide over each if external forces such as shear applied to the liquid crystals. The lamellar gel network is the middle phase of lamellar crystals and lamellar liquid crystals. The bilayers can rotate on the axis direction and the corkscrew-like structure can be observed as shown in figure 3-8[96, 97]. The molecules in lamellar crystals are not mobile.

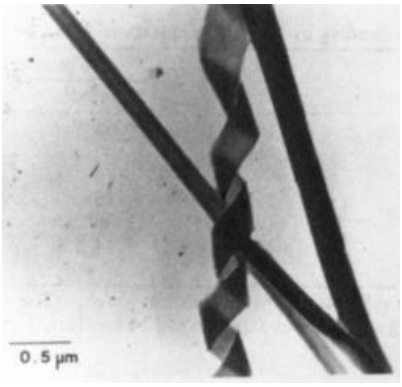

Figure 3-8 The TEM images of unstained hydrated N-dodeca-5,7-diyne galactonamide with corkscrew structure.[94]

Hexagonal liquid crystals are hexagonally packed rod-like micelles surrounded by water layers. The birefringence textures can be observed by polarised microscopy as the 2D arrangement on long-range order.[98] There are two well-established phases of hexagonal liquid crystal, the hexagonal phase (H_1) and the inversed hexagonal phase (H_2). The hexagonal phase (H_1) are rod-like micelles with hydrophilic group outward packed a hexagonal array. The continuous phase such as water or other solvent surrounding the rod-like micelles. The spacing between the rod-like micelles depending on the environment such as concentration and temperature. Although the water content of hexagonal liquid crystal is high, the viscosity is high because only one dimension is disordered, and the other two dimensions are aligned in a hexagonal array. The inverted hexagonal phases form in the solutions with low water content or oily solvent.[97] The water is trapped within the rod-like micelles. The hydrophobic tails face outward and these tails overlapped with each other, which lead the inter-micelle spacing is smaller than the hexagonal liquid crystal (H_1).

The structure of the cubic liquid crystal is not as well established as lamellar liquid crystal or hexagonal liquid crystal. The widely accepted postulation is that the cubic liquid crystal is the micelles or inversed micelles arranged in a cubic array.[95] As the movement of the micelles is restricted in 3 dimensions, the viscosity of cubic liquid crystal is higher than hexagonal liquid crystals.

3.2.3 D-spacing of liquid crystals characterised by SAXS

As discussed in chapter 2.8, small angle X-ray scattering is a powerful method for characterising the size, shape and surface of particles in solution by analysing their

interaction with X-rays. And the SAXS is also quite useful in characterising the structure of liquid crystals. The typical 2-D SAXS pattern of the liquid crystal is shown in figure 3-9 a, several sharp rings can be found in the pattern, which is similar to most powder samples. However, the orientation of the liquid crystal can be changed if applying a force on it. A series of spots in a line can be found in 2-D SAXS pattern as shown in figure 3-9 b.[99] For example, the liquid crystal is injected into a small diameter glass capillary, and the lamellae are preferentially oriented parallel to the surface of the capillary.

a b

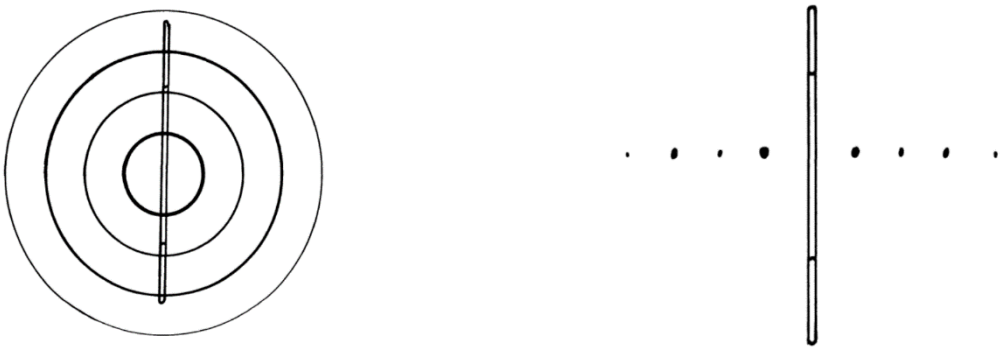

Figure 3-9 2-D SAXS patterns of non-oriented liquid crystals (a) and oriented liquid crystals (b)[99].

As the X-ray scattering following the Bragg's Law, the calculations indicated that there are several orders corresponding with a single repeating d-spacing. As shown in figure 3-10 a, the d100 is the d-spacing of the lamellar liquid crystal:

$$d_{n00} = \frac{n\lambda}{2\sin\ \theta}$$

By combining with the relationship between q and d-spacing calculated in chapter 2.8.1:

$$q_{n00} = \frac{2\pi}{d_{n00}} = \frac{2\pi n}{d_{100}}$$

Hence, the Bragg's repeating ratio of lamellar liquid crystal is $q_{100}: q_{200}: q_{300}: \ldots = 1: 2: 3: \ldots$ The reason of this repeating ratio is because that the lamellar liquid crystals are 1 dimensional regularised and disordered in the other two dimensions.

a b

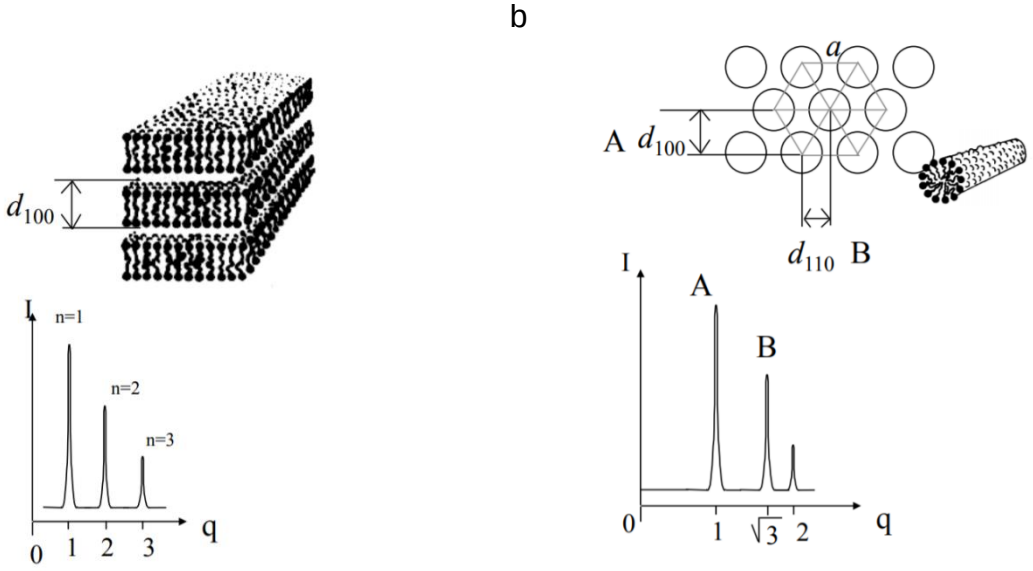

Figure 3-10 Lamellar and hexagonal liquid crystals X-ray patterns[100].

As for the hexagonal liquid crystal shown in figure 3-10 b, there are two d-spacings: d_{100} and d_{110}. Assuming the interparticle spacing is a, the d_{100} and d_{110} can be calculated:

$$d_{100} = \frac{\sqrt{3}}{2}a$$

$$d_{110} = \frac{1}{2}a$$

Hence, the Bragg's repeating ratio of hexagonal liquid crystals is $q_{110}:q_{100}:2q_{110}:\ldots = 1:\sqrt{3}:2:\ldots$ The reason of this phenomenon is because that the hexagonal liquid crystals are two dimensional regularised and disordered in the third dimension.

3.3 Acid-soaps

Soaps are the ionised long chain fatty acids, typically sodium or potassium. It was reported that the physical properties of fatty acids in water are influenced by the neutralisation ratio.[12] The intermediate phase between fully neutralised fatty acids and un-neutralised fatty acids is called acid-soaps.[13] This phenomenon was first reported by Chevreul in 1823[14] and the first systematic research was carried by Ekwall and McBain around 1930s[15-17, 101-103]. The acid-soaps is the stoichiometric crystals of the fatty acid and soap. The wildly accepted postulation is the interaction between fatty acids and soaps is strong hydrogen bonding.[22] . By observing the 1:1 acid-soap in FT-

IR, the acid-soap has both characteristic band (C=O stretching vibration) of fatty acid and soap. The characteristic bands were broadened and some small peaks were observed, which indicated that the fatty acid and soap were affected by hydrogen bonds.[104, 105] However, the mechanism of the interaction between fatty acids and soaps are still elusive as there is no long alkyl chain fatty acid-soaps crystals observed.[24]

Acid-soaps formed by fatty acids and soaps stoichiometrically and typically described as $M_xH_yA_{x+y}$[22]:

$$M_xA_x + H_yA_y = M_xH_yA_{x+y}$$

where M is metal ion, H is hydrogen, A is fatty acids. Although the existence of acid-soaps was confirmed, the ratio of fatty acid and soaps was unclear, and the publications are contradictory. Ekwall[15, 102] reported that the existence of NaH_2P_3, $NaHP_2$ and Na_2HP_3, whereas McBain[16] only reported $NaHP_2$ and Na_2HP_3. Buerger[106] and Lynch[107] suggested that the $NaHP_2$ has two polymorphs, α and β form. The fatty acid used in this project is stearic acid and it has more complex acid-soap forms than palmitic acid. Brouwer[23] reported that the stearic acid system has five forms and x:y ratios are 5:1, 5:2, 3:2, 1:1 and 2:3, whereas Ryer[20] suggested only three forms: 1:1, 2:3 and 1:2. The phase diagram of stearic acid/sodium stearate reported by Brouwer[23] is shown in figure 3-9 and the phase diagram of palmitic acid/sodium palmitate reported by McBain and revised by Lynch is shown in figure 3-10[107]. The melting process of these two systems are quite complex and a series of polymorph were observed. However, the stoichiometric ratios of acid/soap were different. Amazingly, the chemical structures of these two materials are quite similar, whereas the stoichiometric ratios are different.

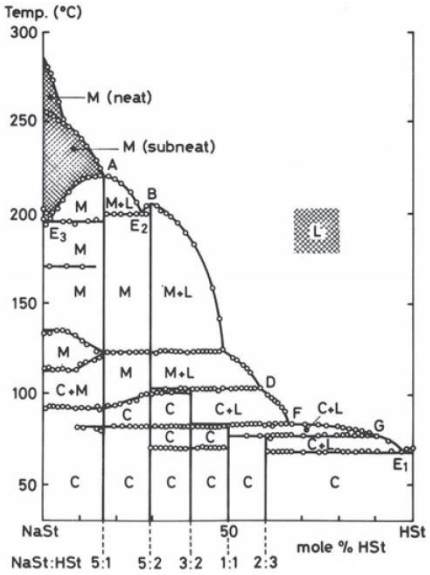

Figure 3-11 Binary phase diagram of sodium stearate and stearic acid. 3:2, 1:1, 2:3, 2:5 and 1:5 are the stoichiometric ratios of acid:soap.[19]

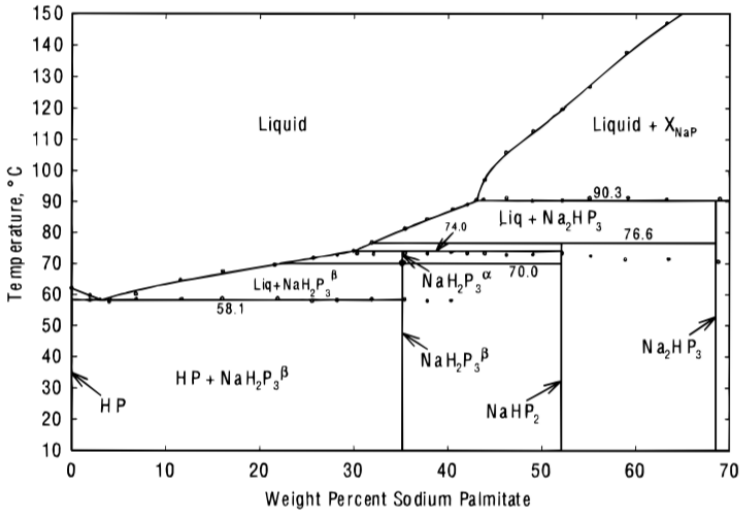

Figure 3-12 Binary phase diagram of sodium palmitate and palmitic acid. The stoichiometric ratios (acid: soap) of acid-soaps are 2:1, 1:1 and 1:2.

The interactions between fatty acids and sodium soaps were characterised by FTIR as the IR is sensitive to the function groups, COO- and COOH. The FTIR spectrum of Na_2HP_3 is shown in figure 3-11[22]. The IR band of the C=O stretch in palmitic acid is at 1694cm^{-1}, and the COO- stretch for NaP is at 1557.1cm^{-1}. The C=O stretch found in Na_2HP_3 is higher than in HP, whereas the COO- stretch is lower than in NaP. The appearance of these two stretch band indicated that the acid-soap has characteristics of fatty acid and soap. And the band shifting was suggested to be the influence of hydrogen bonds.[22, 108]

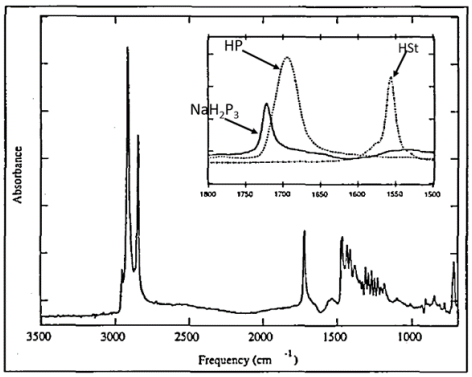

Figure 3-13 FTIR spectra of NaH_2P_3. Inset figure is the comparison of FTIR spectra of HP, NaP and NaH_2P_3[18]

The FTIR spectra were also quantitively analysed by Mantsch and Bian. Although the band positions are similar, the absorptance intensities ratios are different.[109, 110] This phenomenon may because that the acid-soaps formation process is easily affected by the preparation process because of the low solubilities of fatty acids or soaps in the solvent.

Little crystal structure information was published because of the complex phase behaviour of acid-soaps and it is difficult to prepare single crystals.[111] Lynch et al. prepared acid-soap standards by dissolving palmitic acid and sodium palmitate in water with defined ratios. The XRD results indicated that the acid-soaps are bilayer structured. Lynch suggested that there are three kinds of sodium fatty acid-soaps: $NaHP_2$, NaH_2P_3 and $Na_2H_3P_5$. The computational simulation reported by Lynch provided a model of 1:1 palmitate acid-soap as shown in figure 3-12.[24] However, Mary Heppenstall-Butler reported that there are only two kinds of acid-soaps, which is named as asA (acid-soap A) and asB (acid-soap B).[112] The SAXS and WAXS patterns

of stearic acid and the partially neutralised stearic acid in de-ionised water are shown in figure 3-15. It is clear that the peak corresponding with soap appeared in the 0.6 neutralised samples. Although Mary Heppenstall-Butler indicated that there are two kinds of sodium fatty acid-soaps, the stoichiometric ratios of the acid-soaps are still unclear. Similar to the sodium soaps, the amine soaps can also form acid-soaps with fatty acids.[108, 113, 114] S. Zhu indicated that there is only 1:1 acid-soap formed in triethanolamine (TEA) stearic acid-soap system as shown in figure 3-16. And the 1:1 acid-soap crystal is lamellar structured.

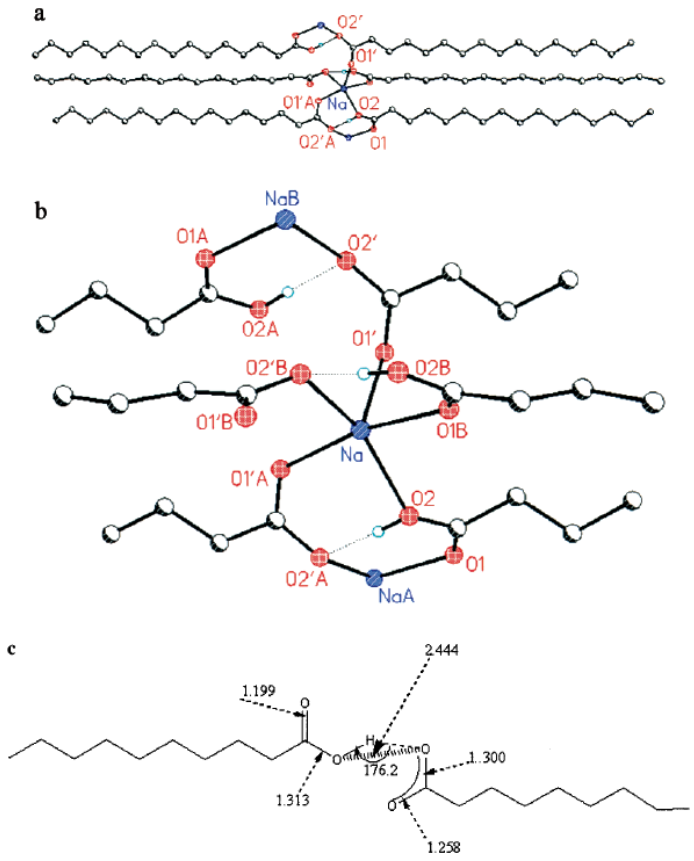

Figure 3-14 Simulated 1:1 palmitate acid-soap crystal structure[24]

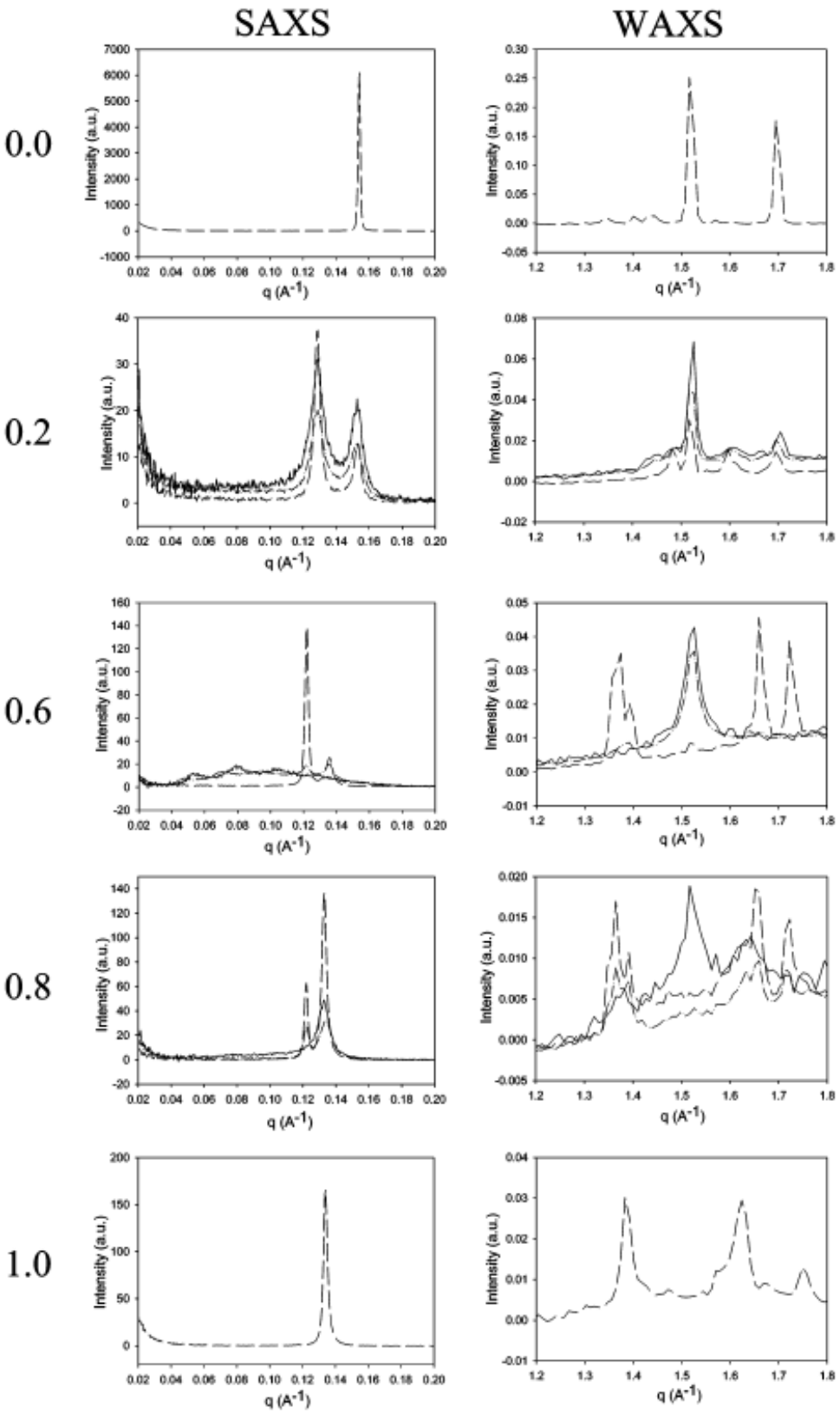

Figure 3-15 SAXS and WAXS patterns taken at 25°C of stearic acid powder (0.0) and the creams of neutralisation 0.2, 0.6, 0.8, and 1.0[112]

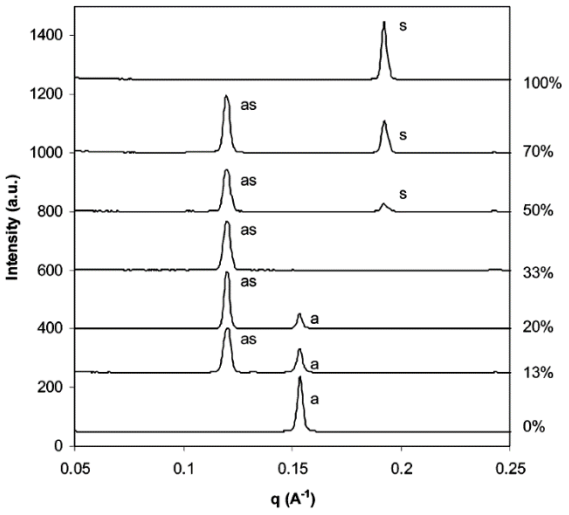

Figure 3-16 SAXS patterns of stearic acid at different neutralisation ratio at room temperature. a: acid; as: acid soap; and s: soap.[108]

3.4 Summary

This chapter has introduced the fundamental knowledge of surfactants structure and the phase behaviours, which is the base knowledge of this project. The literature covering the acid-soap structures and phase behaviour has reviewed, which is the base knowledge of chapter 5. The metallic acid-soaps received lots attention for decades, however, there's still some problems unclear, such as the accurate stoichiometric ratios of stearate system, the influence of chain length, saturation ratio and ionic strength on the stoichiometric ratios, the influence of environmental factors on the stoichiometric ratios. The aim of this project is characterising the crystal structure of stearate acid-soaps and observing the crystallisation process of acid-soaps in environmental of surfactants. And this chapter provided the platform to achieve this.

Chapter 4 Materials and methods

Materials used in this project and the description of instruments and methodologies.

4.1 Introduction

This chapter describes the materials used in this study and the experimental methodologies and techniques used to collect the data in order to meet the objectives of this study. This chapter starts with an overview of the chemicals used in this project, followed by the description of sample preparation and characteristic techniques. These include structural instruments like small angle X-ray scattering, wide angle X-ray scattering and powder-X-ray diffraction and morphology instruments such as polarized light microscopy and scanning electron microscopy.

4.2 Materials

The main chemicals used in this project are fatty acids and two classes of surfactant: non-ionic surfactant - alcohol ethoxylates (AE/AEO) and anionic surfactant - alcohol ethoxy sulphate (AES). Stearic acid (>=95%) was purchased from Sigma-Aldrich. Sodium hydroxide (98%) was purchased from fisher scientific. The non-ionic surfactant is Neodol 45-7, Shell Chemicals. The Neodol 45-7 is mixtures of alcohol ethoxylates with different alkyl chain lengths and ethoxylated degrees. The carbon atoms numbers of alkyl chain are C14 and C15, and the average degree of ethoxylation is 7. The alcohol ethoxy sulphate (AES) used in this project was Tensagex E0370A, KLK Tensachem. This sample contains 70% AES and 30% water. Similar to non-ionic surfactant, the AES is mixture of alcohol ethoxy sulphate with different alkyl chain lengths and ethoxylate degrees. The carbon atoms numbers of alkyl chain are C12 and C14, and the average degree of ethoxylation is 1. All the chemicals were used as received.

4.3 Methods

4.3.1 Preparation of sodium stearate by neutralising stearic acid

The sodium stearate was prepared by neutralising stearic acid with sodium hydroxide solution. A small amount of stearic acid was weighted to a three-neck flask at room temperature. Then a specific amount of de-ionised water was added into the flask. Because of the low solubility of sodium stearate in water, the concentration of stearic acid was controlled at 2 wt%. Then the flask was heated to 80°C on a hot plate with magnetic stirrer, with stirring rate of 300rpm. The condenser was used to keep the

concentration in the flask constant. After the temperature reached 80°C, 15% molar excess NaOH solution was added to the flask slowly to ensure that all the stearic acid was neutralised by caustic and no free stearic acid left. As the solubility of sodium stearate is small in water at low temperature and the caustic is soluble in water, the sodium stearate was precipitated out at 0°C. The fully neutralised samples were washed with 0°C de-ionized water by Büchner flask. Then the sodium stearate precipitate was transferred to the oven and dried at 60°C until constant weight.

Figure 4-1 The instrument used for stearic acid neutralisation.

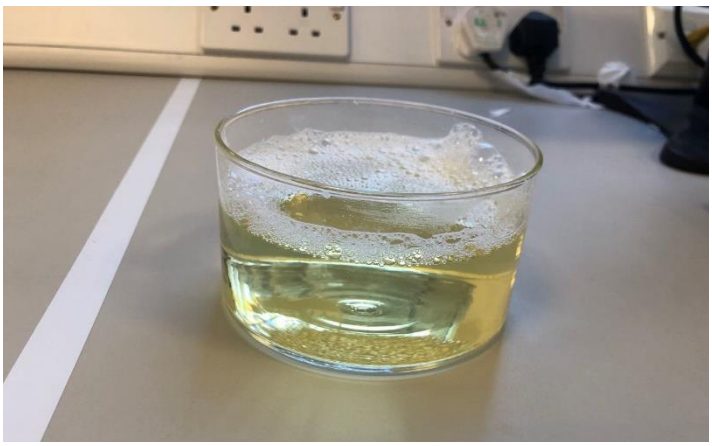

Figure 4-2 The solution obtained after the neutralisation. Clear solution was collected after the neutralisation and no oil layer was observed.

4.3.2 Preparation of stearate acid-soaps

In order to investigate the crystal structure and stoichiometric ratio of acid/soap, the stearate acid-soaps with soap ratio from 0% to 100% with 10% intervals by evaporative crystallisation. The stearic acid and pre-neutralised stearic acid (sodium stearate) were weighted out with molar ratios from 10% to 90%. And then these two materials were transferred to the three-neck flask shown in figure 4-1. The stearic acid and sodium stearate were dissolved in de-ionised water and the concentration was controlled around 2 wt%. The reactor was heated to 80°C and kept for 2 hours to give sufficient time to form acid-soaps. The solutions were transferred to a beaker and placed in an oven at 60°C to evaporate the water until constant weight. The solid acid-soaps were collected from the beaker and ground to powder with ceramic Mortar and pestle.

4.3.3 Preparation of mixtures of non-ionic surfactant and partially neutralised stearic acid

The samples with 90% non-ionic surfactant and 10% partially neutralised stearic acid were prepared to investigate the crystallisation of acid-soaps in the environment of the non-ionic surfactant. The specific amounts of non-ionic surfactant and stearic acid melt were mixed by spatula. As the melting point of stearic acid is 67°C, the mixtures were transferred to the oven at 70°C to keep the samples melt. The mixtures of stearic acid and non-ionic surfactant were mixed with 50 wt% sodium hydroxide solution **in** the IKA magic lab with three-stage disperser. The neutralisation ratio of stearic acid was controlled at 50% by controlling the injecting rates of the mixtures and the NaOH solution. The IKA magic lab was pre-heated to 80°C to avoid the solidification of stearic acid during mixing. The shear rate of IKA magic lab was 8000rpm. The mixtures of non-ionic surfactant and partially neutralised stearic acid (acid-soaps) were kept in the oven at 50°C.

4.3.4 Preparation of mixtures of AES, stearic acid and perfume

A series of samples of AES/stearic acid mixtures were prepared and the AES ratios ranged from 0 wt% to 100 wt% with 10 wt% intervals. At least 3 samples were prepared with same AES ratio to minimal the errors in the measurement. The samples were mixed by overhead mixer. In order to ensure the samples were mixed properly,

samples were collected every 2 minutes from 2 to 16 minutes. The samples were measured by SAXS and the results indicated that there's no difference after 4 minutes mixing. Hence, the mixing time were set to 4 minutes. The AES and stearic acid were weighted to a plastic bottle and melted in the oven at 70°C. And then the samples were mixed by overhead mixer. The temperature was controlled at 70°C by water jacket.

The mixtures of AES/HSt/perfume were prepared with same method with AES/HSt mixtures, whilst the perfume was added to the AES/HSt mixtures during mixing. The mixtures of AES/perfume were prepared with same method with AES/HSt/perfume, whereas the temperature was reduced to 50°C.

The mixtures of stearic acid and perfume were weighted to a 10ml glass vial at room temperature and melted by hot-stage magnetic stirrer with water jacket. The temperature was set to 70°C. All these samples were kept at room temperature.

4.3.5 Powder X-ray diffraction

Powder X-ray diffraction was used to determine the crystal structures of acid-soaps, especially in longer spacing. P-XRD was carried out using a Bruker D8 Eco (figure 4-3a) with Cu Kα radiation in Bragg-Brentano reflection geometry. The radiator was operated at 40kV and 25mA (figure 4-3b). The detector used was Lynxeye XE-T. The samples were measured from 1° to 40° 2θ with 0.005° increment, the exposure time was 1s/step.

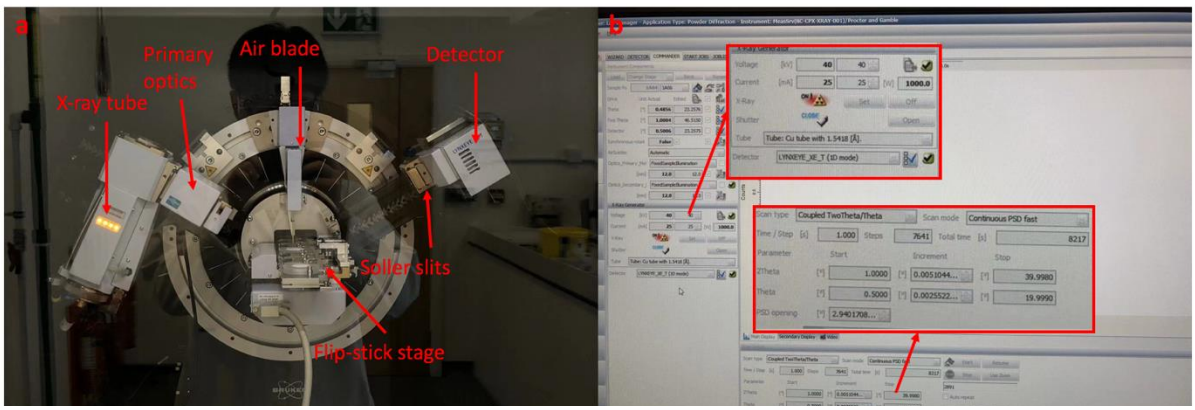

Figure 4-3 a, the Bruker D8 Eco; b, the experimental set ups.

4.3.6 Differential scanning calorimetry

In order to address the thermal transition temperatures of the samples, DSC measurements were carried out on stearate acid-soaps, NI/HSt mixtures and HSt/perfume mixtures using DSC Q2000, TA instruments. 5mg to 10mg samples were weighted and sealed in 40µl aluminum pans. The acid-soaps were equilibrated at 20°C for 5mins before heat to 150°C with heating rate of 1°C/min. The heating ramps were carried out to determine the melting points of the compounds in the mixtures, which could be acid-soaps with different soap ratios, stearic acid and sodium stearate. The samples were also measured with heating rate of 10°C/min, but the endothermal peaks in the samples with low soap ratios overlapped. The cooling ramps were also carried out, but the second heating ramp indicated that an endothermal peak associate with the stearic acid appeared. This phenomenon is because of the stearic acid melted out from the acid-soaps and the acid-soap with low soap ratios transferred to the forms with higher soap ratio. Hence, only the first heating ramps were analysed to characterize the thermal transitions of acid-soaps.

The mixtures of non-ionic surfactants and partially neutralised stearic acid were also measured by DSC. The samples were equilibrized at 20°C for 5mins and then heated to 150°C with heating rate of 10°C/min. After 5min equilibration, the samples were cooled to 20°C with cooling rate of 10°C/min. The reason of choosing 10°C/min is that the ratio of stearic acid in the mixtures are 10% and the endo-thermal/exo-thermal peaks are relatively weak, faster heating/cooling rate can narrow the peaks, which makes the peak more obvious.

4.3.7 Scanning electron microscopy (SEM) and cryo-scanning electron microscopy (cryo-SEM)

The Hitachi SU8230 SEM was used to observe the morphologies of the crystals in the acid-soaps and the mixtures of non-ionic surfactant and stearic acid. The acid-soaps were dissolved in de-ionised water at 80°C. Add several drops of the solutions on the aluminum stub and evaporate the water in oven at 60°C, which is the same conditions with the preparation of acid-soaps. The samples were coated with carbon before insert into SEM because of the weak conductivity of organic materials. The accelerating voltage of the SEM was set to 2kV to 5kV depending on the samples.

The cryo-SEM was used to observe the mixtures of AES/HSt, AES/perfume, HSt/perfume and AES/HSt/perfume because of the existence of volatile compounds such as water and perfume. The samples were crash cooled to -196°C in liquid nitrogen, and then the samples were transferred to the pre-cooled chamber immediately. The surfaces of the samples were cut off as water in air may deposed on it. The samples were coated with platinum to improve the conductivity. The crystal structures on the fractured surface were observed. The accelerating voltage of the electrons were 1kV and 2kV depend on the samples.

4.3.8 Optical microscopy

The polarized optical microscopy was used for observing the crystallisation process of the mixtures of NI/HSt, AES/HSt, AES/perfume, HSt/perfume and AES/HSt/perfume. The temperature was controlled by Linkam LTS120 temperature stage. The samples were transferred to a glass slide by spatula and covered with cover slide as shown in figure 4-4. Some air bubbles were observed in the samples and this is because of the samples were prepared by high shear mixer. The temperature ranges were different between different groups and the temperature ranges are listed in table 4-1. For NI/HSt mixtures, the samples were heated to 120°C and equilibrized for 2 mins, and then the samples were cooled to 20°C with cooling rate of 30°C/min and 10°C intervals, the samples were equilibrized at each temperature for 2 min before shooting. Other samples were measured in similar manner with different temperature ranges.

Figure 4-4 The sample for hot-stage microscopy. Air bubbles were appeared in the sample.

Table 4-1 The temperature ranges of different samples.

Sample	Temperature range (10°C intervals)
NI/HSt	20°C to 120°C
AES/HSt	20°C to 100°C
AES/perfume	20°C to 70°C
HSt/perfume	20°C to 70°C
AES/HSt/perfume	20°C to 70°C

4.3.9 Small angle X-ray scattering (SAXS) and wide angle X-ray scattering (WAXS)

4.3.9.1 Instrumentation

The SAXS/WAXS measurements were carried out using Xeuss system from Xenocs France. The X-ray source was Genix 3Dx using Cu Kα radiation at 0.6mA and 50kV. Two slits were placed in the pencil tube (figure 4-5) to remove the background scattering. And the pencil tube was in vacuum to remove the unwanted air scattering.

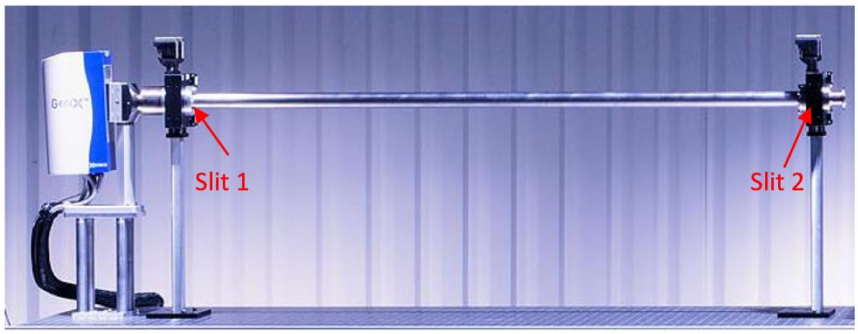

Figure 4-5 X-ray souce of Xeuss system and the two slits in the pencil tube.

The WAXS detector was Pilatus 100k (figure 4-6a) with pixel size of 172 × 172 μm and 487 ×195 pixels. The SAXS detector was Pilatus3 R 200K-A (figure 4-6b) with pixel size of 172 × 172 μm and 487 ×407 pixels. The distance of samples to SAXS detector 372mm. The tube between sample holder and SAXS detector was under vacuum to minimise the air scatter. The temperature was controlled by Forvis temperature stage, which is applied on the sample holder.

Figure 4-6 The detectors in Xeuss system.

4.3.9.2 Sample preparation

Two kind sample holders for solid samples and liquid samples were used in this project as shown in figure 4-7. The mixtures of non-ionic surfactants and partially neutralised stearic acid were melted in the oven at 50°C. And then the samples were injected to borosilicate glass capillary by syringe. The mixtures of AES and perfume are gel-like liquid at room temperature, so the samples were injected to capillary at room temperature. The flowability of the mixtures of AES and stearic acid was depend on the stearic acid ratio. For the samples with low stearic acid percentage, the samples were melted in the oven at 50°C and then injected to the capillary. For the samples with high stearic acid percentage, the solidification process was fast and it is not possible to inject into the capillary. Hence, the solid-like samples were sealed in the sample holder for solid samples (figure 5-5b) by Kapton tape. The acid-soaps were sealed in the solid sample holder at room temperature. As the samples with low soap ratios were melted at high temperature, and the sample holder were placed vertically, the melted samples flowed downside and sometimes no signal can be detected. Also, the stearic acid melted out from the sample during heating process, the stearic acid melts flow downside and the crystallisation process are meaningless. Hence, the SAXS with temperature stage were measured the melting process only for acid-soaps.

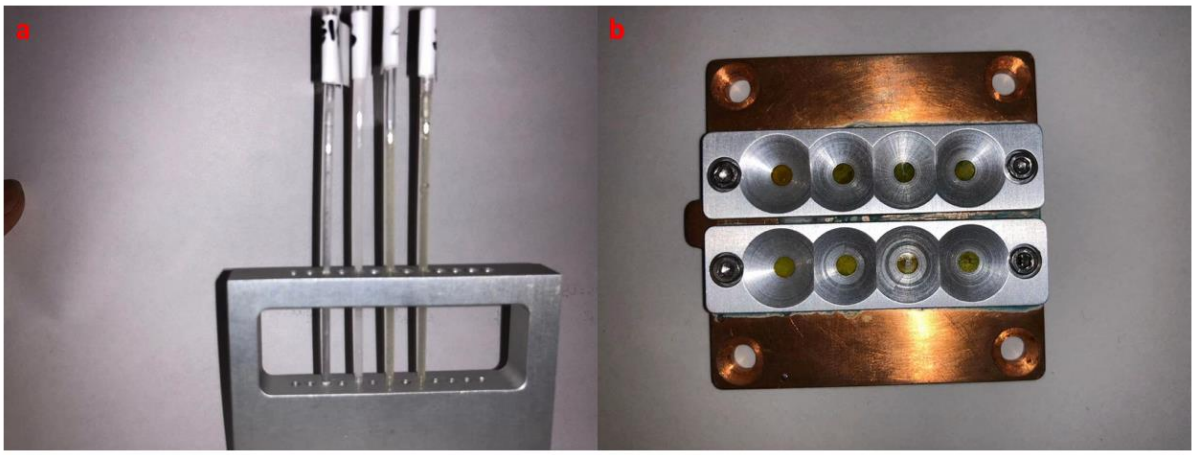

Figure 4-7 Sample holders used in SAXS/WAXS. a, liquid samples were injected into the capillaries. b, the solid samples were sealed in the sample holder by Kapton tape

4.3.9.3 Experimental method

Acid-soaps: The samples were heated from 20°C to 107°C, with 10°C intervals and the heating rate was 30°C/min. The samples were equilibrized at each temperature for 5mins. The exposure time was 300s.

NI/HSt mixtures: The experimental method was similar with acid-soaps and the data was collected at 11°C, 20°C, 29°C, 38°C, 47°C, 56°C, 65°C, and 111°C.

NI/PSFA mixtures: The aim of measuring the NI/PSFA is observing the crystallisation process and comparing with the NI/HSt mixtures. The DSC results indicated that the crystallisation occurred around 30°C. The samples were stored in the oven at 50°C before experiments. The samples were cooled to 35°C and the data was collected after 1min, 5min, 10min, 20min and 30min. And then the samples were cooled to 20°C, the data was also collected after 1min, 5min, 10min, 20min and 30min. The exposure time was 50s.

AES/HSt: The experimental method was similar with acid-soaps, whereas the samples were cooled down from 100°C to 20°C with 10°C intervals.

AES/perfume and HSt/perfume: The experimental method was similar with acid-soaps and the temperature range was 20°C to 70°C.

AES/HSt/perfume: By comparing the SAXS patterns of the samples before and after heating, the peak positions didn't change, whereas the peak intensity increased significantly after heating. Hence, the samples were cooled down from 70°C to 20°C with 10°C intervals. The exposure time was 300s.

The scattering patterns were integrated and transformed from 2D to 1D by Foxtrot software provided by Xenoxs.

Chapter 5 Characterization of the stearic acid/sodium stearate acid-soaps

Stoichiometry ratios determination of stearate acid-soaps, followed by the characterisation of thermodynamic properties.

5.1 Introduction

Soaps are the ionised long chain fatty acids, with typical cations such as sodium or potassium. It was reported that the structures and their physical properties of neutralised or partially neutralised fatty acids in water are influenced by the neutralisation ratio between the acids and neutralising reagent.[12] The intermediate phase between fully neutralised fatty acids and un-neutralised fatty acids is called acid-soaps.[13] The acid-soaps attract attention from the industrial field, and these systems are wildly used in many consumer products like superfatted soap bars, facial cleaners and cosmetics.[18] The wildly accepted postulation is the interaction between fatty acids and soaps is hydrogen bonding. The X-ray diffraction data indicated that crystals formed in the acid-soap systems are lamellar structured and the repeating ratios follow 1:1/2:1/3. The interlayer distances of acid-soaps determined by P-XRD are different from parent materials. Although the existence of acid-soaps was confirmed, the ratio of fatty acid and soaps was unclear, and the publications are contradictory. Ekwall[15, 102] reported that the existence of NaH_2P_3, $NaHP_2$ and Na_2HP_3, whereas McBain[16] only reported $NaHP_2$ and Na_2HP_3. Buerger[106] and Lynch[107] suggested that the $NaHP_2$ has two polymorphs, α and β form. The fatty acid used in this project is stearic acid and it has more complex acid-soap forms than palmitic acid. Brouwer[23] reported that the stearic acid system has five forms and x:y ratios are 5:1, 5:2, 3:2, 1:1 and 2:3, whereas Ryer[20] suggested only three forms: 1:1, 2:3 and 1:2. Despite the interest in the stoichiometric ratio of acid-soaps, the phases and phase transformations of acid-soaps are still unclear.

In this chapter, the stoichiometric ratios of stearic acid-sodium stearate will be confirmed, and the phase transitions of acid-soaps will be studied. The first section is confirming the stoichiometric ratios of acid-soaps at room temperature by P-XRD. The acid-soaps phase transitions as function of temperature will be studied by DSC and SAXS/WAXS with temperature stage. The crystal structure transition around the transition temperature obtained in DSC can be observed by SAXS/WAXS. The phase diagram will be refined based on the information obtained from DSC and SAXS/WAXS.

5.1.1 Characterization of stearic acid/sodium stearate acid-soaps at room temperature

The Powder-XRD patterns of stearic acid – sodium stearate mixtures are shown in figure 5-1. The full P-XRD patterns are shown in figure 5-1 a. Although the short-range d-spacing of the crystals can provide information about the crystals, we are focusing on the long-range d-spacing, which is the interlayer spacing of the lamellar crystals. The d001, d002 and d003 are labelled in 5-1 a, and it is clear that the d003 is sharp and strong, whilst the d001 and d002 are broad and weak. As these three peaks correspond with same crystal structures, only d003 will be discussed in this section. The d-spacing of stearic acid (0% neutralisation sample) are 13.3Å and 19.9Å and these patterns conform with the crystal structure of C-form stearic acid. The C-form crystal is lamellar structure and follows the $d001:d002:d003 = 1:\frac{1}{2}:\frac{1}{3}$ repeating ratios. In this experiment, the strongest intensities are d003 (13.3Å for stearic acid). So the discussion will focus on d003 in this section. The appearance of the peak at 13.3Å in 10%, 20% and 30% (very weak) neutralised samples suggests these three samples contain stearic acid. The intensity of the peak at 13.3Å is weak and hard to be observed in 30% neutralised sample, and it is much easier to confirm the existence of the peak at 13.3Å in 30% neutralised sample by changing the y-scale to logarithmic as shown in figure 5-2. The weak intensity suggests that most of the stearic acid formed acid-soap. As the definition of acid-soap is the stoichiometric crystal of the fatty acid and soap, the acid-soap with lowest soap ratio is approximately 2:1 (NaH_2St_3). Comparing stearic acid and 30% neutralised sample, the new peak appeared at 15.77Å should be correspond with 2:1 acid-soap. The missing of the peak at 13.3Å in 40% neutralised sample also suggests that the soap ratio in the acid-soap is below 40% and close to 30%. Hence, the approximate structure is 2:1 (NaH_2St_3) acid-soap.

The crystal with d-spacing of 16.6Å was observed in 40% neutralised sample and this suggests that the formation of acid-soap with higher soap ratio. 2:1 acid-soap peak can be observed in 30% to 50% neutralised sample, and the intensity decreases with increasing of the neutralisation ratio. In 50% neutralised sample, several small peaks at 15.8Å, 14.9Å and 15.5Å were observed. The 14.9Å and 15.5Å are consistent with the beta and gamma form of sodium stearate[115]. The co-

existence of soap and 2:1 acid-soap is because of the insufficient mixing during preparation. When the neutralisation ratio increased to 60%, the d-spacing of 15.8Å corresponding with 2:1 acid-soap disappeared. This suggests that the new form of acid-soap is 1:1 ($NaHSt_2$) acid-soap and the characteristic peak is at 16.6Å.

From 50% to 100% neutralised samples, the two polymorphs of sodium stearate and 1:1 acid-soap were observed. The soap crystallisation was not well controlled, which leads the ratio of beta and gamma form sodium stearate was not stable. The appearance of the peak at 16.6Å in 100% neutralised sample is because of the 2.20% un-neutralised stearic acid.

The previous reports suggested that the stearic acid - sodium stearate has five forms acid-soaps: 5:1, 5:2, 3:2, 1:1 and 2:3.[20, 23] However, the P-XRD results indicated only 2:1 and 1:1 acid-soaps appeared in the stearic acid – sodium stearate system.

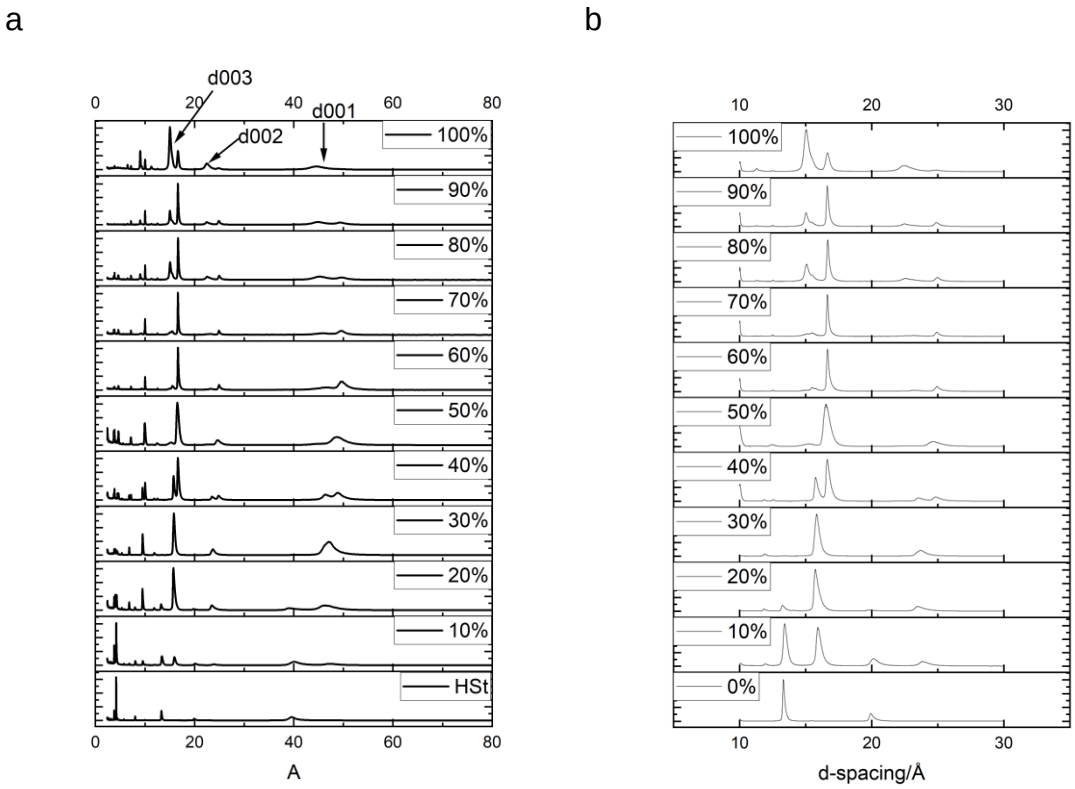

Figure 5-1 The P-XRD patterns of stearic acid-sodium stearate mixtures, a) is the full patterns of the mixtures and b) is the curves from 10Å to 30Å. The soap ratio labelled beside each curve. The peak at 13.3Å (stearic acid) can be observed in 0%, 10% and 20% neutralised samples. The peak at 15.77Å (2:1 acid-soap) appeared in 10% to 50% neutralised samples. The peak at 16.6Å (1:1 acid-soap) appeared in 40% to 100% neutralised samples. The broad peak around 15Å (sodium stearate β form and γ form) with shoulder appeared in 50% to 100% neutralised samples.

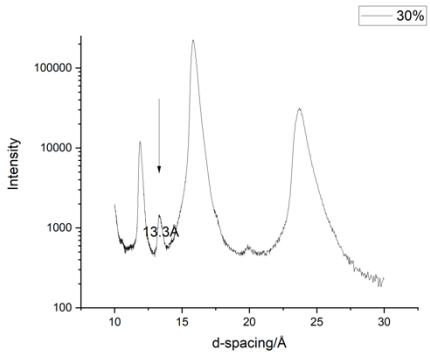

Figure 5-2 The P-XRD pattern of 30% neutralised sample at room temperature. The peak at 13.3Å can be observed with weak intensity.

Table 5-1 Summary of characteristic d-spacings in each sample.

Neutralisation ratio	Stearic acid/Å	1:1 (NaH_2St_3)/Å	2:1 ($NaHSt_2$)/Å	β-NaSt/Å	γ-NaSt/Å
0%	13.30				
10%	13.35	15.83			
20%	13.29	15.77			
30%	Too weak	15.81			
40%		15.78	16.65		
50%			16.64	14.97	15.48
60%			16.66	14.95	15.50
70%			16.64	14.96	15.49
80%			16.66	14.94	15.48
90%			16.65	14.96	15.47
100%			16.65	14.95	15.48

Assuming the carbon chain of stearic acid and sodium stearate are zig-zag configuration and the carboxylic group is not affected by the counter-ion, the fully extended chain length can be roughly calculated:

$$l_{max} = (1.5 + 1.265n_c + 4.2)\text{Å}.$$

Where, 1.5Å is the van de Waals radius of the CH_3, 4.2Å is the size of carboxylic group, 1.265Å is the carbon-carbon bond length on the chain direction, n_c is the number of CH_2.[116, 117]

Hence, the calculated chain length of stearic acid and sodium stearate is 25.94Å. As the crystal of stearic acid, sodium stearate and acid-soaps are double layer lamellar structure, the total chain length should be 51.88Å. The d-spacing obtained from P-XRD is smaller than calculated chain length, which indicates that the 2:1 and 1:1 acid-soaps tilted from the d-001 plane with tilt angle of 66° and 73.7° respectively. The tilt angle is calculated with following equation:

$$\theta = \sin^{-1}\frac{d}{2 \times l}$$

Where, θ is the tilt angle, d is the d-spacing and l is the extended chain length.

As the crystals of 2:1 and 1:1 acid-soaps are lamellar structured, the possible molecules arrangements are shown in figure 5-3.

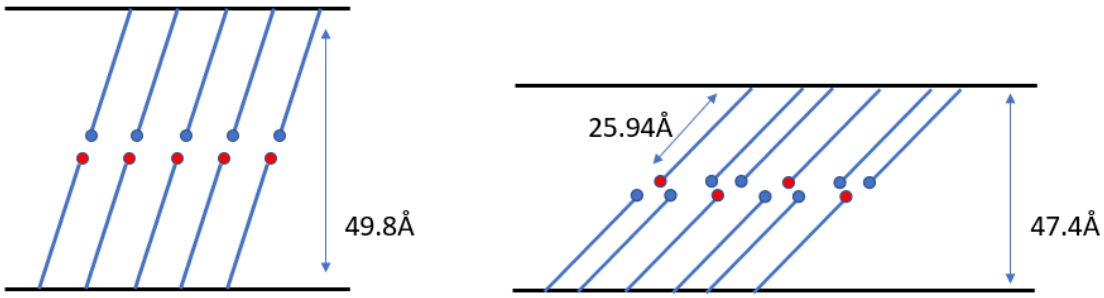

Figure 5-3 Possible molecules arrangement in acid-soaps. Left, 1:1 acid-soap, the tilt angle is around 73.7°; right, 2:1 acid-soap, the tilt angle is around 66°. Red, sodium stearate; blue, stearic acid.

5.2 The DSC results

The DSC traces of 0% to 100% neutralised samples are shown in figure 5.4 and the summary of peak temperature are listed in table 5-2. Only one endo-thermal peak at 69.74°C (peak temperature) can be observed in stearic acid, which is in agreement with previous publications[23, 118, 119]. The melting peak of stearic acid was observed in 10% to 30% neutralised samples and disappeared in 40% neutralised sample. This suggested that the existence of stearic acid in 10% to 30% neutralised samples. The endo-thermal peak corresponding with the melting of stearic acid was disappeared in 40% neutralised sample, which indicated that no stearic acid remains in this sample. This is also evidence of the formation of 2:1 acid-soap. A melting peak appeared at 76°C in 10% neutralised sample. This peak shifted to higher temperature in 20% and 30% neutralised sample and disappeared in 40% neutralised sample. As the 40% neutralised sample consist of 2:1 acid-soap and 1:1 acid-soap and this peak cannot be observed in stearic acid, this peak should be related to the interaction between stearic acid melt and 2:1 acid-soap. The transition peaks around 80°C in 20% and 30% neutralised samples are complex as shown in figure 5-5. Several transitions can be observed in 20% neutralised sample and the endo-thermal peaks are overlapped. The first peak around 77°C is same as the transition of 10% neutralised sample. The peak around 77°C in 30% neutralised sample is smaller than 20% neutralised sample, which also suggested that this peak is corresponding with the interaction between 2:1 acid-soap and stearic acid melt. The main peak around 80°C consists of two peaks and hard to split. The hypothesis is the 2:1 acid-soap transformed to 1:1 acid-soap, the 1:1 acid-soap has several polymorphs and the transitions induced the endo-thermal peaks. This can be verified by the SAXS with temperature stage. The transition around 80°C was also observed in the samples with neutralisation ratio above 50%. This suggested that the 1:1 acid-soap has phase transition in that temperature region. The endo-thermal peak above 80°C was observed in 20%, 30% and 40% neutralised samples. This may because of the phase transition of 1:1 acid-soap and will be verified by SAXS with temperature stage.

When the neutralisation ratio above 33.3%, 1:1 acid-soap formed in the samples and a new transition peak around 101°C was observed, which is the transition peak

corresponding with 1:1 acid- soap. An exo-thermal peak was observed following the endo-thermal peak, which indicated that the melting and reconstruction occurred at the same time. And the broad weak peak may because of the transition of the reconstructed 1:1 acid-soap. The 50% neutralised sample has a broad endo-thermal peak around 120°C. By comparing the 50%, 70% and 100% neutralised samples, the enthalpies of this peak increases as the increasing of soap ratio (figure 5-6). Hence, this peak is corresponding with the sodium stearate. The broad peak may consist of two peaks and this is because of the polymorphs of sodium stearate have different transition temperatures.[120] The DSC curves of 100% neutralised sample is complex, which is because of the heat history of the sample. These transition points are corresponding with the transition of sodium stearate from curd crystal to subwaxy state to waxy state.

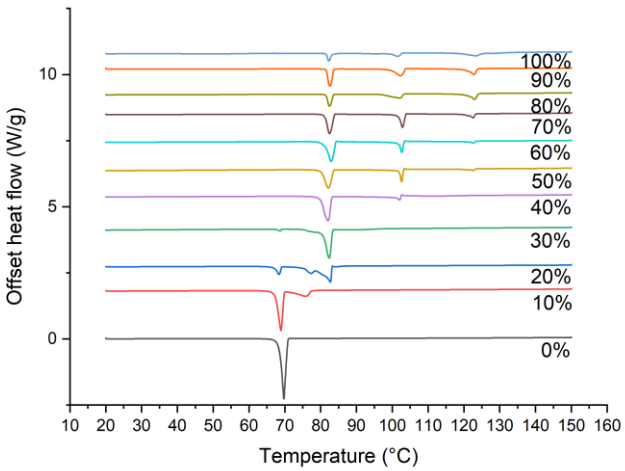

Figure 5-4 DSC heating curves of 0% to 100% neutralised stearic acid

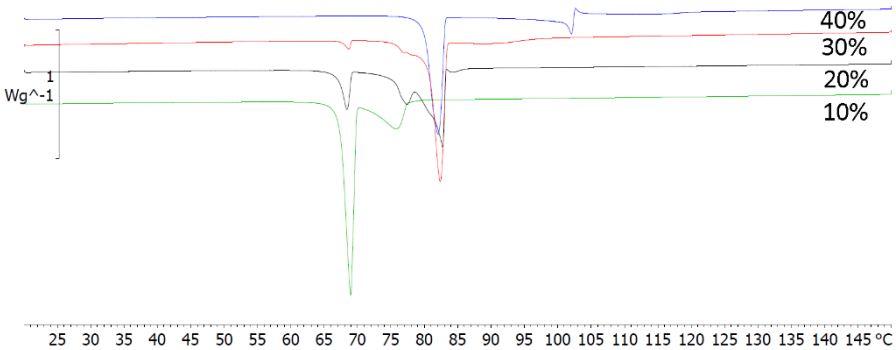

Figure 5-5 The DSC heating curves of 10% to 40% neutralised samples

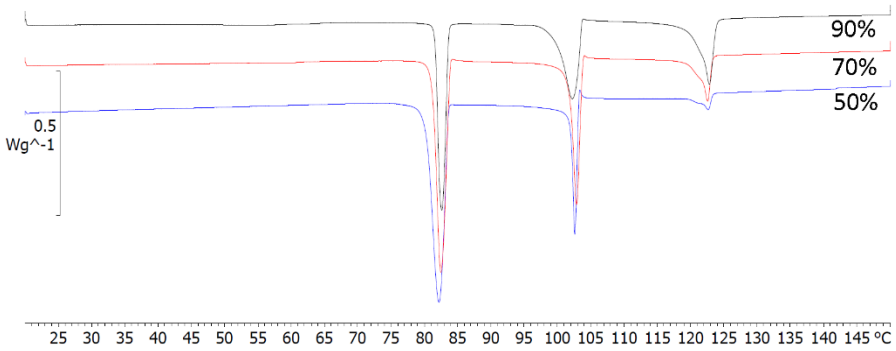

Figure 5-6 Comparing the DSC heating curves of 50% 70% and 90% neutralised samples.

Table 5-2 Summary of stearic acid/sodium stearate mixtures melting points

Samples	Melting points (on-set temperature) (°C)					
0%	68.16					
10%	67.37	70.94				
20%	67.18	75.05	80.25		82.88	
30%	67.56	75.06	80.57			
40%			79.84		100.91	
50%			80.21		101.84	121.35
60%			81.16		101.60	121.52
70%			81.07		101.78	121.36
80%			81.45		97.55	121.27
90%			81.59		98.68	121.16
100%			81.43	95	99.33	119.79

5.3 Characterising the phase transitions and refining the phase diagram

The SAXS patterns of stearic acid as function of temperature are shown in figure 5-7. The SAXS pattern of stearic acid at 50°C has three peaks at 39.8Å, 19.87Å and 13.25Å. These three peaks follow the $1:\frac{1}{2}:\frac{1}{3}$ repeating ratio, which indicates that the stearic acid crystal is lamellar structured. This result is in agreement with the P-XRD pattern. The peak at 39.8Å disappeared when the temperature rises above 70°C. This result conformed with the DSC trace of stearic acid shown in figure 5-4.

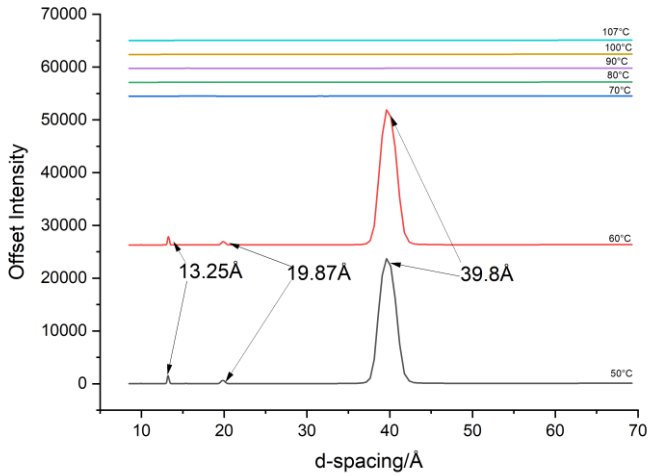

Figure 5-7 The SAXS pattern of Stearic acid as function of temperature.

The 10% neutralised sample has two peaks at 50°C, 39.8Å and 47.3Å (figure 5-8). The 39.8Å is the form C crystal of stearic acid and the 47.3Å is the crystal of 2:1 acid-soap. This result is consistent with the P-XRD result. When the temperature rises to 70°C, the peak associating with stearic acid disappeared. This transition is related with the first endo-thermal peak at 68.9°C in DSC trace. By comparing the SAXS patterns of 10% neutralised sample at 60°C and 70°C as shown in figure 5-9, the peak position didn't change, whilst the peak intensity dropped. As the SAXS patterns were collected from same sample at different temperatures, the intensity change is because of the change of the amount of certain crystal. Because the d-spacing observed at 60°C and 70°C are the same, the intensity change is because of 2:1 acid-soap was partially dissolved in stearic acid melt. The DSC trace of 10% neutralised sample showed

similar phenomenon, the signal following the first endo-thermal peak is away from the baseline, which indicated that there is an endo-thermal phase transition. When the temperature raised to 80°C, all the peaks disappeared in SAXS pattern. Hence, the second endo-thermal peak in DSC is the melting peak of 2:1 acid-soap.

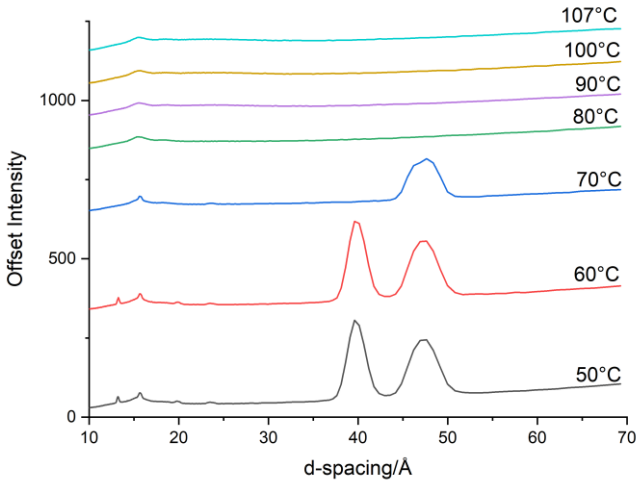

Figure 5-9 Comparing the SAXS pattern of 10% neutralised sample at 60°C and 70°C

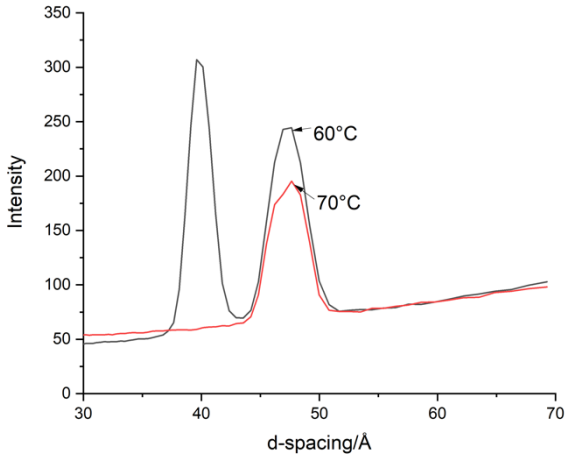

Figure 5-8 Comparing the SAXS pattern of 10% neutralised sample at 60°C and 70°C

The SAXS patterns of 20% neutralised sample as function of temperature is shown in figure 5-10. There are two peaks at 39.8Å and 47.3Å can be observed, which is the same with 10% neutralised sample. The peak associating with stearic acid disappeared at 70°C, which indicated that the endo-thermal peak at 69°C is the

melting peak of stearic acid. The comparison of peak positions and intensities of 20% neutralised sample at 60°C, 70°C, 80°C and 90°C is shown in figure 5-11a. Comparing with 60°C , the intensity of the peak at 47.3Å dropped at 70°C and the peak position didn't change, which is same with the 10% neutralised sample. When the temperature reached 80°C, the peak intensity dropped further and the d-spacing migrated to 47.2Å. Two endo-thermal peaks can be observed at 77°C and 80°C and these two transition peaks are overlapped with each other. The sample at 80°C is in metastable state. As shown in figure 5-11b, the peak migrated to 3.09Å and 3.11Å, which is the characteristic peak for 1:1 acid-soap. Hence, the 2:1 acid-soap transformed to 1:1 acid-soap, and the following transitions are corresponding with 1:1 acid-soap. The peak corresponding with 1:1 acid-soap disappeared at 90°C, which conformed with the DSC results.

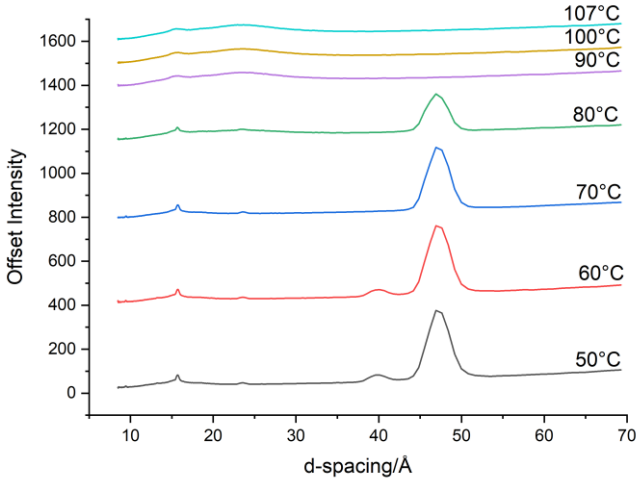

Figure 5-11 The SAXS patterns of 20% neutralised sample as function of temperature

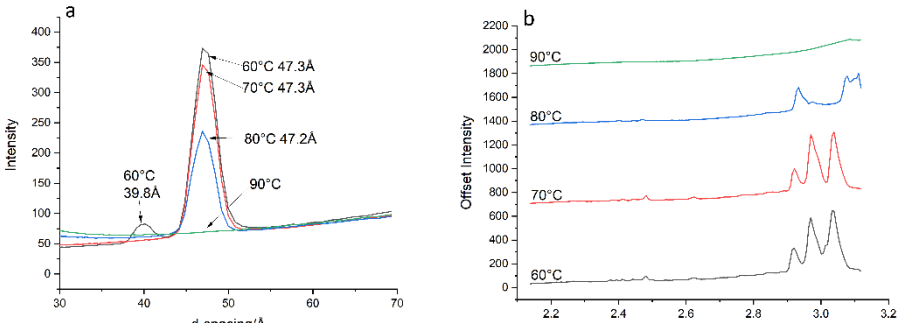

Figure 5-10 a. Comparing the peak positions and intensities of 20% neutralised sample at 60°C, 70°C, 80°C and 90°C. b. The WAXS patterns of 20% neutralised sample as function of temperature.

From the SAXS patterns of 30% neutralised sample shown in figure 5-12, only one peak at 47.3Å can be observed. This is because the intensity of the peak at 39.8Å is too weak to be observed. The P-XRD pattern and DSC trace of the 30% neutralised sample confirmed the existence of stearic acid. The 2:1 acid-soap in 30% neutralised sample is same with the 20%. The peak at 47.3Å migrated to smaller d-spacing, which is same with the 20% neutralised sample (figure 5-13). This confirmed that the transition at around 80°C is the transformation of 2:1 acid-soap to 1:1 acid-soap.

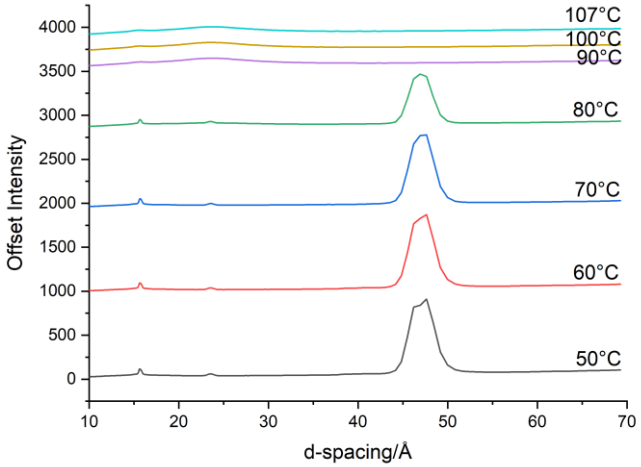

Figure 5-13 SAXS patterns of 30% neutralised sample as function of temperature

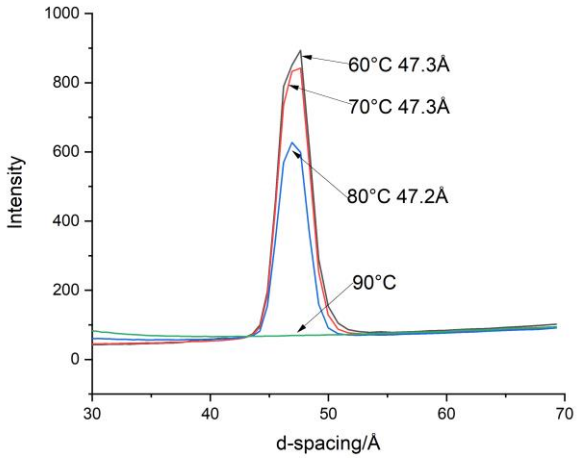

Figure 5-12 Comparing the peak positions and intensities of 30% neutralised sample at 60°C, 70°C, 80°C and 90°C

The 40% neutralised sample consists of 2:1 acid-soap and 1:1 acid-soap. As shown in figure 5-14, one broad peak was found from 45Å to 52Å. The d003 (highlighted) indicated that the broad peak appeared in d001 contains two peaks at 47.3Å and 49.8Å. There's no transition occurred between 60°C and 70°C, which is different with 10% to 30% neutralised sample. This confirmed that the intensity drop of in 10% to 30% neutralised samples is because of the dissolution of 2:1 acid-soap in stearic acid melt. As shown in figure 5-15b, the peak position of 2:1 acid-soap (15.7Å) didn't change from 70°C to 80°C. And the endo-thermal peak at 78°C cannot be observed in 40% neutralised sample. This suggests that the endo-thermal peak at 78°C in 20% and 30% neutralised samples is because of the interaction between stearic acid melt and 2:1 acid-soap. The peak at 49.8Å migreted to 48.8Å at 80°C, this confirmed that the endo-thermal peak around 80°C consists more than one transition. The peak at 48.6Å disappeared at 100°C. This suggests that the endo-thermal peak at 102°C is the melting peak of 1:1 acid-soap. A bump appeared at 40.7Å in the SAXS patterns at 100°C and 107°C. This may be the liquid crystals of 1:1 acid-soap. Hence, the 1:1 acid-soap has three polymorphs and the d-spacing for form I is 49.8Å, form II is 48.6Å and form III is at 40.7Å. The d-spacing at 80°C is 48.8Å, which is larger than form II of 1:1 acid-soap. The hypothsis is the sample at 80°C is at metastable state and this was confirmed by the WAXS results shown in figure 5-16. The characteristic peaks of the sample at 70°C and 90°C were observed in the WAXS pattern of the sample at 80°C, which indicated that the sample at 80°C consists 2:1 acid-soap, form I and form II of 1:1 acid-soap. This confirmed that the endo-thermal peak around 80°C contains two transitions: 2:1 acid-soap transform to 1:1 acid-soap form I, 1:1 acid-soap form I transform to 1:1 acid-soap form II. When the temperature rised to 90°C, a bump at 40.7Å appeared in SAXS pattern and all the peaks disappeared in WAXS. This suggested that the form III of 1:1 acid-soap is liquid crystal.

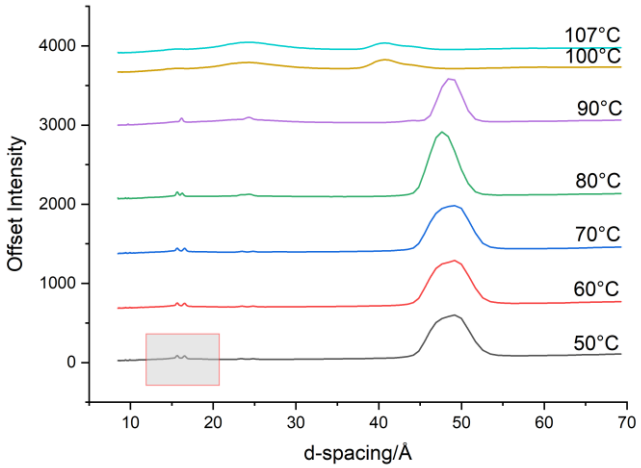

Figure 5-14 The SAXS patterns of 40% neutralised sample as function of temperature. The d003 is highlighted.

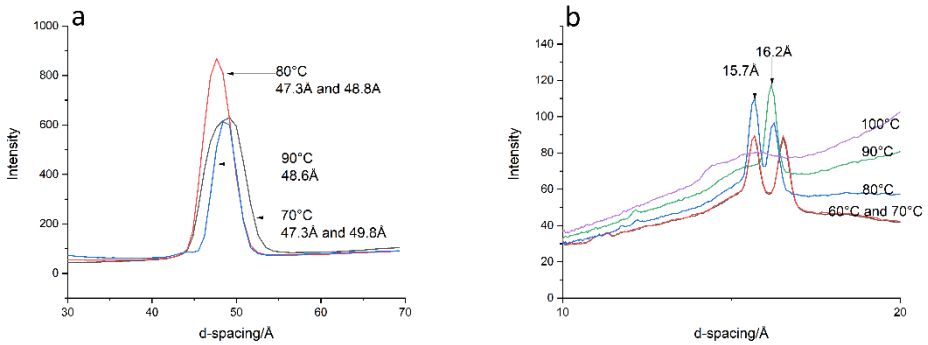

Figure 5-15 Comparing the peak positions of 40% neutralised sample at 60°C, 70°C, 80°C, 90°C and 100°C. a, d001; b, d003.

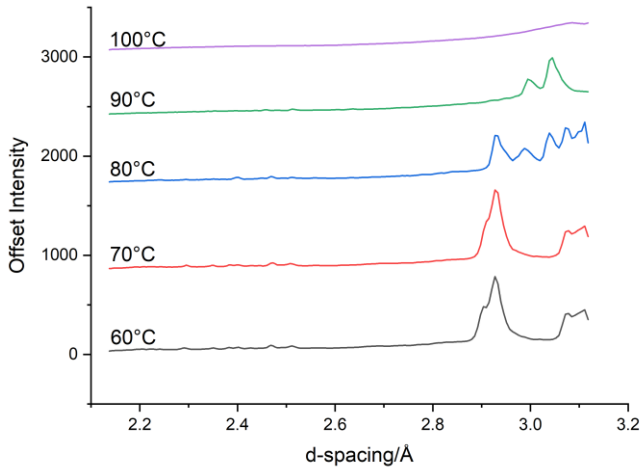

Figure 5-16 The WAXS patterns of 40% neutralised sample as function of temperature.

The DSC trace and P-XRD pattern indicated that the 50% neutralised sample contains some impurities. The shoulder highlighted in figure 5-17 and figure 5-18b also verified this. The phase transitions of 1:1 acid-soap in 50% neutralised sample is same with the 1:1 acid-soap in 40% neutralised sample, which verified the conclusion that the 1:1 acid-soap has three polymorphs.

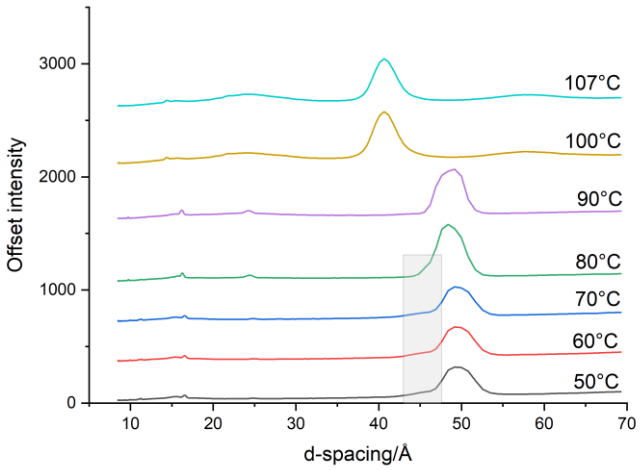

Figure 5-17 The SAXS patterns of 50% neutralised sample as function of temperature.

A new peak at 14.4Å appeared at 100°C as shown in figure 5-17b. And a bump around 57.7Å can be observed at 100°C in figure 5-18a. The SAXS pattern was plotted to log scale to find some very weak peaks to confirm the relationship between these two peaks. Eight peaks have pointed in figure 5-19: 57.7Å, 40.7Å, 28.8Å, 23.6Å, 21.8Å, 20.4Å, 15.4Å and 14.4Å. 57.7Å, 28.8Å and 14.4Å following the repeating ratio $d001:d002:d003:d004 = 1:\frac{1}{2}:\frac{1}{3}:\frac{1}{4}$, which indicated that the crystal with 57.7Å d-spacing is lamellar structure. 40.7Å, 23.6Å, 20.4Å and 15.4Å fowllowing the repeating ratio $d001:d002:d003:d004:d004:d005 = 1:\frac{1}{\sqrt{3}}:\frac{1}{2}:\frac{1}{\sqrt{7}}:\frac{1}{3}:\frac{1}{\sqrt{12}}$, which indicated that the crystal at 40.7Å is hexagonal structure. And the peak at 21.8Å cannot be fitted into these two systems. The hypothsis is these's a small peak around 43.5Å and this peak is overlapped with the peak at 40.7Å.

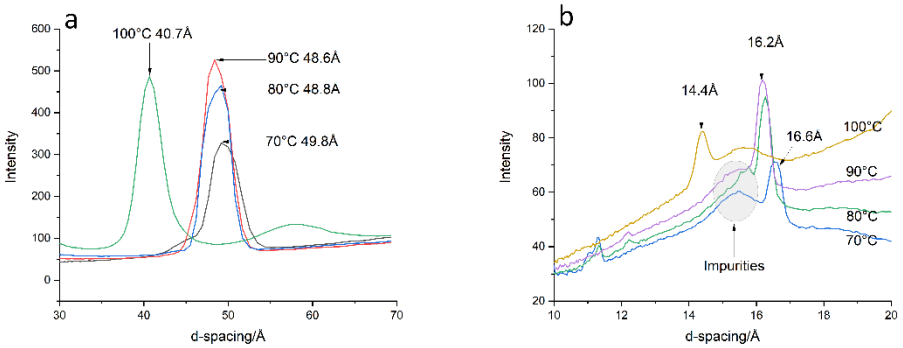

Figure 5-18 Comparing the peak positions of 50% neutralised sample at 60°C, 70°C, 80°C, 90°C and 100°C. a, d001; b, d003.

The WAXS patterns of 50% neutralised sample is shown in figure 5-20. The form I 1:1 acid-soap has two characteristic peaks at 2.90Å and 2.93Å and the form II has two characteristic peaks at 3.00Å and 3.04Å. No peaks can be found at 100°C, this confirmed that only liquid crystals formed in the mixture.

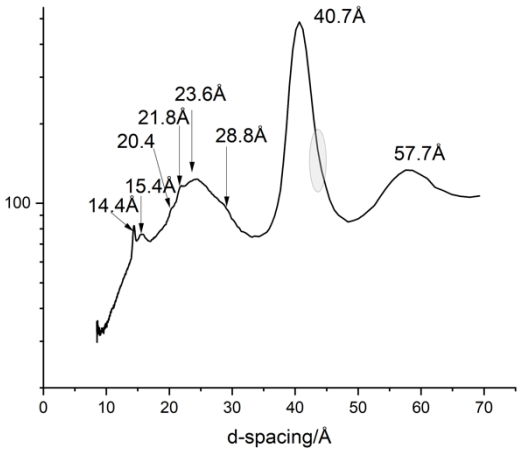

Figure 5-19 The SAXS pattern of 50% neutralised sample at 100°C. This highlighted are may have a small peak.

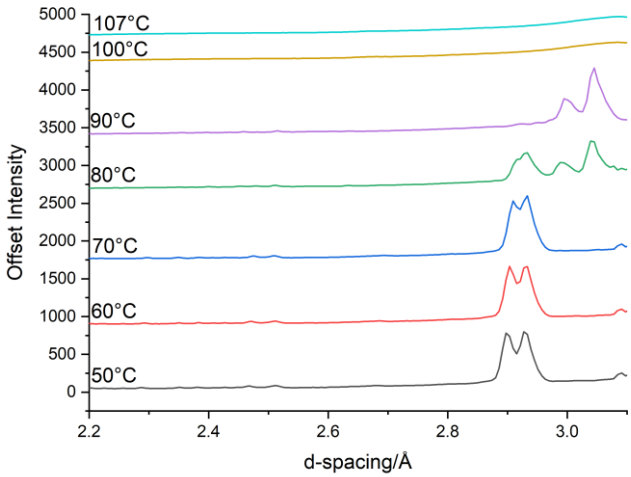

Figure 5-20 WAXS patterns of 50% neutralised sample as function of temperature

When the neutralisation ratio rised to 60%, the samples consist 1:1 acid-soap and sodium stearate. A shoulder around 44Å to 46Å was observed in SAXS patterns as shown in figure 5-21. The XRD patterns suggested that this shoulder contains two peaks at 44.6Å and 46.6Å, which are the β and γ form of sodium stearate. And this

peak migrated to 43.6Å with low intensity as shown in figure 5-22a. This is because of sodium stearate transformed from curd crystals to subwaxy state, which can also explain the endo-thermal peak around 80°C in DSC trace of 100% neutralised sample. The peak migration in 70% neutralised sample showed same trend with 60% neutralised sample (figure 5-23 & 5-24), whilst the peak associated with sodium stearate has stronger intensities because of the higher molar ratio. And the transition temperature corresponding with sodium stearate is higher as the peaks at 15.55Å and 14.90Å were found at 80°C.

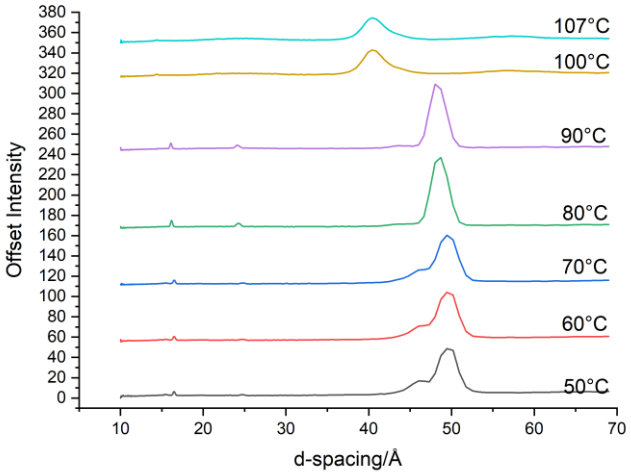

Figure 5-21 The SAXS patterns of 60% neutralised sample as function of temperature

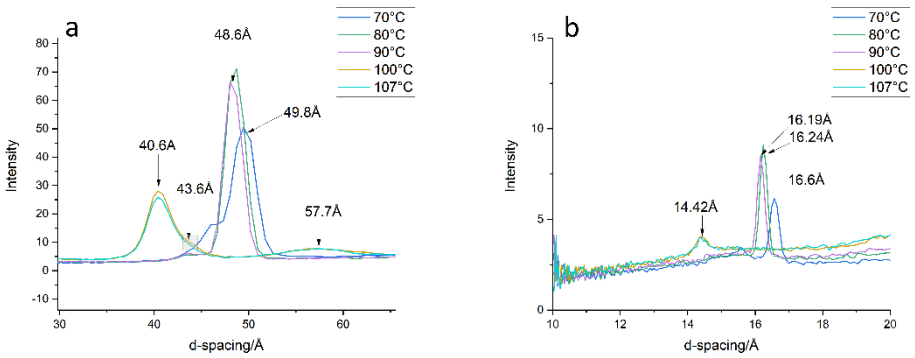

Figure 5-22 Comparing the peak positions of 60% neutralised sample at 70°C, 80°C, 90°C, 100°C and 107°C. a, d001; b, d003.

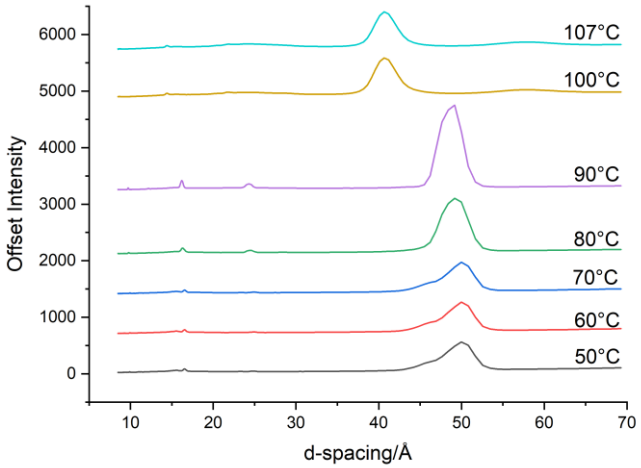

Figure 5-23 SAXS patterns of 70% neutralised sample as function of temperature

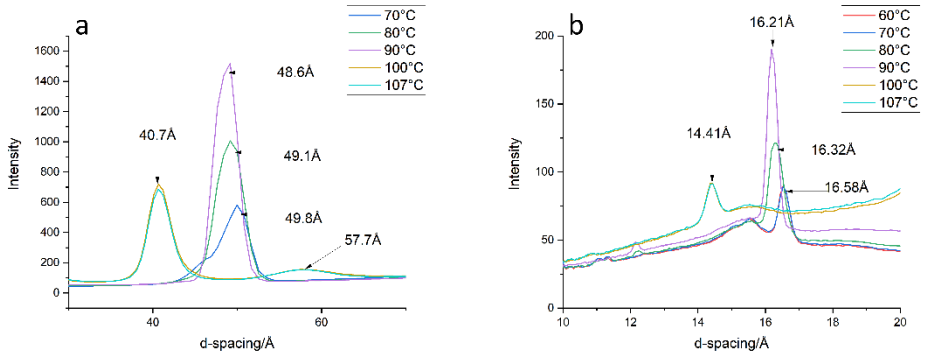

Figure 5-24 Comparing the peak positions of 70% neutralised sample at 70°C, 80°C, 90°C, 100°C and 107°C. a, d001; b, d003.

The SAXS patterns of 80% and 90% neutralised samples are shown in figure 5-25. The peak corresponding with 1:1 acid-soap form I was observed in these two samples, the form II of 1:1 acid-soap was observed at 90°C and 100°C. The DSC confirmed that the transition temperature from form I to form II is at 81°C. The peak at 14.4Å appeared in these two samples at 107°C, which indicated the formation of 1:1 acid-soap form III liquid crystal. The WAXS patterns of 90% shown in figure 5-26 indicated that the sample consists sodium stearate and 1:1 acid-soap form II at 90°C. The soap melted

between 90°C and 100°C. The 1:1 acid-soap form II transformed to form II between 100°C to 107°C. Hence, the broad endo-thermal peak of 90% neutralised sample around 100°C consists two peaks corresponding with the transformation of sodium stearate and 1:1 acid-soap.

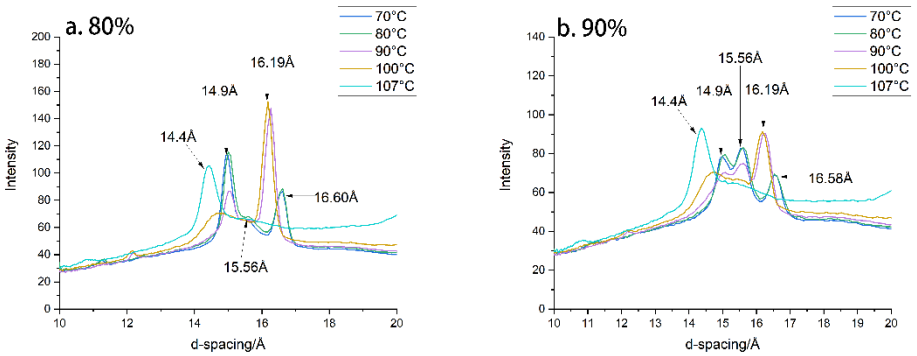

Figure 5-25 Comparing the peak positions of 80% and 90% neutralised sample at 70°C, 80°C, 90°C, 100°C and 107°C. a, 80%; b, 90%.

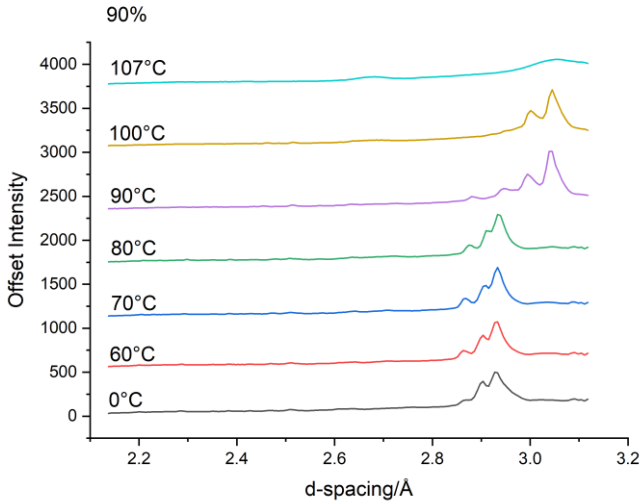

Figure 5-26 WAXS patterns of 90% neutralised sample as function of temperature

The phase transitions of 100% neutralised sample are complex in this experiment (figure 5-23). The peak at 16.61Å was observed in SAXS at 70°C, and the characteristic peaks around 3.09Å corresponding with 1:1 acid-soap were observed in WAXS as shown in figure 5-28. This confirmed that the existence of 1:1 acid-soap. The d-spacing migration of sodium stearate is not clear in SAXS region as shown in

figure 5-27b. The peak corresponding with sodium stearate shown in figure 5-28 migrated to larger d-spacing at 80°C. The peak migration of 1:1 acid-soap occurred between 80°C and 90°C. These two transitions caused the endo-thermal peak around 80°C in DSC. Only large bump was observed at 100°C, which confirmed that the structure in the sample is liquid crystal. The peaks at 14.91Å and 15.54Å were observed in SAXS patterns as shown in figure 5-27a, which confirmed that the sample consists β and γ forms sodium stearate.

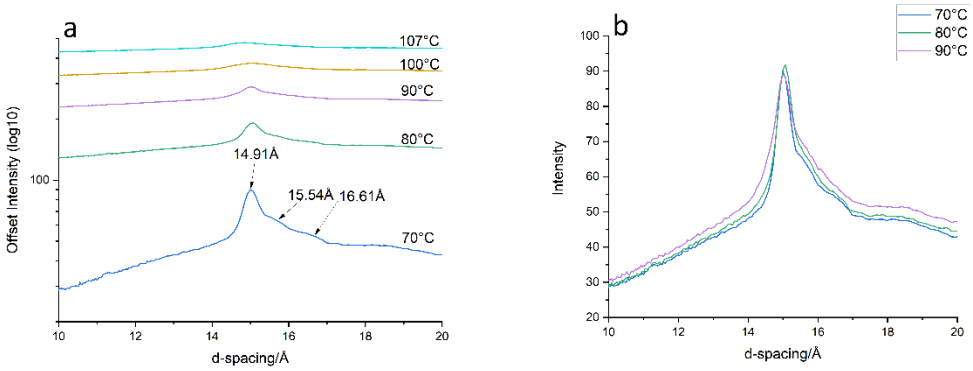

Figure 5-27 The SAXS pattern of 100% neutralised sample as function of temperature. a. d003 (log scale) b. comparing the patterns at 70°C, 80°C and 90°C.

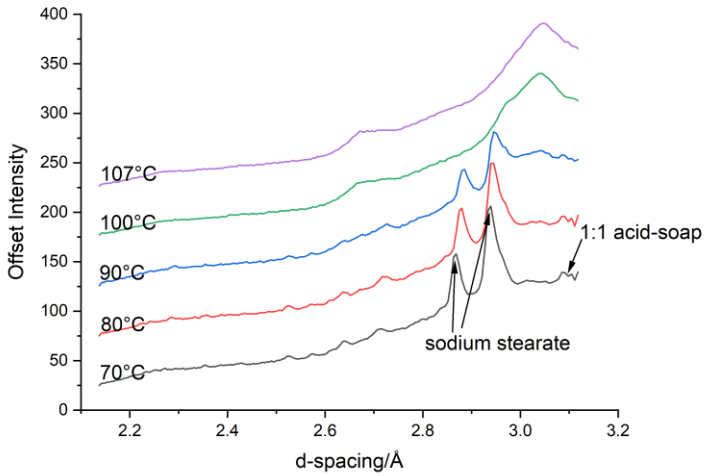

Figure 5-28 WAXS patterns of 100% neutralised sample as function of temperature

According to the experimental results shown previously, the phase diagram of the stearic acid – sodium stearate system was constructed and shown in figure 5-29. The phase diagram is different with the previous publications[121]. Matthew L. Lynch[107] suggested that 2:1, 1:1 and 1:2 acid-soaps were formed in palmitic acid – sodium palmitate system. However, only 2:1 and 1:1 acid-soaps were observed by P-XRD at room temperature.

The first transition corresponding with 2:1 acid-soap (NaH_2St_3) is around 75°C, which is the 2:1 acid-soap dissolved in stearic acid melt and formed liquid crystals. And this transition disappeared when the neutralised ratio above 33.3%. The second transition is the stearic acid melting out from 2:1 acid-soap and formed 1:1 acid-soap ($NaHSt_2$) form I.

The 1:1 acid-soap ($NaHSt_2$) also has phase transition around 80°C, which is associated with the transition from form I to form II. The transition temperature is very close with the transition temperature of 2:1 acid-soap to 1:1 acid-soap form I. The previous publication[107] suggested that the form II is 1:2 acid-soap (Na_2HSt_3). However, the characteristic peak corresponding with form II cannot be found in the samples at room temperature. The form III of 1:1 acid-soap is hexagonal liquid crystal, and the transition temperature is around 100°C. The transition peaks around 100% becomes broader when the neutralisation ratio above 50%. The on-set temperature decreased to 95°C, whilst the peak temperatures were around 101°C (dot-line in figure 5-29). The decreasing of on-set temperature is because of the sodium stearate, the β and γ form of sodium stearate transformed to subwaxy state (liquid crystal). The transition temperature at 101°C is corresponding with the transition of 1:1 acid-soap form II to form III.

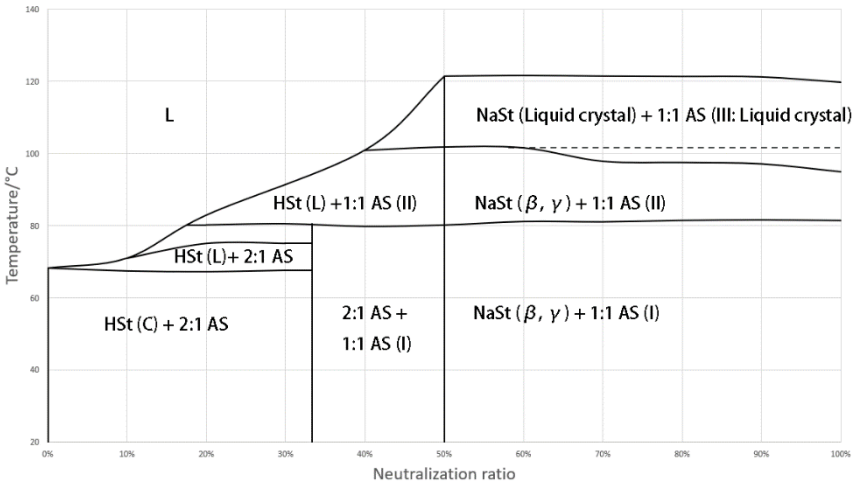

Figure 5-29 Phase diagram of stearic acid-sodium stearate system.

5.4 Morphology of acid-soaps observed by SEM

The aim of this project is solidifying the liquid surfactant by adding partially neutralised stearic acid as organo-gelator. Hence, it is important to know the crystal morphologies of acid-soaps. The P-XRD/SAXS/WAXS confirmed that 2:1 and 1:1 acid-soaps were formed in stearic acid-sodium stearate system. Hence, 0%, 30%, 50%, 70% and 100% neutralised samples were examined by SEM to observe the crystal morphologies. The crystals of stearic acid were plate-like lamellar structures, and the layers were observed by SEM as shown in figure 5-30a. The SAXS/P-XRD results indicated that the 30% neutralised sample consists 2:1 acid-soap and small amount of stearic acid. Hence, the crystals observed in figure 5-30b were 2:1 acid-soap. The 2:1 acid-soap crystals are ribbon-like structure and the size were much smaller than stearic acid. Plate-like crystals were observed in 50% neutralised sample, which should be the 1:1 acid-soap form I. Some rhombus crystals were observed in 50% neutralised sample, these are the fine crystal of 1:1 acid-soap form I. When the neutralisation ratio rised to 70%, some needle-like crystals were observed as shown in figure 5-30e. These needle-like crystals are the γ form sodium stearate. The rhombus crystals were observed in 70% neutralised sample, which confirmed that these crystals are 1:1 acid-soap form I. Some fractured plate-like crystals were observed in 70% neutralised sample, these crystals consists 1:1 acid-soap and β form sodium stearate. The needle

like crystals were observed in 100% neutralised sample, which is the γ form sodium stearate. The P-XRD confirmed that most of the sodium stearate were formed γ-NaSt.

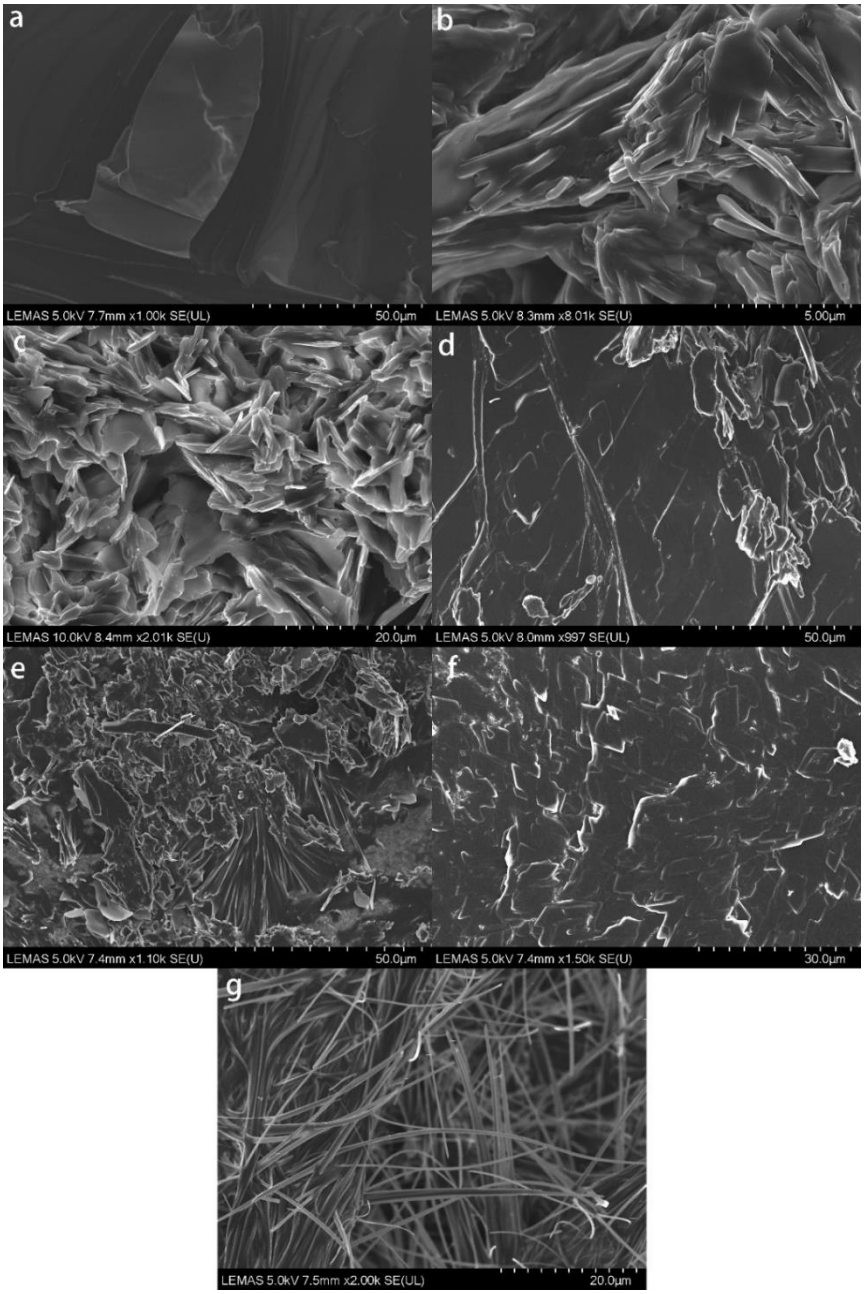

Figure 5-30 SEM images of acid-soaps: a, 0% neutralised sample, 50µm. b, 30% neutralised sample, 5µm. c & d, 50% neutralised sample, 20µm and 50µm. e & f, 70% neutralised sample, 50µm and 30µm. g, 100% neutralised sample, 20µm.

5.5 Conclusions

The stearate acid-soaps have similar structure with palmitate system and the stoichiometric ratios of acid to soap are 2:1 and 1:1. The characteristic long-range d-spacings associate with these two types acid-soaps are 47.4Å and 49.8Å respectively. The repeating peaks follow the $1:1/2:1/3$, which indicated that the crystals are lamellar structure. The fully extended chain length of stearic acid is 25.94Å, which is much smaller than the long range d-spacing. This suggests that the lamellar crystals of 2:1 and 1:1 acid-soaps are bilayer structure with tilt angle of 66° and 73.7° respectively.

The phase behaviour of stearate acid-soaps has been confirmed, and the binary phase diagram of sodium stearate and stearic acid system has generated. The 2:1 acid-soap exhibits two transitions: dissolving in stearic acid melt and form inverted micelles; stearic acid melting out and transform to 1:1 acid-soap. The 1:1 acid-soap has three polymorphs: form I, form II and form III. Form I and form II are lamellar crystals, whereas form III is hexagonal liquid crystal. Form I transform to form II around 80°C, and form II transform to form III around 100°C. The transition temperature of 2:1 acid-soap to 1:1 acid-soap is close to the transition temperature of 1:1 acid-soap form I to form II, which broadened the exo-thermal peak around 80°C in DSC results.

The morphologies of acid-soaps were observed by SEM. The rhombus crystals were observed in 50% and 70% neutralised samples, which is associating with the 1:1 acid-soap form I. However, the amount of the rhombus crystals are relatively small.

Chapter 6 Acid-soaps in surfactants

Characterisation of the acid-soaps formation and crystal structures in environment of non-ionic surfactants and alcohol ethoxylate sulfonates.

6.1 Introduction

The washing powders are typically compositional formulated and varies surfactants are added to the system to achieve desired properties such as detergency and stability. As the main surfactants, linear alkyl benzene sulfonates, were easily affected by the counter-ions, the non-ionic surfactants, alcohol ethoxylates were chosen to improve the detergency in hard water.[122] However, the non-ionic surfactants are gel at room temperature, which cause caking of the washing powder. The partially neutralised stearic acid (acid-soaps) were selected to solidify the gel-like non-ionic surfactants. Although the acid-soaps in aqueous systems were well studied[123-127], these studies were focused on the dilute solution of acid-soaps in water, the influences of the surfactants on the crystallisation process of acid-soaps received little attention. This chapter aims to characterise the stearate acid-soaps formation in the environment of surfactants and the crystallisation process of the acid-soaps. By comparing the SAXS/WAXS patterns of NI/HSt mixtures with stearate acid-soaps presents in chapter 5, the crystals associate with stearate acid-soaps can be characterised. As the industrial requirements, the samples prepared with palm-stearin fatty acids were also prepared to observe the crystallisation process. Another kind surfactant, alcohol ethoxylate sulfonates, were mixed with the stearic acid to compare with the non-ionic surfactants. This also provide fundamental knowledge for understanding the influence of perfume on the crystal structures of AES and acid-soaps in chapter 7.

6.2 The acid-soaps in non-ionic surfactant (Alcohol Ethoxylate)

6.2.1 The mixtures of non-ionic surfactant and partially neutralised stearic acid

6.2.1.1 DSC

The DSC traces of non-ionic surfactant and the mixture of non-ionic surfactant with partially neutralised stearic acid are shown in figure 6-1 and 6-2. The DSC traces of heating cycles of non-ionic surfactant showed a broad bump ranged from 5.61°C to 26.42°C. The bump consists two peaks at 14.09°C and 22.74°C. A broad bump ranged from 11.80°C to -6.86°C with two peaks at 8.88°C and 6.82°C was observed during cooling ramp. The reason is the commercial non-ionic surfactant (Neodol 45-7) consists two main compounds, C14E7 and C15E7. The non-ionic surfactant was supplied by Shell chemicals, and the composition of Neodol 45-7 shown in table 6-1 was determined by GC-MS, which is provided by the supplier. This can explain the two peaks observed in DSC traces of non-ionic surfactant.

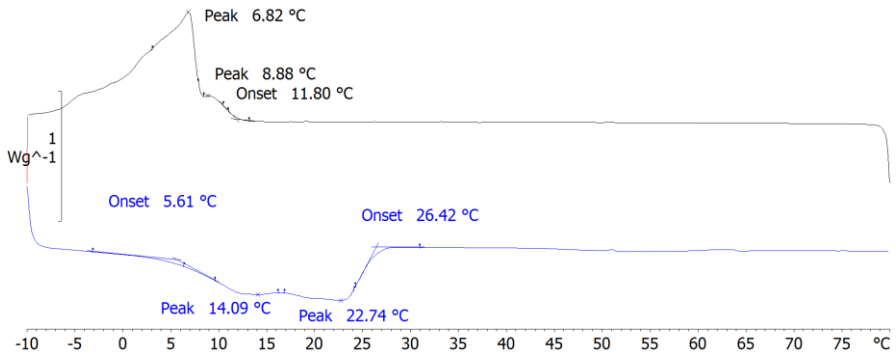

Figure 6-1 The DSC trace of alcohol ethoxylate (non-ionic surfactant). The broad endo-thermal bump ranged from 5.61°C to 26.42°C has two peaks at 14.09°C and 22.74°C. A broad exo-thermal bump ranged from 11.80°C to -6.86°C was observed in cooling ramp.

The DSC traces of samples contains 90% non-ionic surfactant and 10% partially neutralised stearic acid is shown in figure 6-2. A broad bump ranged from 2°C to 25°C was observed during heating ramp. This endo-thermal bump consists two peaks, 13.72°C and 23.16°C, which is similar with the pure non-ionic surfactant. The same phenomenon was observed during cooling cycles. A small peak at 55.03°C was observed in heating ramps and 30.06°C in cooling ramps. These transitions are corresponding with the partially neutralised stearic acid. However, the transition temperature is lower than the stearate acid-soaps measured in chapter 5, which is because the samples only contain 10% partially neutralised stearic acid.

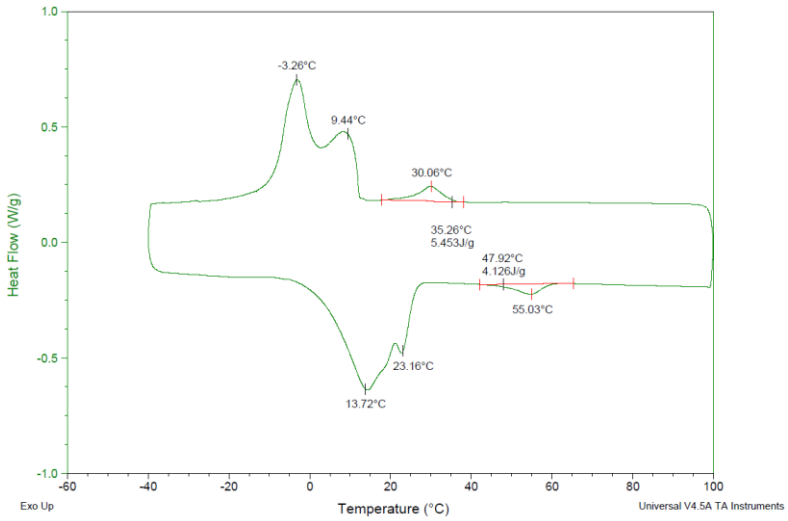

Figure 6-2 The DSC trace of mixture contains 90% non-ionic surfactant and 10% partially neutralised stearic acid. The broad peak from 2°C to 25°C is similar with non-ionic surfactant. The peak at 55°C is corresponding with the partially neutralised stearic acid.

Table 6-1 The composition of Neodol 45-7. The average degree of ethoxylation is 7.

	C12	C13	C14	C15	C16
Neodol 45-7	0	1	48	50	1

6.2.1.2 SAXS with temperature stage

In order to investigate the phase transition of acid-soaps in the environment of non-ionic surfactant, the phase of non-ionic surfactant was observed by SAXS as shown in figure 6-3. A broad weak peak around 35Å was observed from 30°C to 60°C and no

obvious transition occurred. There are no sharp peaks observed in WAXS patterns as shown in figure 6-4, which indicated that the non-ionic surfactant is amorphous.

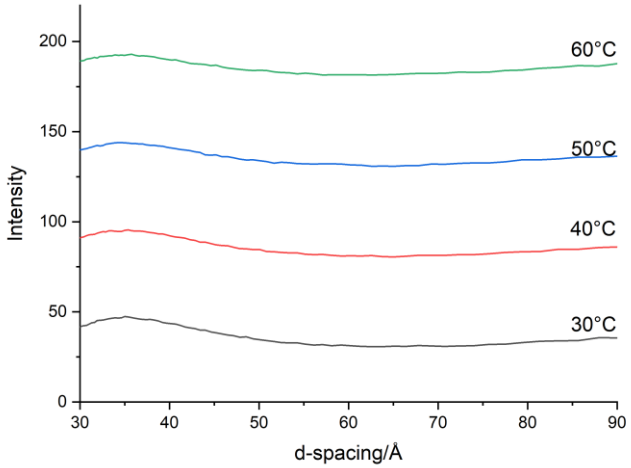

Figure 6-3 The SAXS patterns of non-ionic surfactant as function of temperature. A broad weak peak was observed around 35Å and no obvious transitions occurred.

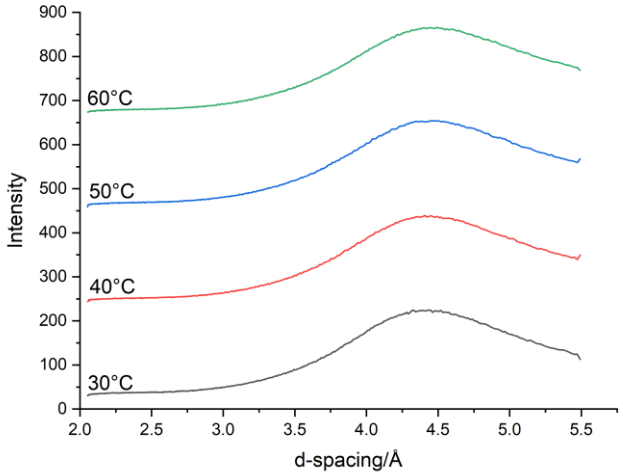

Figure 6-4 The WAXS patterns of non-ionic surfactant as function of temperature. A broad peak around 4.4Å was observed from 30°C to 60°C and no obvious transitions occurred.

The SAXS patterns of the mixture of non-ionic surfactant and partially neutralised stearic acid are shown in figure 6-5. A peak at 44Å with a shoulder at 40.7Å was observed at 111°C. The peak at 40.7Å is corresponding with the 1:1 acid-soap form III. The reported sodium stearate plate-like crystal in solution is at 43.7Å[117], which indicated that the broad peak at 44Å is corresponding with sodium stearate. And the

appearance of sodium stearate in the system indicated that the neutralisation ratio of stearic acid is above 50%. The peaks at 49.7Å and 52Å was observed at 56°C. The peak at 49.7Å is corresponding with the 1:1 acid-soap form I and the peak at 52Å is corresponding with the α-form of sodium stearate.[115] The intensity of the peak at 40.7Å increased at 65°C. This indicated that the 1:1 acid-soap has another phase transition above 107°C (the limit of the temperature stage). A broad bump was observed at 11°C, which is related to the exo-thermal peak of non-ionic surfactant. The WAXS patterns of the mixture is shown in figure 6-6. No peaks were observed at 111°C and 65°C, which confirmed that the sodium stearate and 1:1 acid-soap are liquid crystals. The peaks appeared at 56°C, which indicated that the crystallisation occurred. The broad weak peak around 4.4Å corresponding with non-ionic surfactant was also observed in the mixtures from 20°C to 111°C.

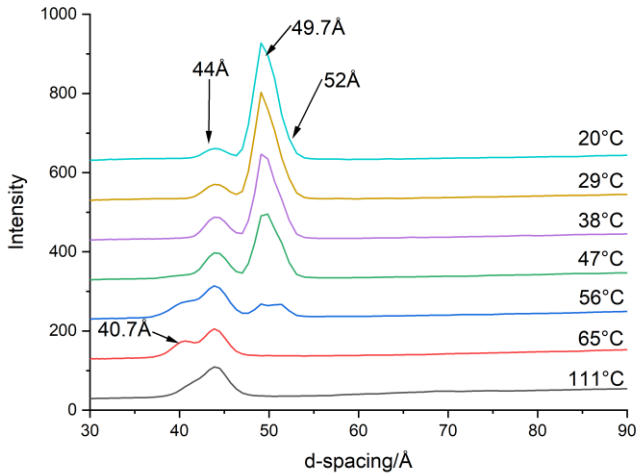

Figure 6-5 The SAXS patterns of non-ionic surfactant/stearic acid mixtures as function of temperature. At 111°C, the peak at 44Å with a shoulder around 40.7Å was observed. Crash cooled to 65°C, the intensity of the peak at 40.7Å increased. The peaks at 49.7Å and 52Å appeared at 56°C.

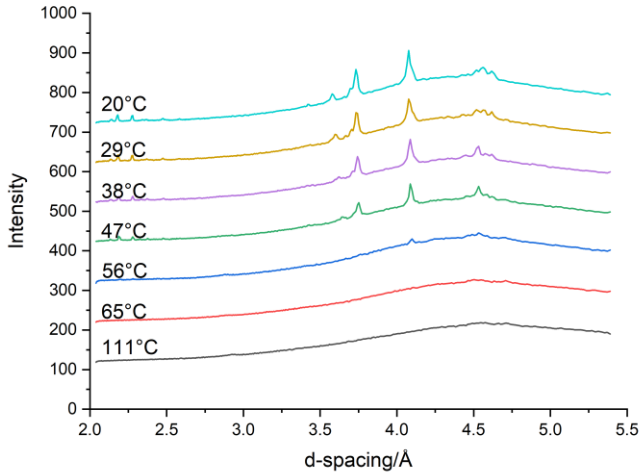

Figure 6-6 The WAXS patterns of non-ionic surfactant/stearic acid mixtures as function of temperature. No peaks were observed at 111°C and 65°C. Small peaks appeared at 56°C.

The samples were prepared with IKA magic lab high shear mixer, the stearic acid was in-situ neutralised with NaOH solution. The neutralisation ratio of stearic acid was controlled at 50%. However, the SAXS results indicated that the samples contains 1:1 acid-soap and sodium stearate. This may because of the “dead zone” (red) in the mixing unit as shwon in figure 6-7. The non-ionic surfactant/ stearic acid premix encountered with NaOH solution before entering the mixing chamber. The viscosity incresed significatantly in the grey zone and the inlet pressure was not enough to push out the samples. The samples with higher viscosity stocked in the red zone (figure 6-7). This was confirmed that some white gels were found after experiments in the red zone, which is also called “dead zone”.

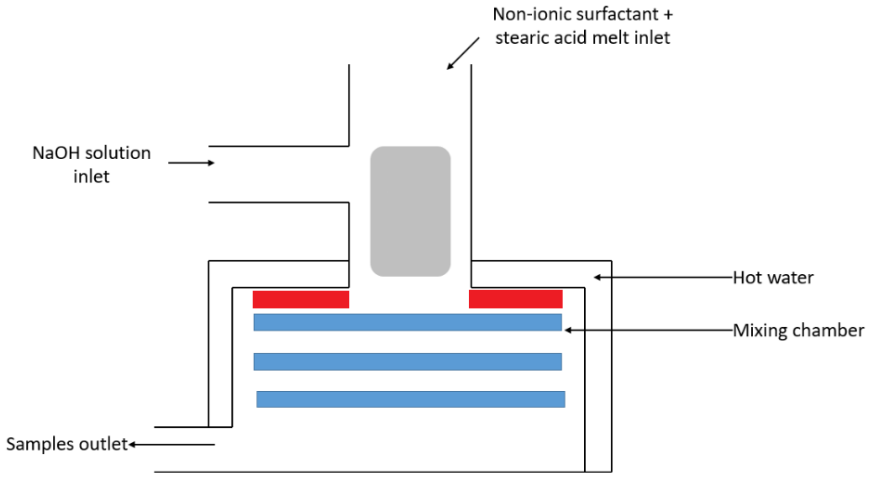

Figure 6-7 The mixing unit of IKA magic lab high shear mixer. The non-ionic/ stearic acid premix encountered with NaOH solution at the grey zone. The blue rectangles are the mixing plates. White gels were found in the red zone, which is also called "dead zone".

6.2.1.3 Polarised microscopy

The images of the mixture of non-ionic surfactant and partially neutralised stearic acid is shown in figure 6-8. The samples are liquid at 120°C and 110°C, and the flowability decreased at 100°C. This phenomenon is because that the formation of 1:1 acid-soap form III liquid crystal increses the viscosity. Needle-like crystals were observed at 50°C and the crystallisation rate is slow. The SAXS patterns also suggested that the crystals formed at 56°C and the peak intensities corresponding with sodium stearate and 1:1 acid-soap form I were weak. When the temperature reached 10°C, the non-ionic surfactant solidified and the sample became semitransparent (figure 6-9).

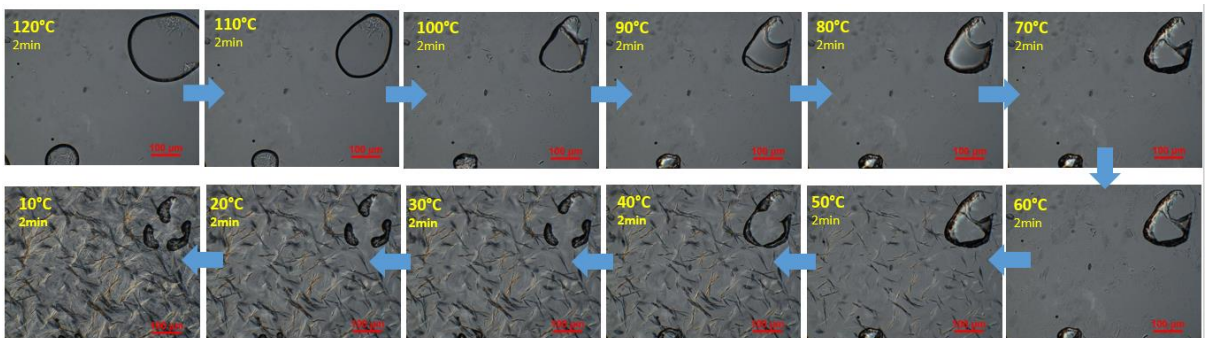

Figure 6-8 The crystallisation of the mixture of 90% non-ionic surfactant and 10% partially neutralised stearic acid. The cooling rate was 10°C/min, and the sample was kept for 2 min for equilibrating. The black circle is air bubble.

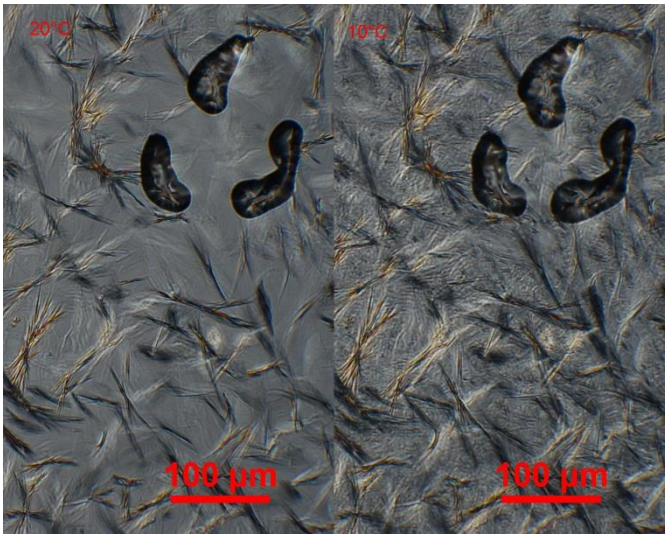

Figure 6-9 Comparing the mixture of 90% non-ionic surfactant and 10% partially neutralised stearic acid at 20°C and 10°C. The transparency of the sample at 20°C is better than 10°C. The edge of the air bubble (dark area) in not smooth at 10°C.

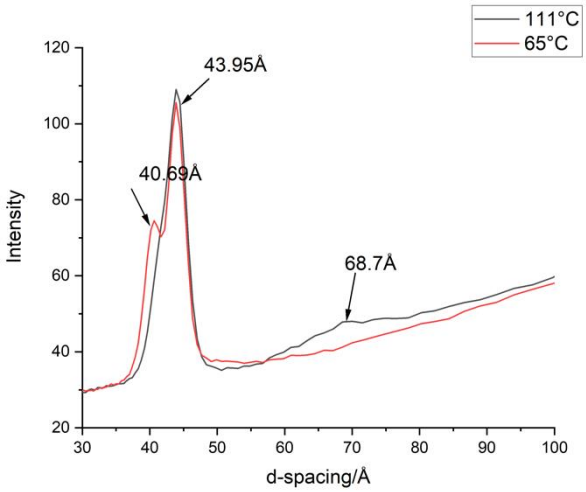

Figure 6-10 Comparing the SAXS patterns of the mixture of 90% non-ionic surfactant and 10% partially neutralised stearic acid at 111°C and 65°C. A broad bump was observed around 68.7Å, and this peak disappeared at 65°C. The peak at 40.7Å appeared at 65°C.

Comparing the SAXS patterns at 111°C and 65°C as shown in figure 6-10, a broad bump around 68.7Å was observed at 111°C and this bump disappeared at 65°C. The appearance of the broad bump indicated that the sample contains some amorphous phases, whilst the molecules have tendency to form bilayer structure. This amorphous chain arrangement transformed to 1:1 acid-soap form III around 100°C. This can explain the decreased flowability of the sample at 100°C. However, only two phase

transitions were observed in these experiments, amorphous to form III and form III to form I. The form II with d-spacing at 48.6Å was not observed.

Possible structural arrangements of sodium stearate and 1:1 acid-soap are shown in figure 6-11. At 111°C, there are two peaks at 44Å and a broad bump around 68.7Å. The d-spacing of 44Å is corresponding with the interlayer spacing of NaSt liquid crystal (vertical). However, the intermolecular spacing (horizontal) are no constant. The broad bump around 68.7Å is corresponding with 1:1 acid-soap amorphous phase. The molecules have tendency to head to head structure. However, the interlayer spacing is not constant. Hence, the broad bump was observed in SAXS patterns. When the temperature dropped to 100°C, the 1:1 acid-soap form III liquid crystal with d-spacing of 40.7Å formed in the mixtures. The sodium stearate and stearic acid molecules formed bilayer structure with fixed intermolecular spacing (40.7Å). After the temperature dropped below the crystallisation temperature, the lamellar crystals of sodium stearate and 1:1 acid-soap form I formed in the mixtures. Both the interlayer spacing and intermolecular spacing are fixed.

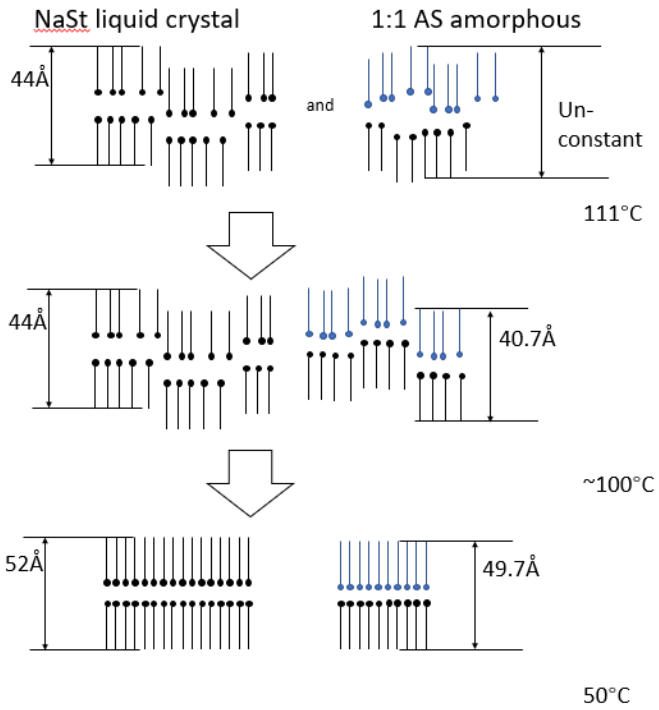

Figure 6-11 Possible molecules arrangements of sodium stearate and 1:1 acid-soap in the mixtures. Blue, acid. Black, soap. At 111°C, the sodium stearate are liquid crystals, the 1:1 acid-soap keeps the head-to-head structure with un-constant d-spacing. At 100°C, 1:1 acid-soap form III liquid crystal appeared. And at 50°C, the lamellar structure crystals of sodium stearate and 1:1 acid-soap formed.

6.2.2 The mixture of non-ionic surfactant and partially neutralised palm-stearin fatty acid (PSFA)

The palm-stearin fatty acid (PSFA) was used as solidifier to solidify the non-ionic surfactant industrially. Hence, the samples consist non-ionic surfactant and PSFA were prepared to observe the formation of acid-soap structures. The PSFA is the mixture of several fatty acids and the composition was determined by GC-MS as shown in table 6-2. The main fatty acids in PSFA are palmitic acid (45.5%) and stearic acid (37.9%).

Table 6-2 The composition of palm-stearin fatty acid. Palmitic acid and stearic acid are the main fatty acids in the mixture.

	Myristic acid	Palmitic acid	Stearic acid	Oleic acid	Linoleic acid
PSFA (%)	6.6	45.5	37.9	9.2	0.8

Comparing with the mixtures prepared with stearic acid, the broad exo-thermal and endo-thermal peak ranged from -5°C to 25°C corresponding with non-ionic surfactant can still be observed in the samples prepared with PSFA. A small endo-thermal peak around 40°C in heating ramps and a small peak around 25°C in cooling ramps were observed in this sample as shwon in figure 6-12. These peaks corresponding with the phase transition of acid-soaps formed by NaPSFA and PSFA. As the experiment set-ups were same with the samples prepared with steaic acid, the acid-soap formed in this sample were 1:1 acid-soap.

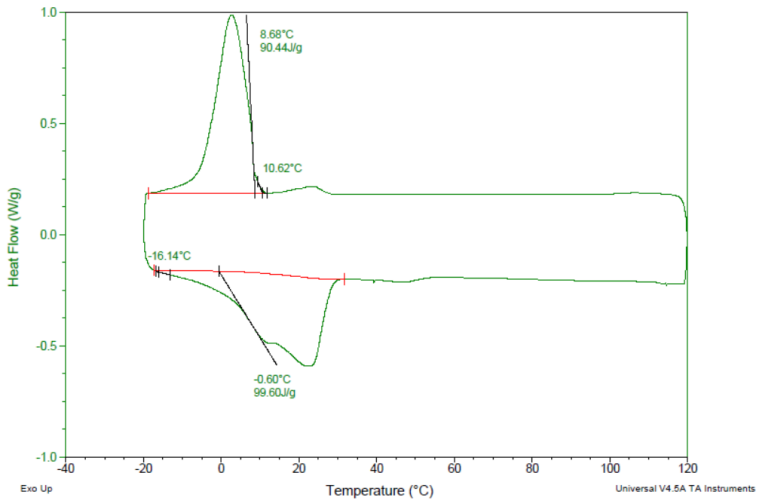

Figure 6-12 The DSC curve of the mixture of 90% non-ionic surfactant and 10% partially neutralised PSFA. The broad peak ranged from -5°C to 25°C in heating ramp was observed. A small endo-thermal peak was observed from 40°C to 50°C in heating ramp, the on-set temperature of the small exo-thermal peak in cooling ramp was observed at 30°C.

As the on-set temperature of the exo-thermal peak in cooling ramp is 27°C and the peak was broad, 35°C and 20°C were choosen for comparing the phase transitions in the mixtures. As shwon in figure 6-13, the samples were crash cooled from 50°C to 35°C and no obvious transition was observed. Only one peak at 39.5Å was observed, and this peak is corresponding with the NaPSFA. The repeating peaks following the 1:2:3 repeating ratios, which indicated that the crystals are lamellar structure. As shown in figure 6-14, another peak at 45Å was observed when the sample crash cooled to 20°C. However, this peak was not observed after 1 min equilibrim, which suggested that the crystallisation rate was slow and the crystal reached equilibrim state after 20 mins. This may because the crystallisation rate of soaps are slow and the viscous non-ionic surfactant restrained the movement of the soaps and fatty acids molecules.

The PSFA contains more palmitic acid than stearic acid, it should performs more like palmitic acid. Lynch[107] reported that the d-spacing of 2:1 palmitate acid-soap is 42.2Å, and this followed the tilt angle of stearate acid-soaps calculated in chapter 5.1.1:

$$l_{\max(HSt)} - l_{\max(HP)} = (1.5 + 1.265n_{16} + 4.2)\text{Å} - (1.5 + 1.265n_{14} + 4.2)\text{Å}$$

$$l_{\max(HSt)} - l_{\max(HP)} = 1.265 \times 2\text{Å} = 2.53\text{Å}$$

As the crystal structure of acid-soaps are bilayer lamellar structure, the alkyl chain length difference is:

$$l_{difference} = 2 \times 2.53\text{Å} = 5.06\text{Å}$$

If the 2:1 palmitate acid-soap has same tilt angle with stearic acid (shown in figure 5-3), the d-spacing can be calculated:

$$\theta = \sin^{-1}\frac{d}{2 \times l}$$

$$d = 2 \times l \times \sin\theta$$

$$d_{difference} = l_{difference} \times \sin\theta = d_{HSt} - d_{HP}$$

$$d_{HP\,2:1} = d_{HSt\,2:1} - l_{difference} \times \sin\theta = (47.4 - 5.06 \times \sin 66°)\text{Å} = 42.78\text{Å}$$

This result is similar with the published result, which indicated that the palmitate acid-soap has similar structure with stearic acid. Hence, the d-spacing of 1:1 palmitate acid-soap can be roughly calculated as:

$$d_{HP\,1:1} = (49.8 - 5.06 \times \sin 73.7°)\text{Å} = 44.94\text{Å}$$

The calculated d-spacing of 1:1 palmitate acid-soap is same with the peak observed in figure 6-14, which suggested that the crystal formed in this sample is 1:1 acid-soap and the crystal structure of PSFA is more like palmitic acid.

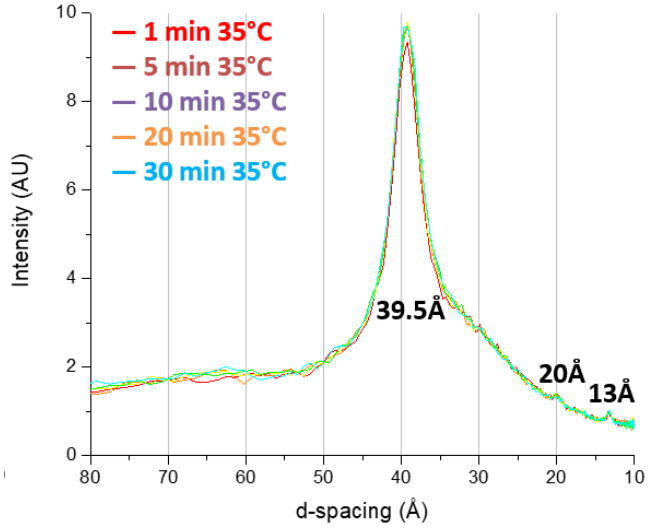

Figure 6-13 The SAXS patterns of sample consists 90% non-ionic surfactant and 10% partially neutralised PSFA. The sample was crash cooled from 50°C to 35°C and kept for 30mins. One peak at 39.5Å was observed, and the repeating peaks indicated that the crystal is lamellar structure.

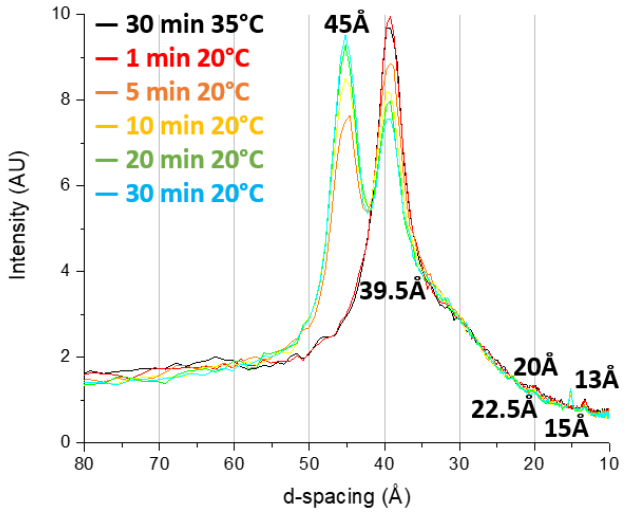

Figure 6-14 The SAXS patterns of sample consists 90% non-ionic surfactant and 10% partially neutralised PSFA. The sample was crash cooled from 35°C to 20°C, and kept for 30mins. A new peak at 45Å corresponding with the 1:1 acid-soap appeared since 5min and reached equilibrium state at 20 min.

The samples prepared with PSFA were also observed by polarized microscopy as shown in figure 6-15. The crystallisation of the samples prepared with PSFA is similar with the samples prepared with stearic acid, whereas the transition temperature is lower. As there's no air bubbles in the observation area, the change of flowability around 100°C cannot be observed. The needle like crystals corresponding with the acid-soaps was observed at 30°C, which is in aggreement with the DSC results. The

solidification of non-ionic surfactant is more obvious than the sample with stearic acid. The crystal size of the needle like crystal in the sample with PSFA is smaller than the sample with stearic acid. This is because the crystallisation of PSFA acid-soaps is harder than stearic acid. As palmitic acid has similar molecule structure with stearic acid, the stearic acid/sodium stearate can get into the crystal of palmitate acid-soaps as shwon in figure 6-16. However, the longer alkyl chain can cause disorder or disrupt the intermolacular packing, which can lead to higher crystallisation energy.[128]

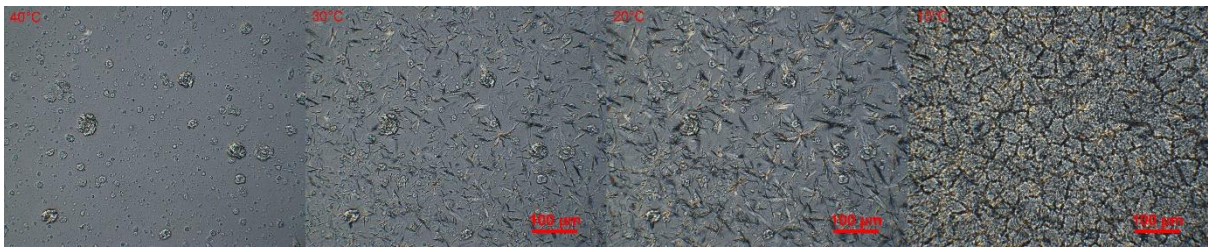

Figure 6-15 The crystallisation of the sample with 90% non-ionic surfactant and 10% partially neutralised palm-stearin fatty acids. The temperature is labelled on the top-left of each image. The needle-like crystal appeared at 30°C. The solidification of non-ionic surfactant was observed at 10°C.

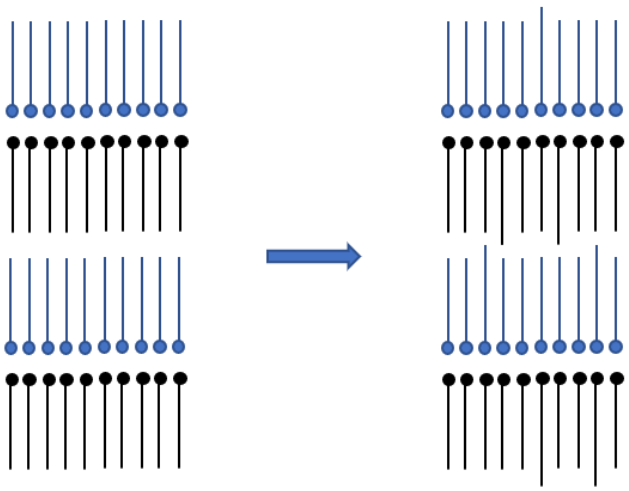

Figure 6-16 Possible molecules arrangement of acid-soaps with and without stearic acid. Left, the 1:1 acid-soap of palmitic acid. Right, the introduce of stearic acid lead the disorder of crystal or disrupt the intermolecular packing.

6.2.3 The morphologies of crystals formed in the mixture of acid-soaps and non-ionic surfactant

Both the samples prepared by PSFA and stearic acid were observed by helium ion microscopy and the images are shown in figure 6-17. The needle-like crystals observed by polarized microscopy were also found in these two samples, whereas the crystals were broken during preparation as the high shear force applied by the mixer. The circled crystal in figure 6-17b is similar with the plate-like sodium stearate crystal. The rhombus crystal observed in stearic acid-sodium stearate was not found in the samples with stearic acid. The crystals formed in the samples with PSFA were sensitive to the helium ions and the boundaries were unclear even very short time exposure, which suggested that these crystals are not as stable as the crystals formed by stearic acid/sodium stearate. This phenomenon is because that the introduce of stearic acid into palmitic acid caused disorder or disrupt the intermolecular packing. Because the stearic acid and palmitic acid have similar molecular structure, the stearic acid can be packed into the crystal of palmitic acid as shown in figure 6-16. The defects caused by stearic acid can increase the crystal strain, which decreased the stability of the crystal.

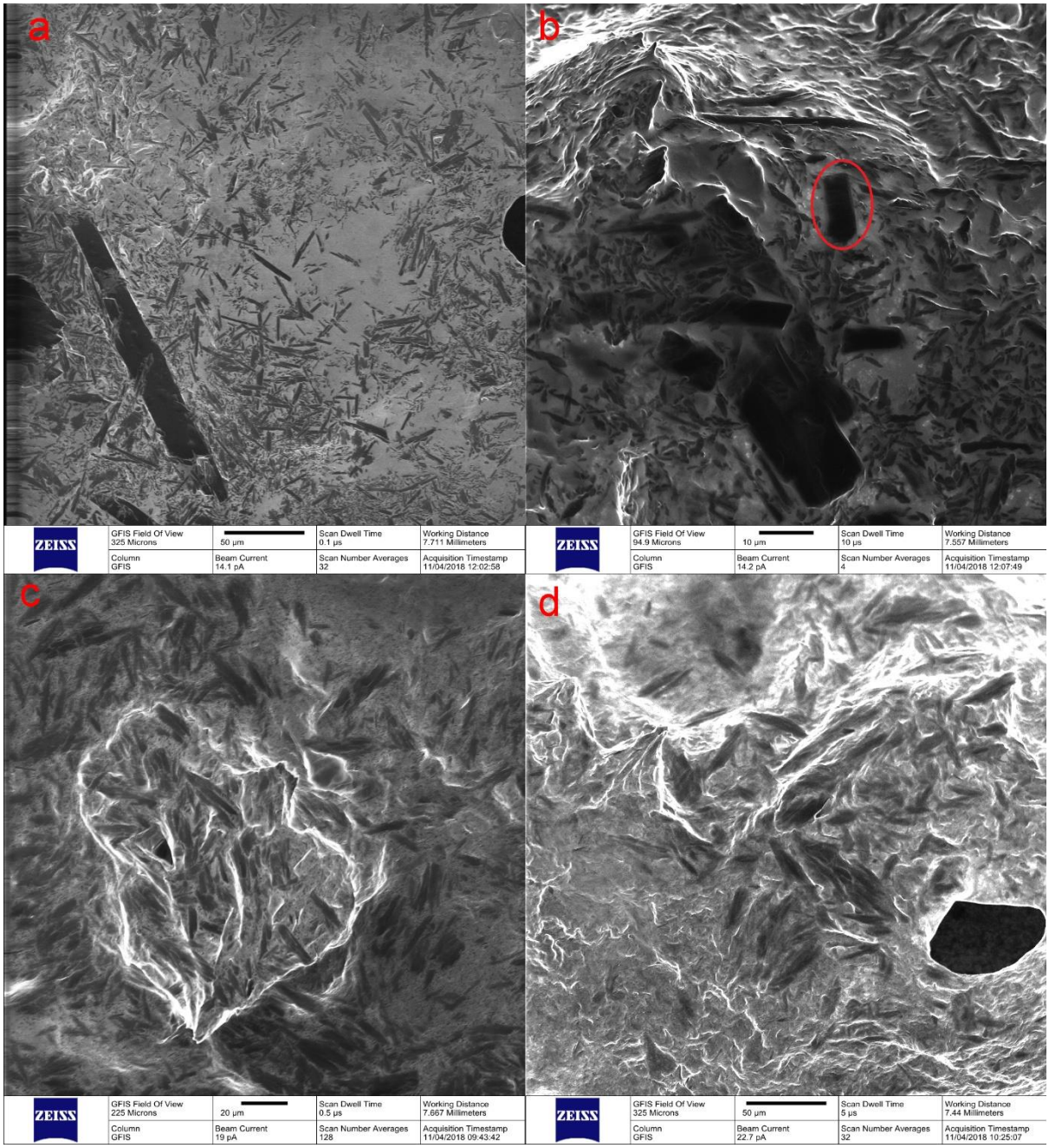

Figure 6-17 The images of mixtures of non-ionic surfactants and partially neutralised stearic acid (a & b) and PSFA (c & d). The scale bars of a, b, c and d are 50µm, 10µm, 20µm and 50µm. The circled crystal is sodium stearate.

The crystal structures of the samples prepared with PSFA was observed by cryo-SEM and the images are shown in figure 6-18. The disperse phase in the samples are lamellar crystals and the layers can be observed. No obvious structure was observed in the continuous phase, which suggested that the continuous is amorphous. As the sample was crashed cooled from room temperature to -196°C, the crystals are

corresponding with the soaps and acid-soaps of PSFA and the amorphous phase is corresponding with the non-ionic surfactant. The interfacial area between amorphous and lamellar crystals was sharp and obvious as shown in figure 6-18a, which indicated that there's no strong interactions between these two phases. This is in aggreement with the SAXS results, the acid-soaps of stearic acid was observed in the samples and the non-ionic surfactant has no influence on the intermolecular structure.

Figure 6-18 The cryo-SEM images of the sample prepared with PSFA. Lamellar crystals dispersed in amorphous non-ionic surfactant. The sharp interfacial area was observed in a. The scale bars are: 2µm (a) and 3µm (b).

6.3 The acid-soaps in alcohol ethoxy sulphates (AES)

6.3.1 The composition of AES

The alcohol ethoxy sulphates provided by Procter & Gambles consist 70% active ingredients, 30% water and some NaOH to modify the pH. The composition was measured by GC-MS. The degree of ethoxylation is shown in table 6-3, 49% of the AES does not contain ethoxy group, and the average ethoxylation degree is 1.03. The alkyl chain length of the AES are 12 and 14 as shown in table 6-4. The titration results indicated that the AES contains 0.6% NaOH and the soap ratio of AES/HSt mixture was calculated as shown in table 6-5.

Table 6-3 The ethoxylate distribution of AES. The average ethoxylation degree is 1.03.

Ethoxylation	AE1S (%)
0	49.0
1	24.0
2	13.0
3	7.0
4	4.0
5	2.0
6	1.0
7	0.0

Table 6-4 The chain length distribution of the AES provided by P&G.

	C12	C13	C14	C15	C16
AE1S (%)	67	0	26	0	6

Table 6-5 The calculated NaSt molar ratio vs stearic acid base on the titration results of AES.

AES paste (wt%)	HSt (wt%)	Neutralisation ratio of HSt(mol%)
100	0	
80	20	14.28%
70	30	8.85%
60	40	5.88%
50	50	4.00%
40	60	2.70%
30	70	1.75%
20	80	1.03%
10	90	0.46%
0	100	0%

6.3.2 The crystal structure of acid-soap and AES determined by SAXS/WAXS

6.3.2.1 SAXS/WAXS

The WAXS pattern of AES at 20°C is shown in figure 6-19. One broad peak around 4.5Å and no sharp peak was observed, which suggested that the AES paste is liquid crystal. The SAXS patterns of AES/HSt mixture are shown in figure 6-20. A peak at 37.97Å was observed at 100°C. The d-spacing of this peak increses as the temperature drcresing and the d-spacing incresed to 41.17Å at 20°C. The same phenomenon was observed in d002 and d003 of AES as shown in figure 6-21. The repeating ratios of d002 and d003 follow $1:\frac{1}{2}:\frac{1}{3}$, which indicated that the AES liquid crystals are lamellar structure.

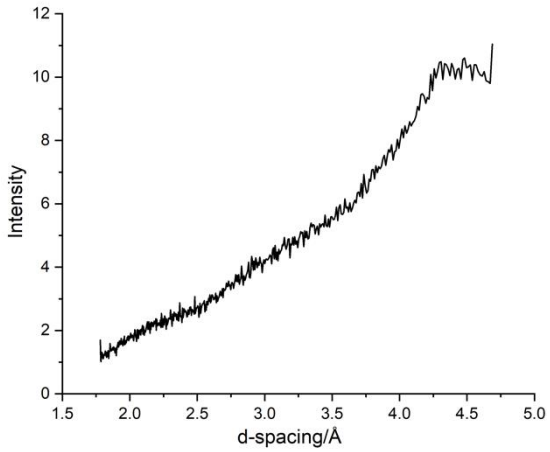

Figure 6-19 The WAXS pattern of AES paste at 20°C.

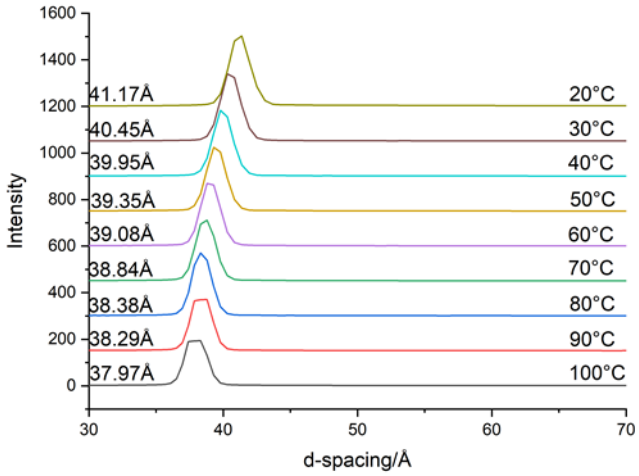

Figure 6-20 The SAXS patterns of AES as function of temperature. The d-spacing of AES increases as temperature decreasing.

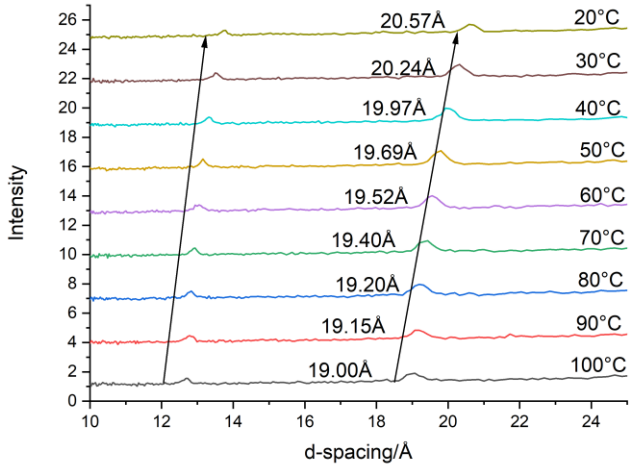

Figure 6-21 The d002 and d003 of AES paste. The d-spacing also increases as temperature decreasing. The d001, d002 and d003 following the 1:1/2:1/3 repeating ratios.

The d-spacing change is because of the temperature dependence of tilt angle.[129] As the average ethoxylation degree is 1 and the C12 is the main chain length in AES, the chain length of CH_3-(CH_2)-(O-CH_2-CH_2)-SO_3Na is calculated as the average chain length of AES. Assuming the van de Waals radius of -SO_3 is same with -COOH, the chain length is:

$$l_{max} = \left(1.5 + 1.265n_c + l_{C-O} \times \sin\frac{\theta_1}{2} + l_{C-S} \times \sin\frac{\theta_2}{2} + 4.2\right) \text{Å} = 24.4\text{Å}$$

Where the l_{C-O} is the carbon oxygen bond length and l_{C-S} is the carbon sulphur bond length, θ_1 and θ_2 are the bond angle of C-O and C-S bond respectively.

Assuming the molecular chain length of AES does not affected by temperature, the tilt angle of the AES at different temperatures can be calculated as:

$$tilt\ angle = (\sin^{-1}\frac{d-spacing}{24.4\times 2})^{\circ}$$

And the results is shown in table 6-6 and figure 6-22.

Table 6-6 The possible tilt angle of AES as function of temperature.

Temperature/°C	d-spacing/Å	Tilt angle/°
20	41.17	57.53
30	40.45	55.99
40	39.95	54.95
50	39.35	53.74
60	39.08	53.21
70	38.84	52.74
80	38.38	51.86
90	38.29	51.69
100	37.97	51.08

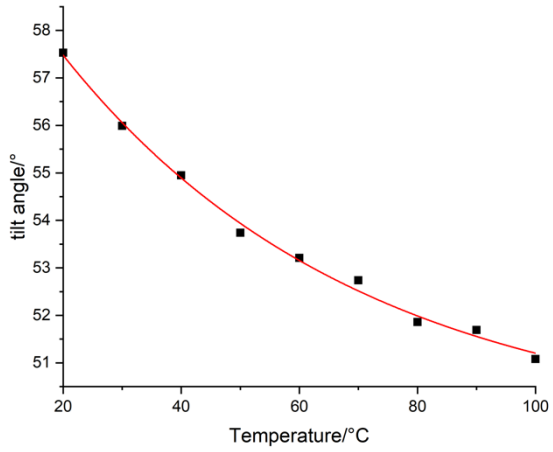

Figure 6-22 The possible tilt angle of AES liquid crystals as function of temperature. The tilt angle decreases gradually as temperature increasing.

The SAXS patterns of the sample consists 80% AES and 20% stearic acid are shown in figure 6-23a and the d002 and d003 patterns are shown in figure 6-23b. The repeating ratios indicated that the crystals formed in this sample were lamellar

structure. The WAXS patterns shown in figure 6-24 indicated that the crystals above 50°C are liquid crystal. The peak information is listed in table 6-7.

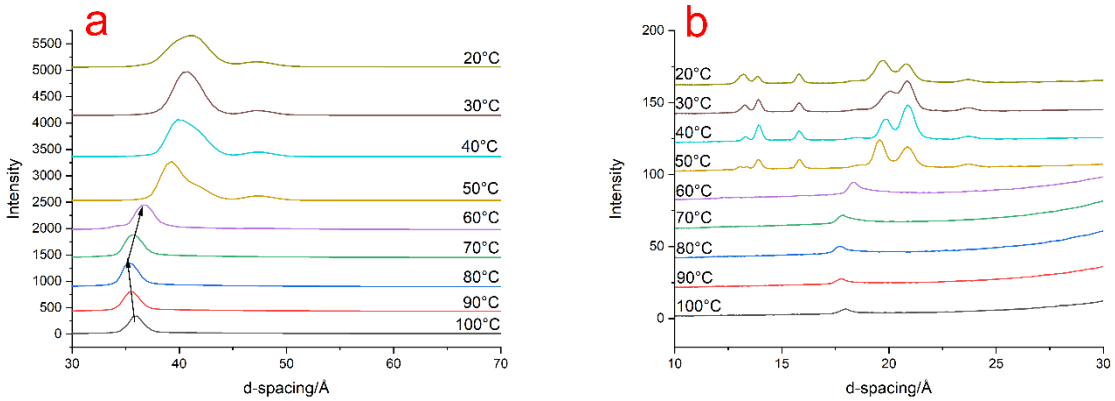

Figure 6-23 The SAXS patterns of AES/HSt (80/20) mixtures as function of temperature. a, d001; b, d002 and d003.

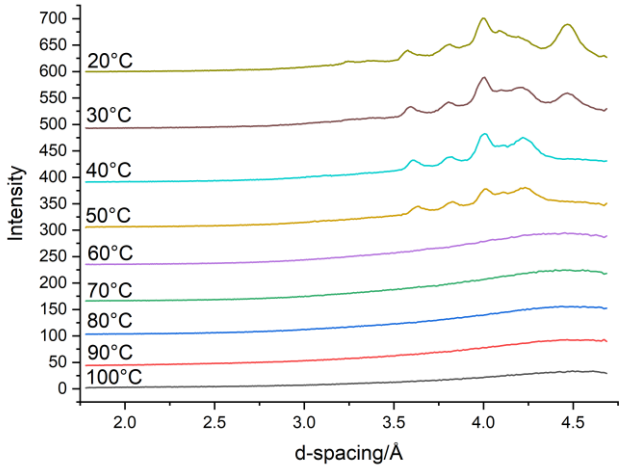

Figure 6-24 The WAXS patterns of AES/HSt (80/20) mixtures as function of temperature. The crystals formed above 50°C are liquid crystals as no peak was observed in WAXS region.

Table 6-7 The summary of peak positions of AES/HSt (80/20) at different temperatures. The broad peak around 40Å observed from 40°C to 20°C consist two peaks at 42Å and 39.8Å.

Temperature/°C	d001/Å	d002/Å	d003/Å	Repeating ratios	Structure
100	35.91	17.97		1:1/2	Lamellar
90	35.53	17.77		1:1/2	Lamellar
80	35.45	17.72		1:1/2	Lamellar
70	35.66	17.84		1:1/2	Lamellar
60	36.69 42.11 47.41	18.35		1:1/2	Lamellar
50	47.40 42.11 39.31	23.72 20.85 19.57 18.69	15.81 13.91 13.35	1:1/2:1/3 1:1/2:1/3 1:1/2:1/3	Lamellar Lamellar Lamellar
40	47.41 40.07	23.71 20.86 19.81 18.48	15.82 13.91 13.31	1:1/2:1/3 1:1/2:1/3 1:1/2:1/3	Lamellar Lamellar Lamellar
30	47.41 40.62	23.72 20.86 20.02 18.54	15.81 13.91 13.28	1:1/2:1/3 1:1/2:1/3 1:1/2:1/3	Lamellar Lamellar Lamellar
20	47.40 40.95	18.55 23.72 20.82 19.69	15.81 13.91 13.26	1:1/2:1/3 1:1/2:1/3 1:1/2:1/3	Lamellar Lamellar Lamellar

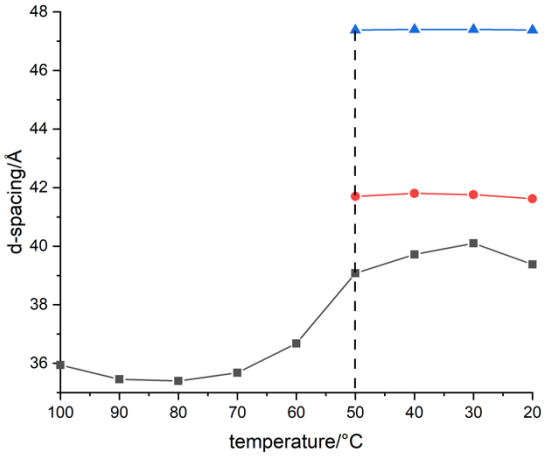

Figure 6-25 Peak position migration vs temperature of AES/HSt (80/20).

As shwon in figure 6-25, the peak at 47.4Å corresponding with 2:1 stearate acid-soap appeared at 50°C. The peak at 41.70Å appeared at the same time, which is corresponding with the AES. The peak around 39Å is corresponding with the stearic

acid. However, the peak position is not stable, which may because of the interaction with AES. When the temperature above 50°C, only one peak was observed in SAXS and the WAXS patterns indicated that the crystals were liquid crystal. The peak migration is different with the AES paste, several transitions may occurred during cooling ramp.

The SAXS patterns of the samples consist 70% AES paste and 30% stearic acid are shown in figure 6-26. The peak around 40Å are complex and the broad peak may consists several peaks. Hence, the peak position confirmation was based on the d002. The peak informations are listed in table 6-8.

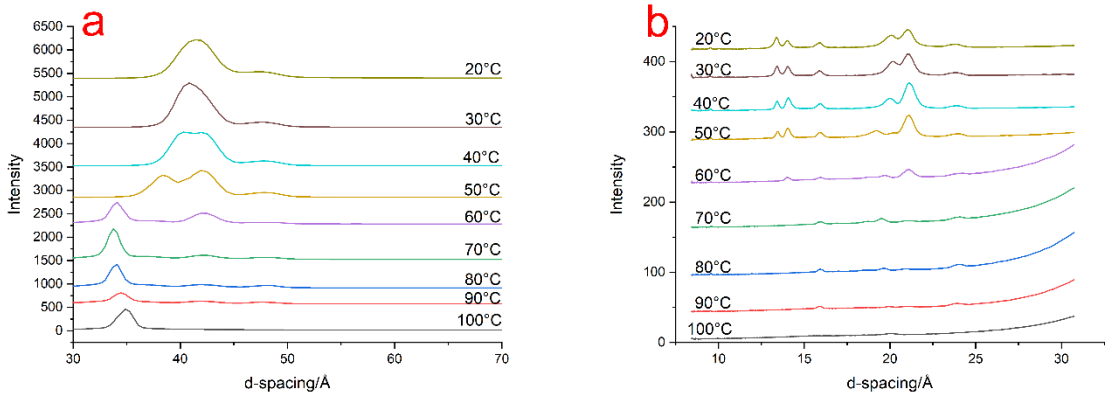

Figure 6-26 The SAXS patterns of AES/HSt (70/30) as function of temperature. a. d001; b, d002 and d003.

Table 6-8 The summary of peak positions of AES/HSt (70/30) at different temperatures.

Temperature/°C	d001/Å	d002/Å	d003/Å	Repeating ratios	Structure
100	34.87	20.07		$1:1/\sqrt{3}$	Hexagonal
90	47.74 41.98 34.4	23.86 20.97 19.86	15.92	$1:1/2:1/3$ $1:1/2$ $1:1/\sqrt{3}$	Lamellar Lamellar Hexagonal
80	48.06 42.37(w) 34.05	24.02 20.92 19.6	15.97	$1:1/2:1/3$ $1:1/2$ $1:1/\sqrt{3}$	Lamellar Lamellar Hexagonal
70	48.01 42.02 37.11 33.80	24.07 21.06 19.48 18.72	16.89 15.9	$1:1/2:1/3$ $1:1/2:1/3$ $1:1/2$ $1:1/\sqrt{3}$	Lamellar Lamellar Lamellar Hexagonal
60	47.89 42.07 37.31 34.00	23.90 21.07 19.67 18.93	15.93 14.04	$1:1/2:1/3$ $1:1/2:1/3$ $1:1/2$ $1:1/\sqrt{3}$	Lamellar Lamellar Lamellar Hexagonal
50	47.72 42.05 38.31	23.94 21.09 20.17 19.21	15.91 14.05 13.45	$1:1/2:1/3$ $1:1/2:1/3$ $1:1/2$ $1:1/2$	Lamellar Lamellar Lamellar Lamellar
40	47.75 42.12 40.3	23.85 21.10 20.02	15.91 14.08 13.41	$1:1/2:1/3$ $1:1/2:1/3$ $1:1/2$	Lamellar Lamellar Lamellar
30	47.71 40.96(b)	23.85 21.07 20.14	15.90 14.04 13.40	$1:1/2:1/3$ $1:1/2:1/3$ $1:1/2$	Lamellar Lamellar Lamellar
20	47.68 41.41(b)	23.80 21.04 20.04	15.90 14.02 13.39	$1:1/2:1/3$ $1:1/2:1/3$ $1:1/2$	Lamellar Lamellar Lamellar

The peaks at 34.87Å and 20.07Å was observed at 100°C, which indicated that the liquid crystal was hexagonal structure. Comparing with the samples contians 20% stearic acid, the d-spacing is smaller and the crystal structure changed from lamellar to hexagonal structure. This is because the increasing amount of stearic acid disrupted the lamellar structure of AES. The possible hexagonal structure is shown in figure 6-27. The chain length of AES is 24.4Å as calculated previously. The d-spacing of hexagonal crystals is smaller than 48.8Å (2×24.4Å), which is because the stearic acid melt dispersed in the hydrophobic tails of AES and the flexibility of alkyl chain was improved.

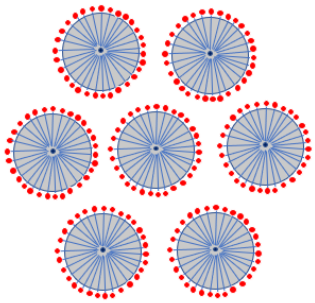

Figure 6-27 The possible hexagonal structure formed at 100°C.

The peak positions of AES/HSt (70/30) is plotted vs temperature as shown in figure 6-28. The peak at 47.74Å corresponding with 2:1 stearate acid-soap formed at 90°C, and the peak corresponding with AES lamellar crystal with d-spacing of 42Å appeared at the same time. Although the samples contains 21.15% stearic acid, the peak at 39.8Å was not observed. Comparing with the AES paste, a peak at 40Å appeared in the mixtures of AES with stearic acid at low temperature. Hence, this peak should be related with stearic acid. The peak corresponding with 2:1 acid-soap is larger than the d-spacing of 2:1 stearate acid-soap determined in chapter 6, whilst the d-spacing corresponding with stearic acid crystals is larger than the results in chapter 5. This

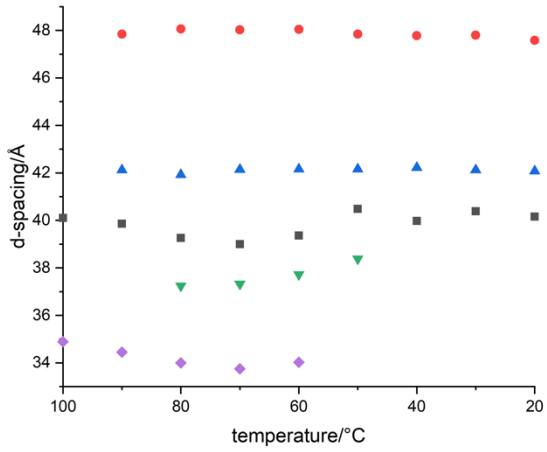

Figure 6-28 The summary of peak position migration of AES/HSt (70/30).

may because that the molecular structure of stearic acid is similar with AES as shown in figure 6-29, the AES can get into the crystals of stearic acid and 2:1 acid-soaps. The introduce of AES in the lamellar crystals also decresed the stability of the crystals and

the peaks were broder than pure materials. As the 70/30 (AES/HSt) samples consists 21 wt% water, the inter-molecular spacing can also be expanded by the water layer. The ethoxylation degree of the AES shwon in figure 6-29 is one. The AES with 0 ethoxylation degree, 49% of the AES used in this project, is more similar with stearic acid. Hence, it is easier to introduce into the crystals of stearic acid and acid-soaps.

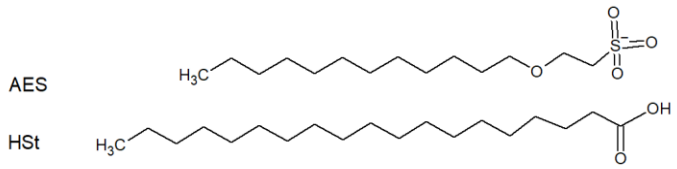

Figure 6-29 The molecule structures of AES and stearic acid.

When the stearic acid ratio increased to 40%, the composition of the mixture is: 18 wt% H_2O, 42 wt% AES, 40 wt% HSt (5.88 mol% neutralised). According to the SAXS patterns shown in figure 6-30, only a very weak peak around 34.86Å was observed in this sample at 100°C. As the intensity is too weak, the repeating peaks cannot be observed. The peak position of the sample contains 30% stearic acid suggested that this peak corresponding with the hexagonal liquid crystal. The peak positions are listed in table 6-9. The peak migrations of 60/40 sample is similar with the 70/30 sample.

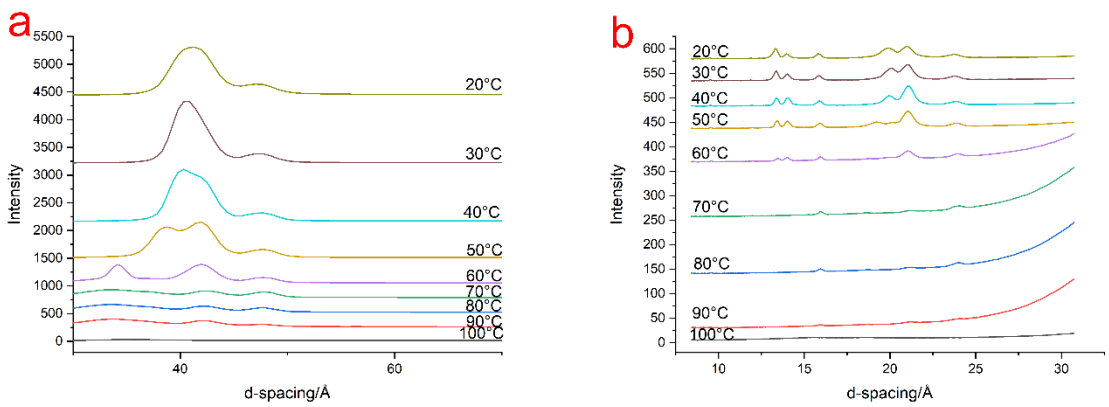

Figure 6-30 The SAXS patterns of AES/HSt (60/40) as function of temperature. a, d001; b, d002 and d003.

Table 6-9 The summary of peak positions of AES/HSt (60/40) at different temperatures. The repeating peaks of the peak at 34.84Å was not observed because of weak intensity, the liquid crystal structure is hexagonal as the position is same with the 70/30.

Temperature/°C	d001/Å	d002/Å	d003/Å	Repeating ratios	Structure
100	34.86				Hexagonal
90	47.77 42.23 33.74	23.95 21.25	15.93	1:1/2:1/3 1:1/2	Lamellar Lamellar Hexagonal
80	47.77 42.17 36.83(w) 33.73	23.94 21.13 18.57(w)	15.96	1:1/2:1/3 1:1/2 1:1/2	Lamellar Lamellar Lamellar Hexagonal
70	47.78 42.42 36.88(w) 33.73	23.97 21.21 18.65(w)	15.97	1:1/2:1/3 1:1/2 1:1/2	Lamellar Lamellar Lamellar Hexagonal
60	47.82 41.97 36.95(w) 34.12	23.93 21.05 19.91(w) 18.85(w)	15.98 14.00 13.46	1:1/2:1/3 1:1/2:1/3 1:1/2:1/3 1:1/2	Lamellar Lamellar Lamellar Lamellar Hexagonal
50	47.77 42.04 38.75	23.92 21.05 20.10 19.24	15.93 14.01 13.42	1:1/2:1/3 1:1/2:1/3 1:1/2:1/3 1:1/2	Lamellar Lamellar Lamellar Lamellar
40	47.75 42.10 40.30	23.85 21.09 19.99	15.90 14.04 13.39	1:1/2:1/3 1:1/2:1/3 1:1/2:1/3	Lamellar Lamellar Lamellar
30	47.63 40.76(b)	23.81 21.03 20.04	15.83 13.99 13.34	1:1/2:1/3 1:1/2:1/3 1:1/2:1/3	Lamellar Lamellar Lamellar
20	47.40 40.69(b)	23.73 20.99 19.92	15.83 13.99 13.34	1:1/2:1/3 1:1/2:1/3 1:1/2:1/3	Lamellar Lamellar Lamellar

The peak positions are plot vs temperature as shown in figure 6-31. Similar with the 70/30 sample, the peak around 47.8Å and 42Å appeared at 90°C. The peak at 47.7Å is corresponding with the 2:1 stearate acid-soap and the peak around 42Å is corresponding with the AES lamellar crystal. With the temperature decresing, a weak peak at 36.8Å appeared at 80°C. The repeating peak corresponding with the peak at 36.8Å was observed around 18.57Å as listed in table 6-9, and the repeating peak corresponding with AES lamellar crystals around 21Å was not affect. Hence, the crystal with d-spacing of 36.8Å is lamellar structure. As temperature decreasing, the d-spacing of this crystal incresed as shown in figure 6-3. This structure is the metastable state of the transformation of hexagonal liquid crystal to AES1 crystal and

stearic acid crystal. The peak corresponding with this metastable crystal disappeared at 40°C.

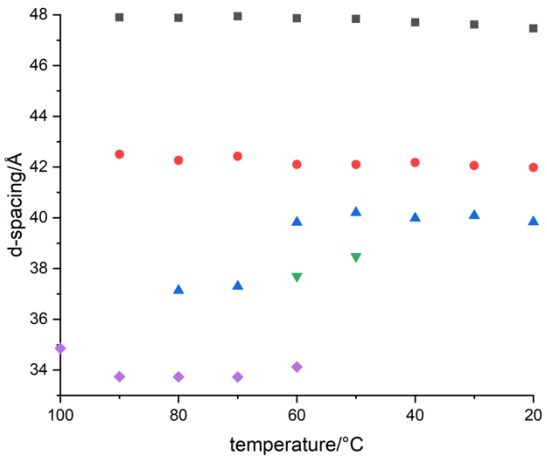

Figure 6-31 The summary of peak position migration of AES/HSt (60/40).

The SAXS patterns of AES/HSt (50/50) are shown in figure 6-32. A weak and broad peak around 32Å was observed at 100°C and no repeating peaks were found. The peaks around 47.7Å and 42Å was appeared at 80°C, which is lower than the samples with higher AES ratios. At 60°C, a broad peak around 42Å with a shoulder was observed. The repeating peaks indicated that this peak consists two peaks at 42.5Å and 40.5Å. When the stearic acid and AES lamellar crystals formed in the samples, the peak at 32Å migrated to larger d-spacing. The peak at 32Å migrated to 37.3Å, and the repeating peaks indicated that the crystal is lamerllar structure. Although the broad peak around 40Å has a shoulder around 38Å at 30°C, the peak cannot be separated because of the weak intensity.

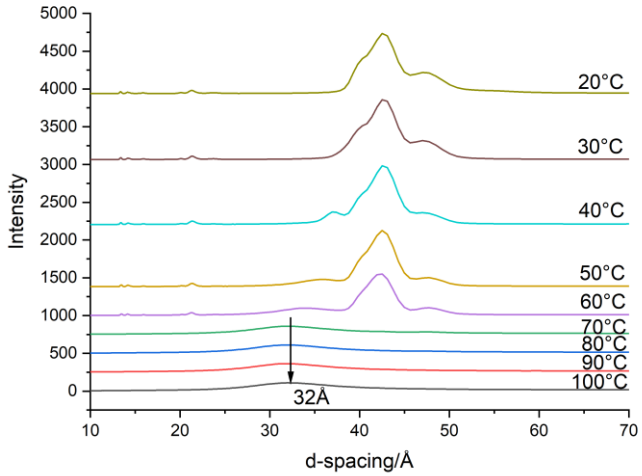

Figure 6-32 The SAXS patterns of AES/HSt (50/50) as function of temperature.

Table 6-10 The summary of peak positions of AES/HSt (50/50) at different temperatures.

Temperature/°C	d001/Å	d002/Å	d003/Å	Repeating ratios	Structure
100	31.96				Micelles
90	31.96				Micelles
80	47.65 31.96				Lamellar Micelles
70	47.65 42.81 32.01				Lamellar Lamellar Micelles
60	47.81 42 33.88	23.92 21.27 20.27	15.96 14.18 13.49	1:1/2:1/3 1:1/2:1/3 1:1/2:1/3	Lamellar Lamellar Lamellar Micelles
50	47.75 42.66 40.41 35.57	23.94 21.34 20.21	15.96 14.19 13.44	1:1/2:1/3 1:1/2:1/3 1:1/2:1/3	Lamellar Lamellar Lamellar
40	47.56 42.73 40.34 37.28	23.78 21.33 20.12 18.61	15.92 14.20 13.43	1:1/2:1/3 1:1/2:1/3 1:1/2:1/3 1:1/2	Lamellar Lamellar Lamellar Lamellar
30	47.56 42.73 40.34	23.72 21.35 20.13	15.91 14.19 13.41	1:1/2:1/3 1:1/2:1/3 1:1/2:1/3	Lamellar Lamellar Lamellar
20	47.56 42.73 40.34	23.73 21.31 20.10	15.91 14.18 13.39	1:1/2:1/3 1:1/2:1/3 1:1/2:1/3	Lamellar Lamellar Lamellar

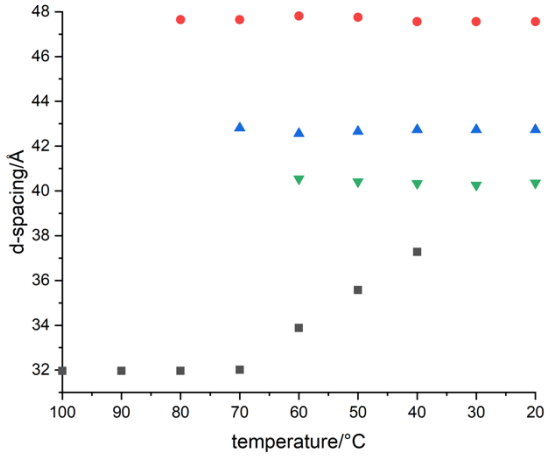

Figure 6-33 The summary of peak position migration of AES/HSt (50/50).

As shown in figure 6-34, a broad peak around 33Å was observed from 100°C to 70°C in AES/HSt (40/60). As the peaks around 33Å are braod and weak, these peaks should be same with the peak around 32Å observed in 50/50 samples. A weak peak at 47.8Å appeared at 80°C and the intensity incresed significantly at 60°C. The peak at 40.68Å corresponding with crystals of stearic acid appeared at 60°C. The repeating peaks indicated that this peak has a shoulder at 42Å, which is corresponding with the AES crystals. As shwon in figure 6-35, the peak around 33Å migrated to 37.38Å at 50°C and disappeared at 40°C. Although the broad peak around 40Å may consists a shoulder, the peak around 38Å cannot be separated because of the weak intensity. This phenomenon is same with the 50/50 samples.

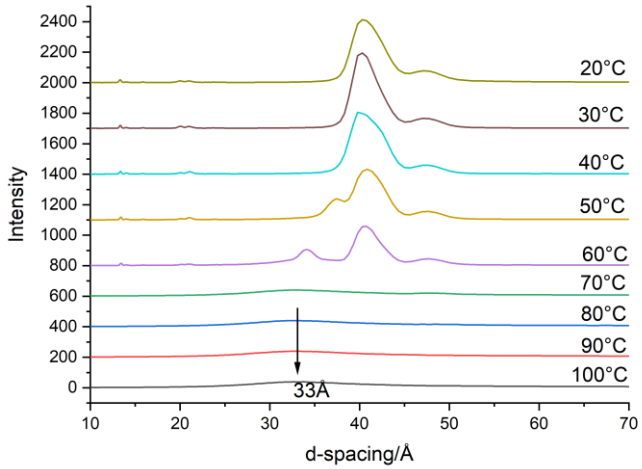

Figure 6-34 The SAXS patterns of AES/HSt (40/60) as function of temperature.

Table 6-11 The summary of peak positions of AES/HSt (40/60) at different temperatures.

Temperature/°C	d001/Å	d002/Å	d003/Å	Repeating ratios	Structure
100	33				Micelles
90	33				Micelles
80	47.8 33				Lamellar Micelles
70	47.8 33				Lamellar Micelles
60	47.76 40.68 34.08	23.91 21.00 20.19	15.89 14.01 13.44	1:1/2:1/3 1:1/2:1/3 1:1/2:1/3	Lamellar Lamellar Lamellar Micelles
50	47.68 40.82 37.38	23.85 21.01 20.15 18.89	15.88 14.02 13.40	1:1/2:1/3 1:1/2:1/3 1:1/2:1/3 1:1/2	Lamellar Lamellar Lamellar Lamellar
40	47.40 40.16	23.83 21.07 20.05	15.89 14.04 13.39	1:1/2:1/3 1:1/2:1/3 1:1/2:1/3	Lamellar Lamellar Lamellar
30	47.31 40.23	23.72 21.00 20.06	15.87 14.01 13.36	1:1/2:1/3 1:1/2:1/3 1:1/2:1/3	Lamellar Lamellar Lamellar
20	47.36 40.52	23.72 21.01 20.01	15.88 13.99 13.33	1:1/2:1/3 1:1/2:1/3 1:1/2:1/3	Lamellar Lamellar Lamellar

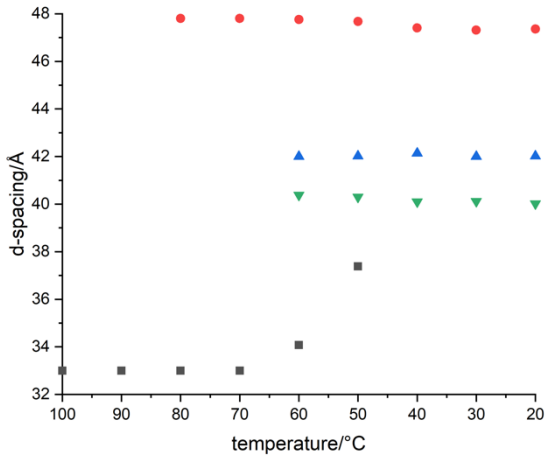

Figure 6-35 The summary of peak position migration of AES/HSt (40/60).

The SAXS patterns of AES/HSt (30/70) is shown in figure 6-36. The broad and weak peak around 31.13Å was observed from 100°C to 60°C. The peak at 47.6Å appeared at 80°C, and the intensity increased as temperature decreasing. The peak corresponding with stearic acid crystals at 40Å appeared at 60°C, which is reasonable that the melting point of stearic acid is around 68°C. And this peak migrated to 39.8Å at 20°C, which is the d-spacing of stearic acid form C crystal. The repeating peaks also suggested that the peak corresponding with the crystal of stearic acid was at 39.8Å. The peak migration of the AES/HSt (30/70) samples is shown in figure 6-37. Comparing with the 40/60 samples, the peak corresponding with AES lamellar crystals disappeared in 30/70 samples, whereas the peak at 37.8Å can still be observed at 20°C.

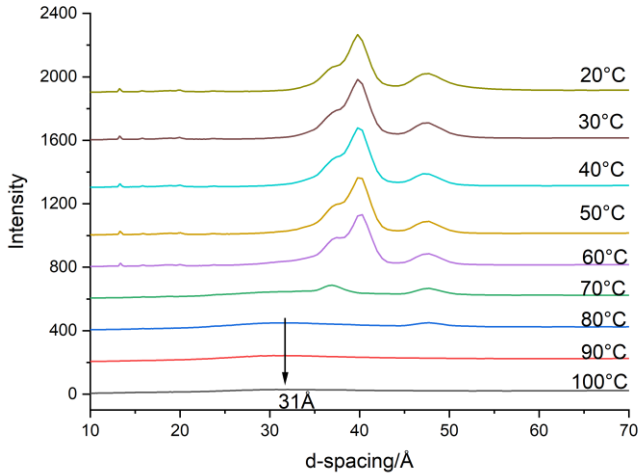

Figure 6-36 The SAXS patterns of AES/HSt (30/70) as function of temperature.

Table 6-12 The summary of peak positions of AES/HSt (30/70) at different temperatures.

Temperature/°C	d001/Å	d002/Å	d003/Å	Repeating ratios	Structure
100	31.13				Micelles
90	31.13				Micelles
80	47.59 31.13		15.84	1:1/3	Lamellar Micelles
70	47.64 36.93 31.11	23.83 18.55	15.85	1:1/2:1/3 1:1/2	Lamellar Lamellar Micelles
60	47.58 40.08 37.50 31.18	23.81 20.06 18.71	15.88 13.37 12.65	1:1/2:1/3 1:1/2:1/3 1:1/2:1/3	Lamellar Lamellar Lamellar Micelles
50	47.45 40.08 37.41	23.81 20.01 18.75	15.87 13.34 12.69	1:1/2:1/3 1:1/2:1/3 1:1/2:1/3	Lamellar Lamellar Lamellar
40	47.41 39.93 37.44	23.72 19.98 18.81	15.82 13.31 12.64	1:1/2:1/3 1:1/2:1/3 1:1/2:1/3	Lamellar Lamellar Lamellar
30	47.45 39.84 37.74	23.72 19.93 18.90	15.80 13.29 12.62	1:1/2:1/3 1:1/2:1/3 1:1/2:1/3	Lamellar Lamellar Lamellar
20	47.46 39.85 37.33	23.75 19.91 18.83	15.78 13.28 12.58	1:1/2:1/3 1:1/2:1/3 1:1/2:1/3	Lamellar Lamellar Lamellar

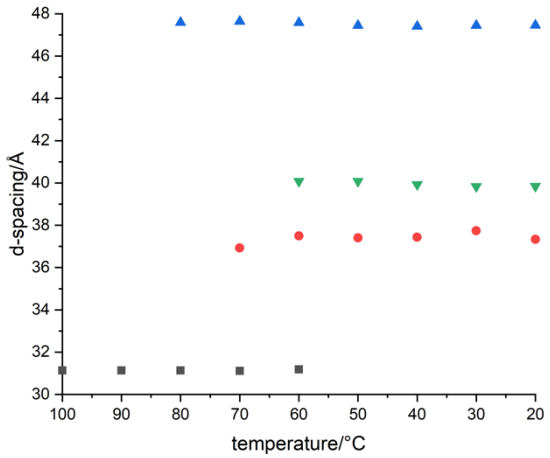

Figure 6-37 The summary of peak position migration of AES/HSt (30/70).

The SAXS patterns of AES/HSt (20/80) are shown in figure 6-38. Two weak peaks at 31Å and 47.4Å were observed at 100°C. The intensity of the peak at 47.4Å increased at 80°C and the repeating peak corresponding with this peak was observed at 80°C. The peak at 31Å migrated to 37.5Å at 70°C. The peak corresponding with stearic acid crystals at 40.05Å was observed at 60°C, which is same with the samples with higher AES ratios. The peak position migration is shown in figure 6-39, the peak migration of 20/80 samples is similar with the 30/70 samples. The peak corresponding with AES lamellar crystals at 42Å was not observed, and the peak around 37.5Å can still be observed at 20°C.

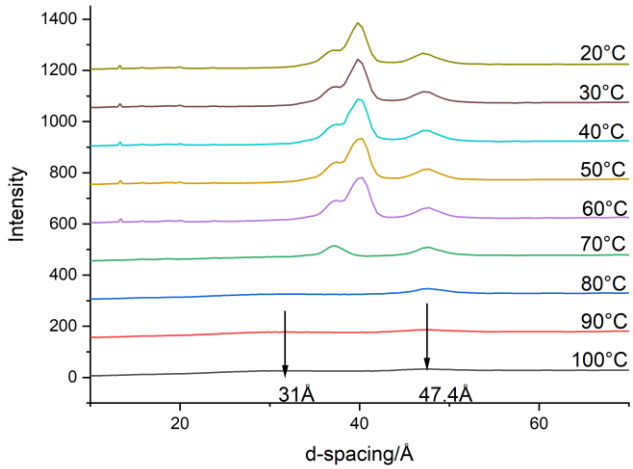

Figure 6-38 The SAXS patterns of AES/HSt (20/80) as function of temperature.

Table 6-13 The summary of peak positions of AES/HSt (20/80) at different temperatures.

Temperature/°C	d001/Å	d002/Å	d003/Å	Repeating ratios	Structure
100	47.45 30.62				Lamellar Micelles
90	47.64 30.55				Lamellar Micelles
80	47.57 30.55		15.83	1:1/3	Lamellar Micelles
70	47.61 37.15	23.86 18.57	15.88 12.67	1:1/2:1/3 1:1/2:1/3	Lamellar Lamellar
60	47.56 40.05 37.22	23.81 20.05 18.74	15.84 13.38 12.67	1:1/2:1/3 1:1/2:1/3 1:1/2:1/3	Lamellar Lamellar Lamellar
50	47.57 39.98 37.37	23.89 20.00 18.77	15.85 13.38 12.68	1:1/2:1/3 1:1/2:1/3 1:1/2:1/3	Lamellar Lamellar Lamellar
40	47.44 39.96 37.41	23.77 19.99 18.75	15.84 13.35 12.63	1:1/2:1/3 1:1/2:1/3 1:1/2:1/3	Lamellar Lamellar Lamellar
30	47.41 39.88 37.30	23.68 19.93 18.83	15.77 13.32 12.60	1:1/2:1/3 1:1/2:1/3 1:1/2:1/3	Lamellar Lamellar Lamellar
20	47.32 39.85 37.10	23.60 19.90 18.82	15.74 13.29 12.85	1:1/2:1/3 1:1/2:1/3 1:1/2:1/3	Lamellar Lamellar Lamellar

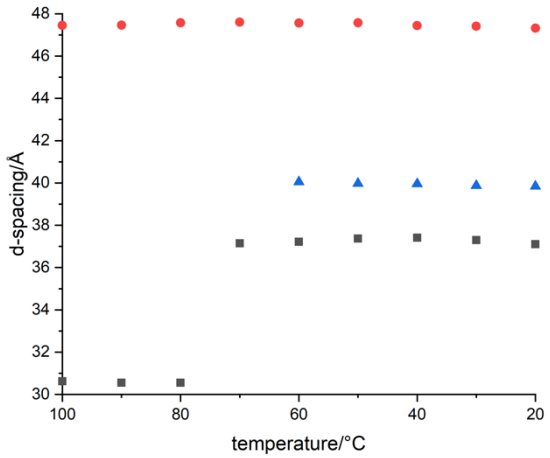

Figure 6-39 The summary of peak position migration of AES/HSt (20/80).

The SAXS patterns of AES/HSt (10/90) is shwon in figure 6-40. The peak at 31Å can still be observed at 100°C and this peak disappeared at 60°C. The intensity of this peak was weak and no repeating peaks were observed. The peak at 37.44Å was appeared at 70°C with weak intensity. A weak peak around 48Å was also observed at 70°C and this peak should be related with the 2:1 acid-soap. The repeating peaks cannot be observed because of the weak intensities. As only 0.46% stearic acid was neutralised by the caustic in AES paste, the 10/90 samples contains 0.42% 2:1 acid-soap. Hence, it is reasonable that the intensity of the peak corresponding with 2:1 acid-soap is weak. The peak corresponding with stearic acid was observed around 40Å. The broad peak around 40Å may consists two peaks at 39.8Å and 40.8Å as observed from 60°C to 40°C.

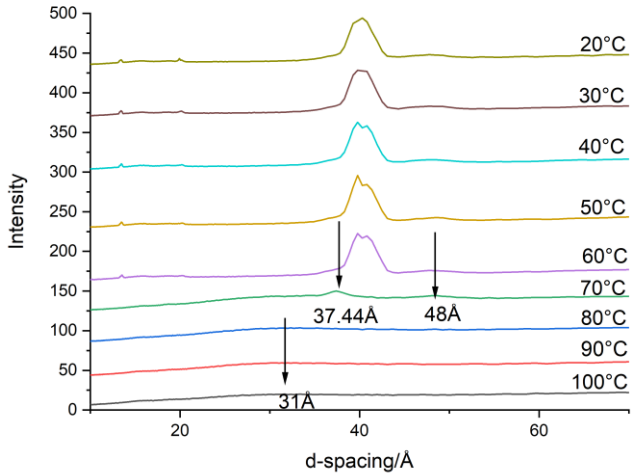

Figure 6-40 The SAXS patterns of AES/HSt (10/90) as function of temperature.

Table 6-14 The summary of peak positions of AES/HSt (10/90) at different temperatures.

Temperature/°C	d001/Å	d002/Å	d003/Å
100	31.23		
90	31.23		
80	31.23		
70	48.28 37.44 31.23		
60	47.86 40.85 39.84 37.41	20.03 18.85	15.85 13.51
50	48.13 40.85 39.85 37.40	20.21 18.76	15.90 13.48
40	48.06 40.85 39.85 37.42	20.23 18.68	15.82 13.47
30	47.89 40.01 37.41	20.16 18.72	15.76 13.43
20	47.84 40.11 37.41	19.91 18.66	15.82 13.42

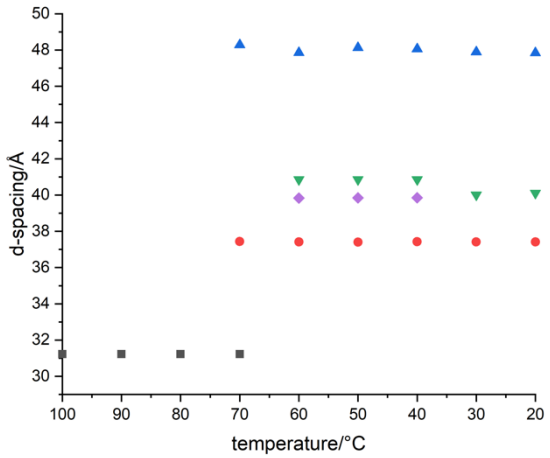

Figure 6-41 The summary of peak position migration of AES/HSt (10/90).

6.3.2.2 Further discussion of the crystal structures

The peak corresponding with 2:1 stearate acid-soap at 47.7Å was observed in the mixtures of AES and stearic acid, which indicated that the 2:1 acid-soap formed in the mixtures. However, the d-spacing of 2:1 acid-soap determined in chapter 6 is 47.3Å, which is smaller than the acid-soap in the mixtures. This is because of the existence of water in the mixtures. The water layer can expand the intermolecular spacing of sodium stearate and stearic acid as shown in figure 6-42. As the molecule structures of AES is similar with stearic acid (figure 6-29), and the strong electronegativity of sulphate group can form hydrogen bonding with the carboxylic group in stearic acid. The chain length of AES is 24.4Å and the chain length of stearic acid is 25.94Å as calculated previously. Assuming the AES formed acid-soaps with stearic acid and the molecules arrangement is same with stearate acid-soaps, the d-spacing can be calculated as:

$$d_{1:1} = \left(24.2\text{Å} + 25.94\text{Å}\right) \times \sin 73.7° = 48.31\text{Å}$$

$$d_{2:1} = \left(24.2\text{Å} + 25.94\text{Å}\right) \times \sin 66° = 45.98\text{Å}$$

The peak at 48.28Å was observed in the AES/HSt (10/90) at 70°C and no peak around 45.98Å was observed in the mixtures.

The peak around 48Å was appeared at 90°C in 70/30 and 60/40 samples, 80°C in 50/50, 40/60 and 30/70. However, the transition point of 2:1 stearate acid-soap is around 80°C. The transition point of the 2:1 acid-soap in the mixtures should be smaller as the neutralisation ratio is small (table 6-3). For instance, the neutralisation ratio of stearic acid in 70/30 samples was 8.85%. And the transition point of 10% neutralisation stearic acid corresponding with 2:1 acid-soap was 70.94°C, which is lower than 80°C. Hence, the broad peak around 48Å consists two peaks: 2:1 stearate acid-soap and 1:1 AES-HSt acid-soap. However, the crystals corresponding with stearic acid and AES lamellar crystals were observed in the mixtures, which suggested that the AES and stearic acid are preferring to form the lamellar crystals respectively, rather than forming the 1:1 acid-soap. Hence, the 1:1 AES-HSt acid-soap are broaden the peak around 48Å and the overlapping caused the d-spacing shifted to higher d-spacing.

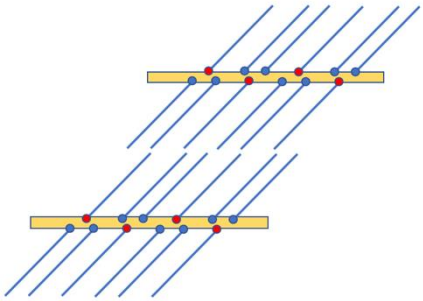

Figure 6-42 The possible molecules arrangement of 2:1 acid-soap with water layer (yellow regions).

The peak positions of the mixtures at 100°C is shown in table 6-15. The samples with 80% AES has a peak at 35.91Å with a repeating peak at 17.97Å, which indicated that the crystal is lamellar crystal. The peak migrated to 34.87Å in the samples with 70% AES, and the repeating peak at 20.01Å indicated that the crystal is hexagonal structure. The peak at 34.86Å was also observed in the samples with 60% AES, and the repeating peaks were not observed, which is because of the weak intensity. When the AES ratio decreased to 50%, the peak migrated to 32Å with no repeating peaks. However, the slop in intermediate q is around -0.37, which indicated that this is not the micelle structure. The peak position and peak shape of 40/60 sample is similar with the 50/50 as shwon in figure 6-41a. When the stearic acid ratio increased to 70%, the

peak intensity decreased significantly and the peak migrated to 31Å (figure 6-43b). The slop of intermediate q is apprx. -1, which is indicated that wormlike micelles formed in the samples.[130] As the peak position of hexagonal liquid crystal and micelles are close, and the intensities of the peak corresponds with micelles are weak, the samples with 50% and 60% stearic acid may contain hexagonal liquid crystals and wormlike micelles at the same time. And the transitions occurred are: lamellar liquid crystal to hexagonal liquid crystal, and then transformed to wormlike micelles.

Table 6-15 The d-spacings of AES/HSt mixtures at 100°C.

AES ratio/%	d-spacing 001/Å	d-spacing 002/Å	Repeating ratio	Structure
80	35.91	17.97	$1:\frac{1}{2}$	Lamellar liquid crystal
70	34.89	20.07	$1:\frac{1}{\sqrt{3}}$	Hexagonal liquid crystal
60	34.86			Hexagonal liquid crystal
50	31.96			Mixtures
40	33			Mixtures
30	31.13			Wormlike micelles
20	30.06			Wormlike micelles
10	31.23			Wormlike micelles

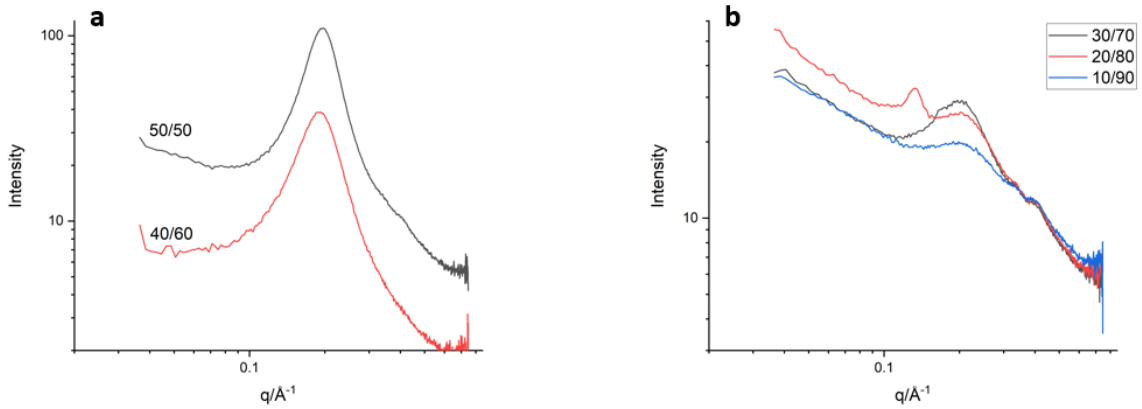

Figure 6-43 The SAXS patterns of AES/HSt mixtures at 100°C on a log-log plot. a. 50/50 and 40/60, one broad peak around 32Å and no repeating peaks were observed. b, 30/70, 20/80 and 10/90.

The d-spacing of the liquid crystal of AES paste at 100°C is at 37.97Å, and the d-spacing of the samples with 20% stearic acid is at 35.91Å, which is smaller than the AES paste. This is because of the stearic acid were penetrated into the hydrophobic

tail of AES surfactant and the flexibility of the alkyl chain is improved. When the AES ratio decreased to 70%, the samples contains 21% water and 30% partially neutralised stearic acid. And the samples with 60% AES contains 18% water and 40% partially neutralised stearic acid. The crystals with d-spacing of 34.86Å were observed in these two samples, as the samples contains more stearic acid than water, the liquid crystal formed should be reversed hexagonal liquid crystal.

The peaks observed in the samples with lower AES ratios has a broad peak around 32Å with no repeating peaks, which is related with the AES micelles. The possible molecules arrangement of these three structures is shown in figure 6-44: a is the liquid crystal of AES with d-spacing of 35.91Å, the structure is similar with the AES, whereas the stearic acid melt dispersed in the hydrophobic tails; b is the reversed hexagonal liquid crystal of AES; c is the micelles of AES formed in stearic acid melt, the water is in the blue circle and the micelles are dispersed in stearic acid melt.

Both the peaks at 35.91Å, 34.86Å and 32Å migrated to 37.5Å when the temperature decreased below the melting point of stearic acid. As the stearic acid crystallized, the flowability of the alkyl chain decresed and the d-spacing of lamellar liquid crystal with d-spacing of 35.91Å increased. And the hexagonal liquid crystals and micelles transformed to lamellar crystals as the decreasing of stearic acid melt.

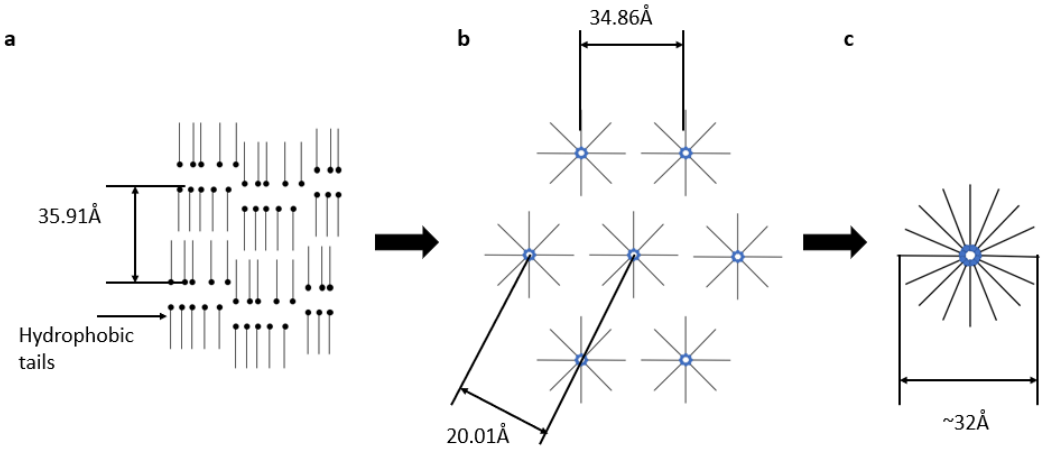

Figure 6-44 The possible crystal structure formed in AES and stearic acid mixtures. a, the lamella liquid crystal with d-spacing of 35.91Å; b, hexagonal liquid crystal with d-spacing of 34.64Å; c, the wormlike micelles with diameter around 32Å and the length is unknown.

6.3.3 The morphologies of crystals formed in the mixture of AES and stearic acid

As the aim of this section is solidifying the surfactant with partially neutralised fatty acid, the crystal morphologies were observed by hot stage microscopy. The liquid crystals of AES at 20°C is shwon in figure 6-45 and there's no obvious transition obseved from 100°C to 20°C. The birefringence obseved in AES indicated that the crystals with d-spacing of 41.17Å is liquid crystal. The crystallisation of AES/HSt (80/20) is shown in figure 6-46. The birefringence was observed from 100°C to 60°C, which indicated that the existence of liquid crystals. Combining with the SAXS/WAXS patterns of AES/HSt (80/20) shown in figure 6-23 and 6-24 and the peak migration shown in figure 6-25, the liquid crystals observed by polarized microscopy is corresponding with the peak around 35.5Å. When the sample was cooled to 60°C, a cloudy area was observed in the visual filed, whilst the birefringence indicated the existence of liquid crystals. The peak corresponding with lamellar liquid crystals at 35.5Å migrated to 36.69Å, and the weak peak at 47.4Å and 42.1Å appeared at 60°C. The intensity of the peaks at 47.4Å and 42.1Å incresed significantly at 50°C. The cloudy area observed at 60°C confirmed that the appearance of crystals, and the cloudy area filled the visual area at 50°C. And there's no other transition observed from 50°C to 20°C.

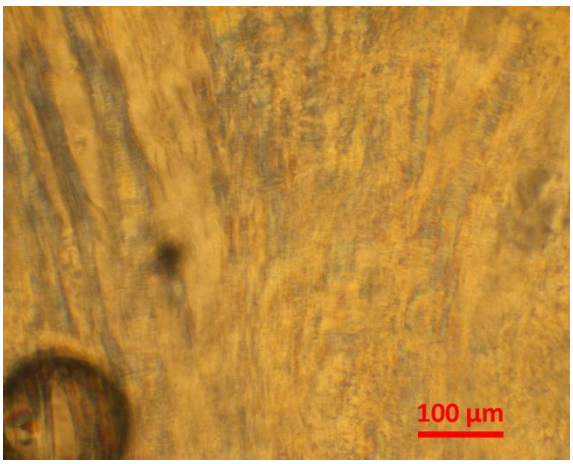

Figure 6-45 The lamellar liquid crystals of AES at 20°C.

When the ratio of stearic acid increased to 50%, the crystallisation process was differnent with the samples with 20% stearic acid. As shown in figure 6-47, the birefringence was not observed at from 100°C to 60°C, which indicated that no liquid crystals formed in the samples and the peak around 32Å is corresponding with the micelle structure. A crystal was observed at 80°C as shown in the red circle in figure 6-46 and the crystal size is around 42µm. The appearance of this crystal verified that the weak peak at 47.65Å observed at 80°C in SAXS pattern. More crystals were formed at 70°C, and it is not possible to link these crystals with the specific crystals as

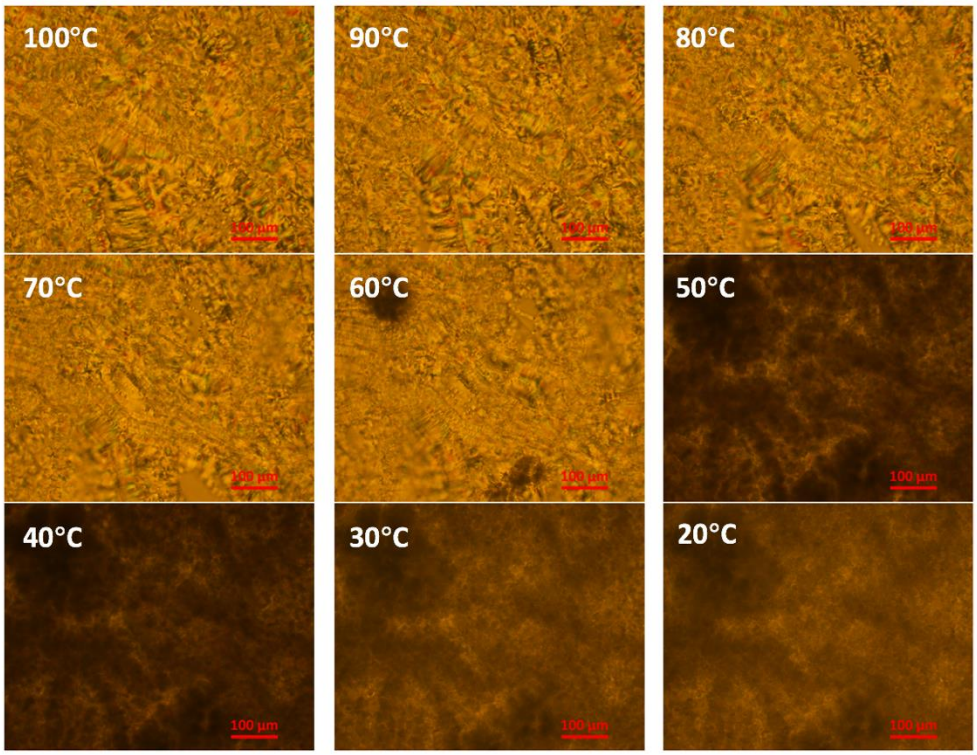

Figure 6-46 The crystallisation of AES/HSt (80/20). The sample was cooled down from 100°C to 20°C, 10°C/min, and equilibrium for 2mins.

there were two peaks at 47.65Å and 42.81Å appeared at 70°C in SAXS pattern. The visual area became cloudy at 60°C and this is because of the transition of micelles to lamellar crystals. The peak migration of 50/50 shown in figure 6-33 indicated that the peak corresponding with micelles around 32Å migrated to 33.9Å at 60°C, and this peak migrated to higher d-spacing as temperature decreasing. This transition was observed by the polarized microscopy at 50°C, a dard area was formed in the samples as shwon in the yellow circle in figure 6-47. And this dark area growing larger as temperature decreasing, and this transition reached stable state at 30°C as no obvious

differences were observed between 30°C and 20°C. The SAXS patterns also comfirmed this conclusion.

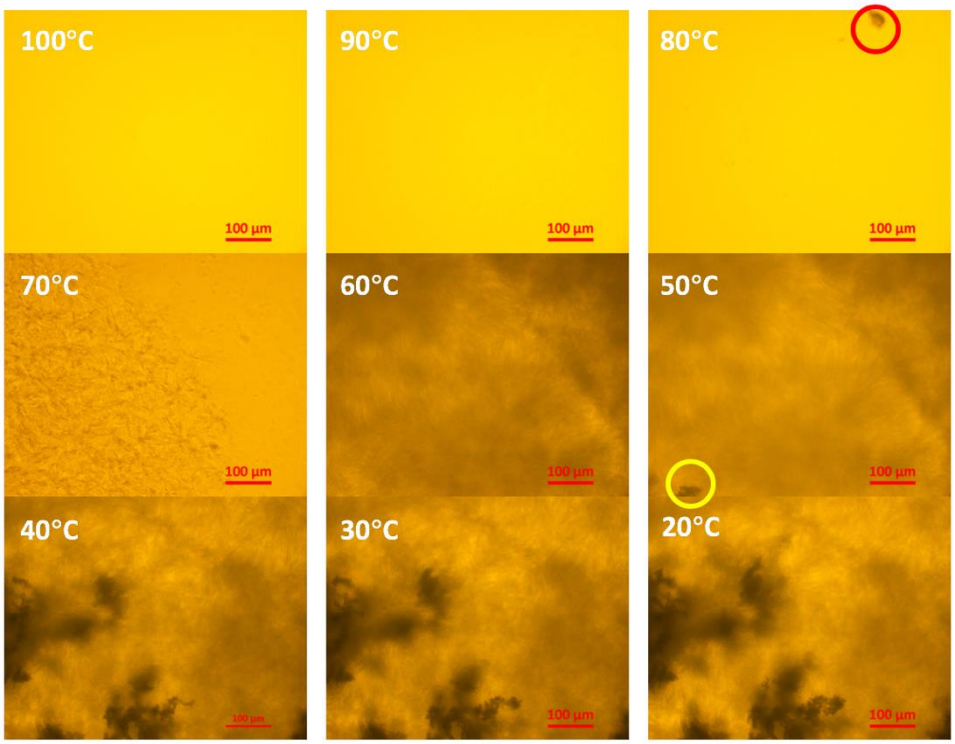

Figure 6-47 The crystallisation of AES/HSt (50/50). The sample was cooled down from 100°C to 20°C, 10°C/min, and equilibrium for 2mins.

As shwon in figure 6-48, the transparency of the sample decreased at 80°C, whereas the peak at 48.28Å and 37.44Å appeared at 70°C in SAXS patterns. The decrese of transparency may because of the crystallisation and this was not observed in SAXS pattern is because of the weak intensities. The crystallisation corresponding with the stearic acid was observed at 60°C, and the peak corresponding with stearic acid around 40Å were observed in SAXS pattern at 60°C. There's no obvious transition observed from 60°C to 20°C and the SAXS patterns also confirmed this. As the crystals stacked together and it's hard to observe the morphologies, the edge of the 10/90 sample was observed as shown in figure 6-49: the ribbon-like crystals corresponding with stearic acid was found and the birefringence was observed in the red circle.

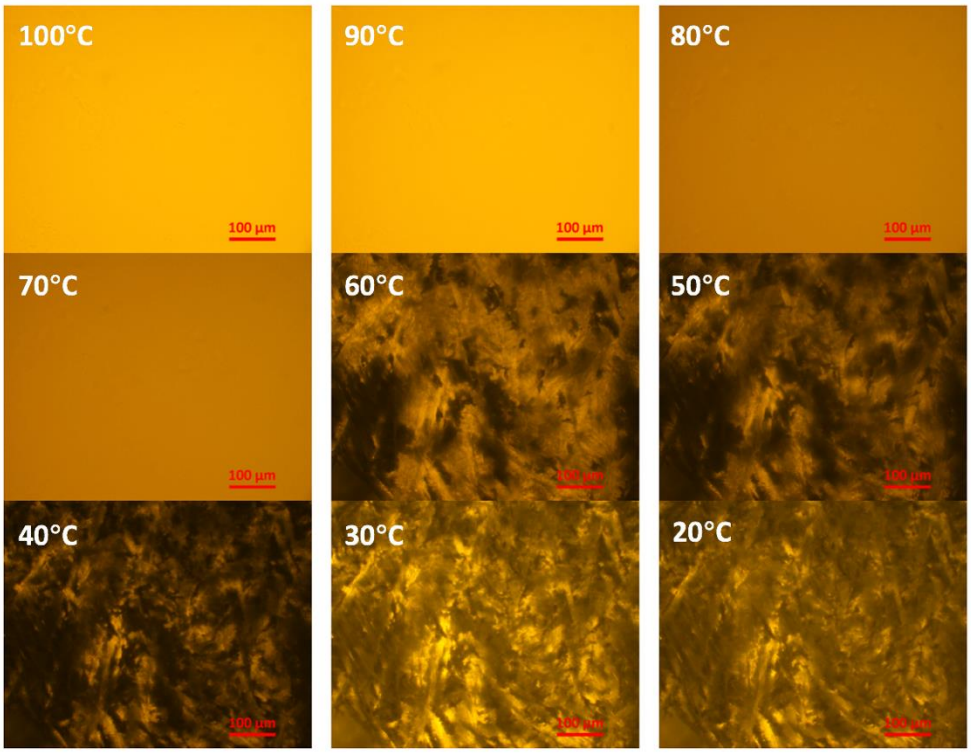

Figure 6-48 The crystallisation of AES/HSt (10/90). The sample was cooled down from 100°C to 20°C, 10°C/min, and equilibrium for 2mins.

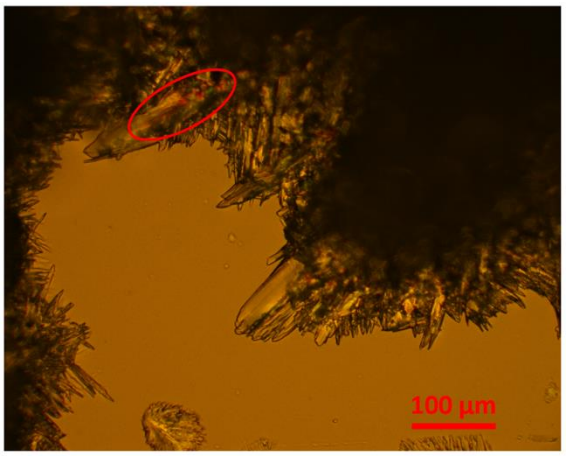

Figure 6-49 The edge of the AES/HSt (10/90) at 20°C. Ribbon-like crystals were observed.

The samples with 75% AES and 25% stearic acid was observed by the cryo-SEM as shown in figure 6-50. The lamellar crystals corresponding with stearic acid and acid-soaps were dispersed in AES lamellar crystals (figure 6-50a). The layers of AES lamellar liquid crystals were clear in figure 6-50c. Comparing the orientation of AES liquid crystals in b and c, the liquid crystals near the stearic acid/acid-soap crystals are following the orientation of the crystals of stearic acid/acid-soaps, whereas the orientation away from the crystals of stearic acid/acid-soaps were random. The AES was penetrated into the lamellar crystals of stearic acid/acid-soaps as shwon in figure 6-50b, and the bend in the red circle may because of the AES interupted the lamellar structure of stearic acid/acid-soaps. Another evidence is the lamellar crystals corresponding with stearic acid/acid-soaps are more sensitive to the electrons than pure materials. As shwon in figure 6-50d, the crackles on the surface of lamellar crystals were induced by the electrons, which is because of the materials sensitive to the electrons penetrated into the lamellar structures.

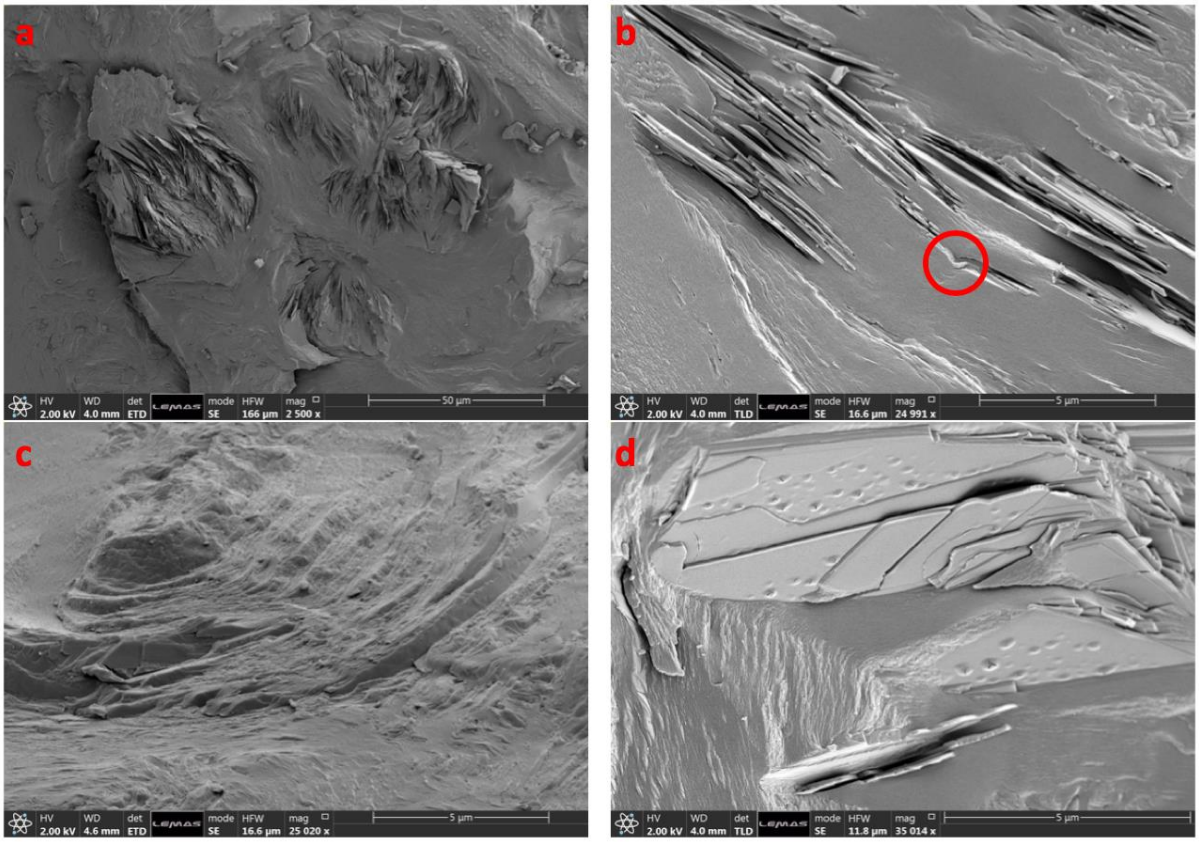

Figure 6-50 The Cryo-SEM images of the mixture of AES/HSt (75/25).

6.4 Conclusions

The characteristic peak associates with 1:1 acid-soap at 49.8Å was observed in the NI/HSt mixtures, which confirmed the formation of acid-soaps. However, the phase transition temperatures were lower than pure acid-soaps, which suggested that there's interactions between acid-soaps and non-ionic surfactants. A crystal with similar phase behaviour with 1:1 stearate acid-soaps was observed in the NI/PSFA mixtures. The d-spacing calculated with extended alkyl chain length and tilt angle of stearate acid-soaps is close to the experimental results, which indicated that the acid-soap formed by palm-sterin fatty acid has similar structure with stearic acid.

The d-spacing of 2:1 acid-soap formed in AES/HSt mixtures migrated to higher d-spacing, which is different with the non-ionic surfactant. The calculated d-spacing of the crystals formed by AES and stearic acid is close to the bump observed in SAXS patterns, which indicated that the AES has tendency to form acid-soap lamellar structures. This is because the hydrophilic head group of AES are electronegative, which can form hydrogen bond with stearic acid. This phenomenon could be side evidence of the interactions in acid-soaps are hydrogen bonds. This phenomenon cannot be observed in non-ionic surfactant is because the hydrophilic head group does not ionised.

Chapter 7 The influence of perfume on the crystal structure of AES and stearic acid

Characterisation of influence of perfumes on the crystals of acid-soaps and liquid crystals of alcohol ethoxylate sulfonates

7.1 Introduction

The perfumes are common ingredients of consumer products and they were added to the products at low percentage. The perfumes are complex mixtures contain synthetic materials and natural products.[131] The perfumes for laundry products are typically mixtures of small molecular weight and oil soluble components. As the perfumes are sensitive to temperature, which caused the high weight loss during manufacturing. The propose of this chapter is trapping the perfumes in the hydrophobic tails of AES and reduce the evaporation. The crystal structures of AES/HSt mixtures were determined in last chapter, and the influence of the perfume oils on the structures of AES, HSt and AES/HSt mixtures will be investigated.

This chapter begins with the influence of the perfumes on the stearic acid crystals. SAXS/WAXS was the main technique used to determine the crystal structure of stearic acid, and the polarized hot-stage microscopy was used to observe the crystallisation process of stearic acid and verifying the SAXS/WAXS results. Following this, the influence of the perfumes on the liquid crystal structure of AES was examined. And then, the mixtures of these three components were examined by SAXS/WAXS, hot-stage microscopy and cryo-SEM.

7.2 The influence of perfume on stearic acid crystals

7.2.1 The DSC of stearic acid and perfume mixtures

The DSC curves of stearic acid/perfume mixtures are shown in figure 7-1. The melting point of stearic acid is 68.7°C, which is consistent with the previous results. The melting point decreased to 62°C in the samples consist 90% stearic acid and 10% perfume. The hackly peak indicated that the crystals of stearic acid were disrupted by the perfume. The melting point corresponding with stearic acid was not stable as shown in table 7-1. The melting temperatures were decreased as the perfume content increasing and the Tm has linear relationship with the perfume content as shown in figure 7-2. The baseline of the samples contain perfume are not flat, especially when the ratio above 50%, which is because of the evaporation of perfume. It is clear that the sample contains 10% stearic acid has a broad and weak peak appeared after the melting peak corresponding with stearic acid, and that broad peak covered from 67.7°C to 150°C (the end temperature of the heating ramp).

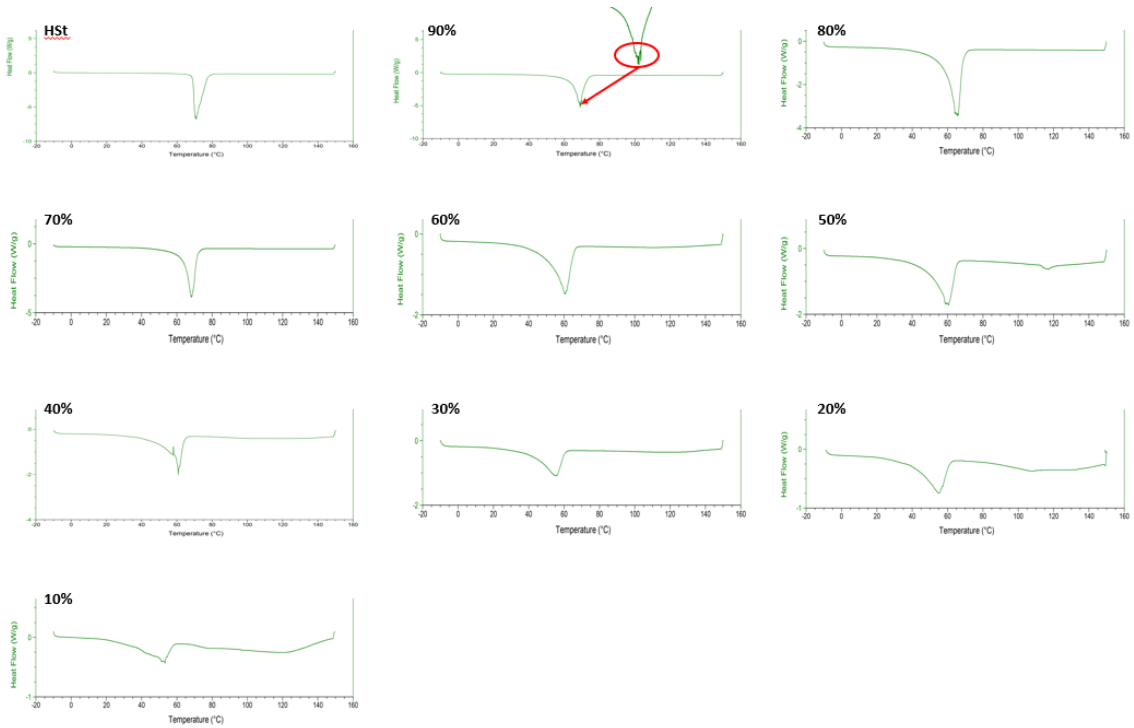

Figure 7-1 The DSC curves of the stearic acid/perfume mixtures. The red circle is the hackly peak of the sample contains 10% perfume.

Table 7-1 The onset temperature of stearic acid/perfume mixtures.

HSt ratio/ wt%	100	90	80	70	60	50	40	30	20	10
Melting temperature/°C	68.7	62.0	55.7	62.7	48.3	45.4	43.4	37.3	36.1	25.5

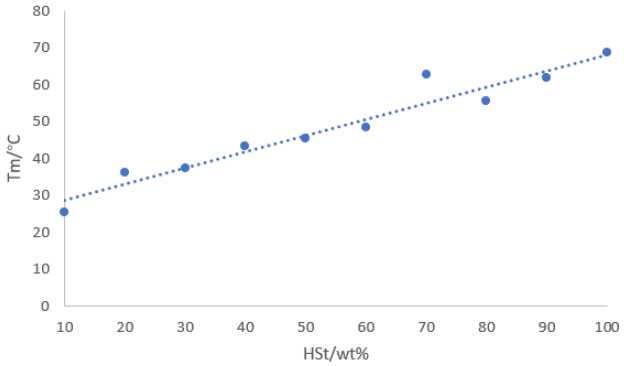

Figure 7-2 The melting temperature corresponding with stearic acid in the mixtures of stearic acid and perfume. And the melting temperature showed linear relationship with the stearic acid ratio.

7.2.2 The SAXS patterns of stearic acid and perfume mixtures

Based on the DSC results, the crystal structures of stearic acid were measured by SAXS from 20°C to 70°C. The intensity of the crystals corresponding with stearic acid is weak in the samples contain 10% stearic acid as shown in figure 7-3a, which is because the stearic acid was dissolved in the perfume and this had been verified that no peaks were observed in the samples contain 5% stearic acid (figure 7-3b). Three peaks at 39.8Å, 45.1Å and 46.6Å was observed in the samples with 10% stearic acid, and the peak at 39.8Å has a shoulder with larger d-spacing. The crystals with d-spacing of 39.8Å is corresponding with the stearic acid. And the crystals with larger d-spacing is because of the perfume penetrated into the lamellar crystals of stearic acid, the increased flexibility of the alkyl chain changed the molecules arrangement of stearic acid. The observed repeating peaks indicated that the crystals with d-spacing of 39.8Å, 45.1Å and 46.6Å are lamellar structure (table 7-2). A peak at 40.7Å appeared at 30°C, which is the shoulder of the peak at 39.8Å observed at 20°C. The intensity

of the peaks at 45.1Å and 46.6Å decreased at 30°C, and this consist with the DSC result that the melting point of the samples with 10% stearic acid is at 25.5°C.

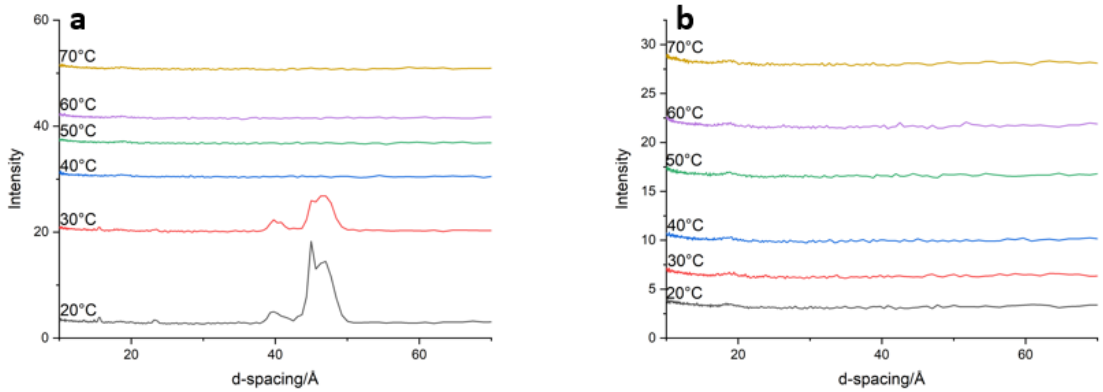

Figure 7-3 The SAXS patterns as function of temperature. a, the samples with 10% stearic acid, the peak at 39.8Å is corresponding with stearic acid, the peak at 45.1Å and 46.6Å is the expanded lamellar crystals of stearic acid. b, the samples with 5% stearic acid, the stearic acid was dissolved in the perfume and no peak was observed.

Table 7-2 The d-spacing of the crystals formed in the samples with 10% stearic acid. No peaks were observed above 40°C. Some of the repeating peaks were not observed because of the weak intensities.

Temperature/°C	d-spacing (d001)/Å	d-spacing (d002)/Å	d-spacing (d003)/Å	Repeating ratios	Structure
20	39.8				Lamellar
	45.1		14.9	1:1/3	Lamellar
	46.6	23.3	15.5	1:1/2:1/3	Lamellar
30	39.8				Lamellar
	40.7		13.5	1:1/3	Lamellar
	45.1		14.9	1:1/3	Lamellar
	46.6	23.4	15.5	1:1/2:1/3	Lamellar
40					
50					
60					
70					

When the stearic acid ratio increased to 20%, the peak at 40.0Å was from 20°C to 40°C. As shown in figure 7-4b, a small peak around 45Å was observed in log-log plot at 20°C. This peak was also observed at 30°C. Hence, the stearic acid lamellar crystals formed in the samples contain 20% stearic acid and the intermolecular spacing of part of the crystals was expanded because of the perfume. The peak

intensity of the peak at 40.0Å decreased from 30°C to 40°C, and the peak disappeared at 50°C. This phenomenon consists with the DSC results that the melting point of the samples with 20% stearic acid is 36.1°C. The repeating ratios indicated that the crystals with d-spacing of 40.0Å is lamellar structure (table 7-3). As the intensity of the peak around 45Å is too weak, the repeating peaks corresponding with this peak cannot be observed. As this peak is similar with the peak at 45.1Å in the samples contain 10% stearic acid, the crystal with d-spacing around 45Å should be lamellar structure.

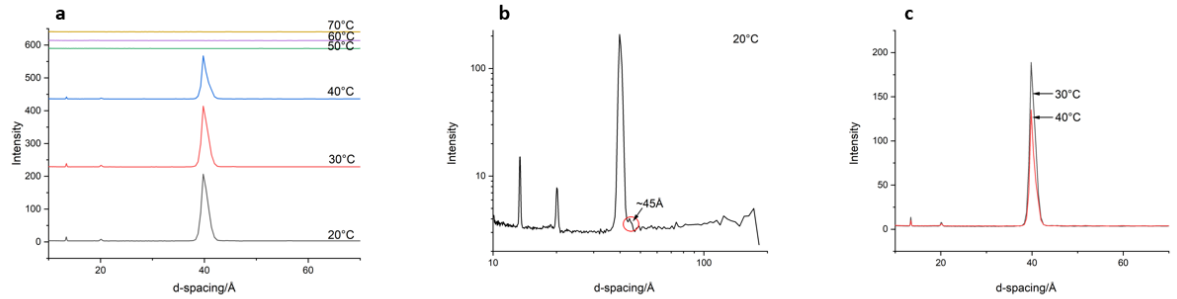

Figure 7-4 The SAXS patterns of the samples with 20% stearic acid and 80% perfume. a, the SAXS patterns from 20°C to 70°C. b, log-log plot of SAXS data at 20°C. c, comparing the peak intensity of the peak at 40.0Å at 30°C and 40°C.

Table 7-3 The d-spacing of the crystals formed in the samples contain 20% stearic acid and 80% perfume. The expanded lamellar crystals of stearic acid with d-spacing around 45Å was observed at 20°C and 30°C. No peak was observed above 50°C.

Temperature/°C	d-spacing (d001)/Å	d-spacing (d002)/Å	d-spacing (d003)/Å	Repeating ratios	Structure
20	40.0 ~45	20.1	13.4	$1:1/2:1/3$	Lamellar
30	40.0 ~45	20.1	13.4	$1:1/2:1/3$	Lamellar
40	39.9	20.1	13.4	$1:1/2:1/3$	Lamellar
50					
60					
70					

The samples contain 30% stearic acid have two peaks at 39.8Å and 40.8Å at 20°C. The peak at 39.8Å is corresponding with the form C lamellar crystal of stearic acid, and the peak at 40.8Å is the expanded lamellar crystals of stearic acid (figure 7-4a). When the temperature reached 40°C, the peak intensities decreased and a shoulder

with larger d-spacing appeared (figure 7-4b). This consist with the DSC results that the melting point of the samples contain 30% stearic acid is at 37.3°C. A broad peak around 16Å was observed in the samples and this peak is corresponding with the Kapton tape mount the samples in the holder. As the peak intensities were weak and the peak position of the two peaks were close, it's not possible to separate the repeating peaks.

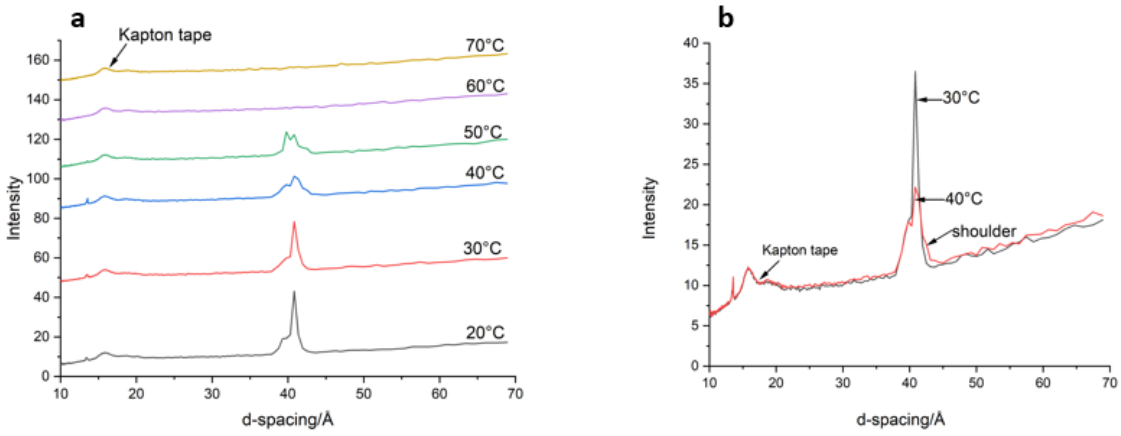

Figure 7-5 The SAXS patterns of the samples with 30% stearic acid and 70% perfume. a, the SAXS patterns from 20°C to 70°C. b, comparing the peak intensities at 30°C (black) and 40°C (red). The peak intensities drop indicated that the melting occurred between 30°C and 40°C. A shoulder at larger d-spacing was observed at 40°C, this shoulder was also observed at 50°C.

Table 7-4 The d-spacing of the samples contain 30% stearic acid and 70% perfume. Two peaks were observed at 20°C and 30°C. A shoulder around 42.5Å appeared at 40°C. No peak was observed above 60°C.

Temperature/°C	20	30	40	50	60	70
d-spacing (d001)/Å	40.8 39.8	40.8 39.8	40.8 39.8 ~42.5 (shoulder)	40.8 39.8 ~42.5 (shoulder)		

As shown in figure 7-6a, two peaks at 39.2Å and 40.8Å were observed at 20°C in the samples with 40% stearic acid and 60% perfume. The repeating peaks corresponding with the peak at 39.2Å were at 19.8Å and 13.2Å, which indicated that the d-spacing of the crystals is slightly larger than 39.2Å. And the repeating peaks following the $1: 1/2 : 1/3$ repeating ratios, which indicated that the crystal is lamellar structure. The

peak at 40.8Å was also observed in the samples with 30% stearic acid and 70% perfume, which is the expanded lamellar crystal of stearic acid. No obvious transition was observed below 40°C and this consists with the DSC results that the melting point of this sample is 43.4°C. By comparing the peaks of the sample at 40°C and 50°C as shown in figure 8-6b, the intensity of the peak at 39.3Å decreased significantly and the peak at 40.8Å split into two peaks at 41.3Å and 40.4Å. As the repeating peaks corresponding with the peak at 40.8Å were at 20.2Å and 13.4Å, which is close to the peak at 40.4Å. This phenomenon indicated that the peak at 40.8Å consists two peaks at 40.4Å and 41.3Å, the intermolecular spacing of the crystal with d-spacing of 39.3Å increased to 40.4Å as the temperature increasing.

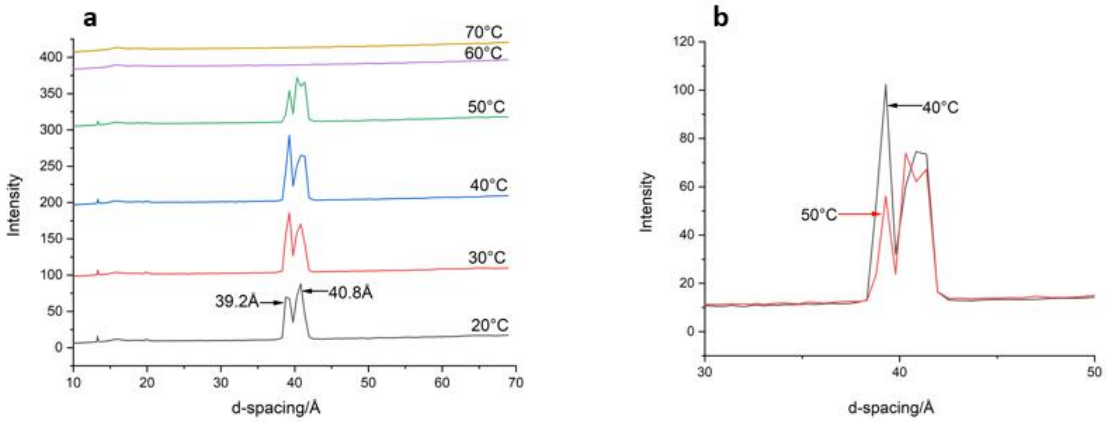

Figure 7-6 The SAXS patterns of the samples with 40% stearic acid and 60% perfume. a, the SAXS patterns from 20°C to 70°C. b, comparing the peak intensities at 40°C (black) and 50°C (red). The peak at 40.8Å split into two peaks at 40.4Å and 41.3Å.

Table 7-5 The d-spacing of the crystals formed in the samples contain 40% stearic acid and 60% perfume. The repeating peaks indicated that the crystals are lamellar structure. The peaks were disappeared at 60°C.

Temperature/°C	d-spacing (d001)/Å	d-spacing (d002)/Å	d-spacing (d003)/Å	Repeating ratios	Structure
20	40.8 39.2	20.1 19.8	13.4 13.2	1:1/2:1/3 1:1/2:1/3	Lamellar Lamellar
30	40.8 39.2	20.2 19.8	13.4 13.3	1:1/2:1/3 1:1/2:1/3	Lamellar Lamellar
40	41.0 39.3	20.2 19.8	13.4 13.3	1:1/2:1/3 1:1/2:1/3	Lamellar Lamellar
50	41.3 40.4 39.3	20.2 19.8	13.4 13.3	1:1/2:1/3 1:1/2:1/3	Lamellar Lamellar
60					
70					

The SAXS patterns of the samples contain 50% stearic acid and 50% perfume is shown in figure 7-7. As the intensities of the peaks were weak, it's not easy to fit the peaks and configure the peak positions. The broad peak around 40Å consists two peaks at 40.4Å and 39.2Å at 20°C, which is similar with the samples with 40% stearic acid and 60% perfume. The melting of the crystals occurred between 40°C and 50°C as shown in figure 7-7b, the intensities of the peaks decreased significantly at 50°C and all the peaks disappeared at 60°C. The d-spacings of the crystals are listed in table 7-6, the repeating peaks were not listed because of the weak intensities. As the peak positions of the samples contains 50% stearic acid are similar with the samples contains 40% stearic acid, the crystals formed in these two samples should be the same.

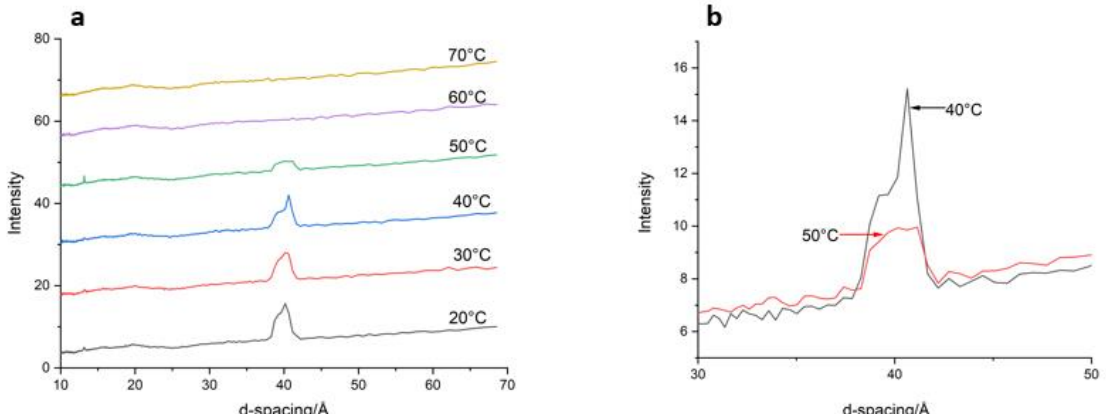

Figure 7-7 The SAXS patterns of the samples with 50% stearic acid and 50% perfume. a, the SAXS patterns from 20°C to 70°C. b, comparing the peak intensities at 40°C (black) and 50°C (red). The intensities of the peaks decreased, which indicated that part of the crystals were melted at 50°C. This conformed with the DSC result that the melting point is 45.4°C.

Table 7-6 The d-spacing of the samples contain 50% stearic acid and 50% perfume. The repeating peaks were not observed because of the weak intensities. A broad peak around 40Å was observed at 50°C and this peak may consist three peaks, which is similar with the samples contain 40% stearic acid and 60% perfume.

Temperature/°C	20	30	40	50	60	70
d-spacing (d001)/Å	40.4 39.2	40.4 39.2	40.6 39.2	~40		

It is obvious that the samples contain 60% stearic acid and 40% perfume have two peaks at 39.2Å and 41.4Å at 20°C. However, the d002 and d003 corresponding with these two peaks indicated that the peak positions are at 39.6Å and 40.8Å (table 7-7). The repeating ratios are following $1: 1/2 : 1/3$, which indicated that the crystals are lamellar structure. The intermolecular spacing of the crystals with d-spacing of 41.4Å was expanded to 41.7Å at 50°C, whilst no obvious intensity change was observed. The peak intensities dropped between 50°C to 60°C. This phenomenon conformed with the DSC results that the melting point of this sample is at 48.3°C.

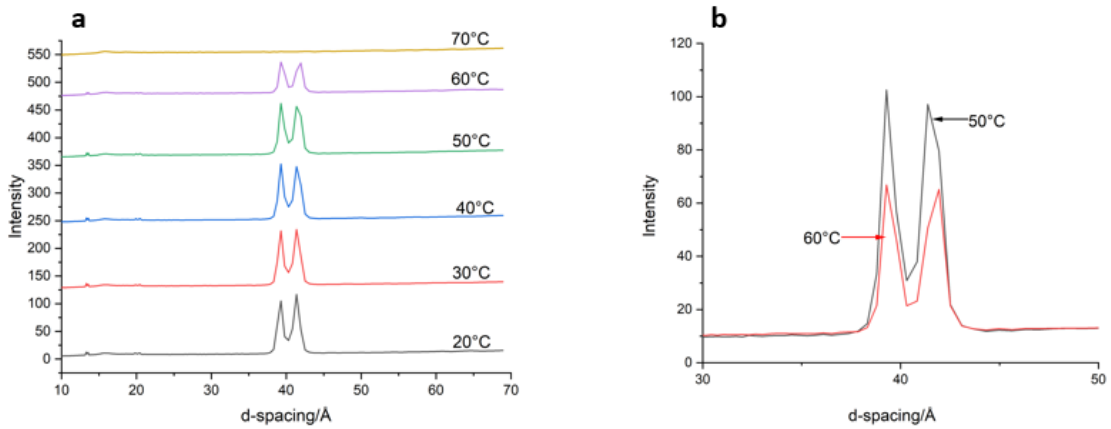

Figure 7-8 The SAXS patterns of the samples with 60% stearic acid and 40% perfume. a, the SAXS patterns from 20°C to 70°C. b, comparing the peak intensities at 50°C (black) and 60°C (red).

Table 7-7 The d-spacing of the crystals formed in the samples contain 60% stearic acid and 40% perfume. The repeating peaks indicated that the crystals are lamellar structure. The peaks were disappeared at 70°C.

Temperature/°C	d-spacing (d001)/Å	d-spacing (d002)/Å	d-spacing (d003)/Å	Repeating ratios	Structure
20	39.2 41.4	19.8 20.4	13.3 13.6	1:1/2:1/3 1:1/2:1/3	Lamellar Lamellar
30	39.2 41.4	19.8 20.4	13.3 13.6	1:1/2:1/3 1:1/2:1/3	Lamellar Lamellar
40	39.2 41.4	19.9 20.4	13.3 13.6	1:1/2:1/3 1:1/2:1/3	Lamellar Lamellar
50	39.2 41.7	19.9 20.5	13.4 13.6	1:1/2:1/3 1:1/2:1/3	Lamellar Lamellar
60	39.4 41.7	20.0 20.6	13.4 13.6	1:1/2:1/3 1:1/2:1/3	Lamellar Lamellar
70					

When the stearic acid ratio increased to 70%, only one broad peak at 40.2Å was observed from 20°C to 50°C and no peak split was observed in the repeating peaks. A shoulder around 41.4Å was observed at 60°C as shown in the red circle in figure 7-9a and blue circle in figure 7-9b. This peak was observed in the samples with 60% stearic acid and 40% perfume, which is corresponding with the expanded lamellar crystals of stearic acid. The melting point of the samples contain 70% stearic acid and 30% perfume determined by DSC is 62.7°C, which is away from the linear relationship of melting point with stearic acid ratio. The melting process was observed between 50°C and 60°C, which conformed with the linear relationship.

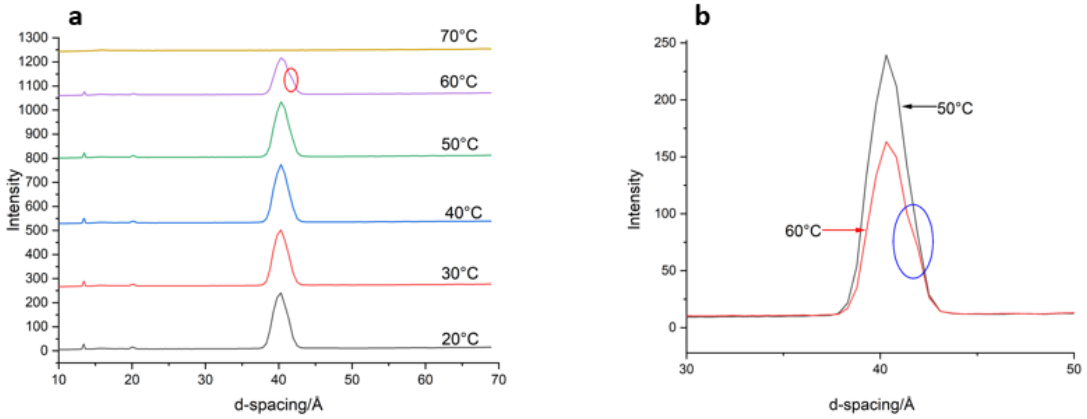

Figure 7-9 The SAXS patterns of the samples with 70% stearic acid and 30% perfume. a, the SAXS patterns from 20°C to 70°C. b, comparing the peak intensities at 50°C (black) and 60°C (red). The red circle in a and blue circle in b is the shoulder around 41.4Å at 60°C.

Table 7-8 The d-spacing of the crystals formed in the samples contain 70% stearic acid and 30% perfume. The repeating peaks indicated that the crystals are lamellar structure. The peaks were disappeared at 70°C. No repeating peak of the peak at 41.4Å was observed because of the weak intensity.

Temperature/°C	d-spacing (d001)/Å	d-spacing (d002)/Å	d-spacing (d003)/Å	Repeating ratios	Structure
20	40.2	20.1	13.4	$1:1/2:1/3$	Lamellar
30	40.2	20.1	13.4	$1:1/2:1/3$	Lamellar
40	40.2	20.1	13.4	$1:1/2:1/3$	Lamellar
50	40.2	20.1	13.4	$1:1/2:1/3$	Lamellar
60	40.2 41.4	20.1	13.4	$1:1/2:1/3$	Lamellar
70					

One peak at 40.2Å was observed in the samples with 80% stearic acid and 20% perfume at 20°C. And this peak has two shoulders around 39.2Å and 41.4Å as shown in figure 7-10. Although the shoulders were observed in d001, the repeating peaks were not observed. This may because that the intensities of the peaks are weak and the d-spacing of too close. No obvious transition was observed from 20°C to 50°C, and the peak intensity decreased from 50°C to 60°C as shown in figure 7-10b. The shoulder around 41.4Å didn't change at 60°C, which indicated that the crystals with d-spacing at 41.4Å is more stable than the crystals with d-spacing of 39.2Å. All the peaks disappeared at 70°C. This conformed with the DSC results that the melting point of the samples with 80% stearic acid is at 55.7°C.

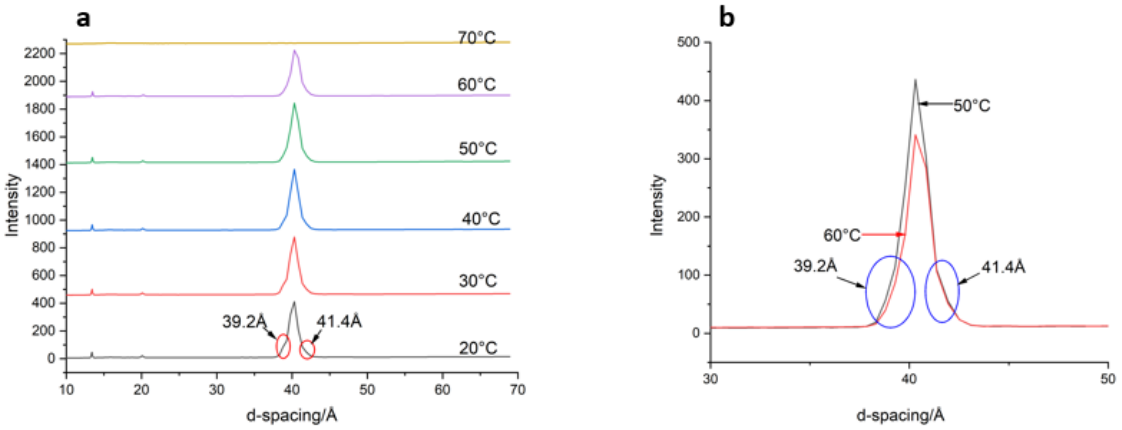

Figure 7-10 The SAXS patterns of the samples with 80% stearic acid and 20% perfume. a, the SAXS patterns from 20°C to 70°C. b, comparing the peak intensities at 50°C (black) and 60°C (red). The red circle in a and blue circle in b are the shoulders around 39.2Å and 41.4Å.

Table 7-9 The d-spacing of the crystals formed in the samples contain 80% stearic acid and 20% perfume. The repeating peaks indicated that the crystals are lamellar structure. The peaks were disappeared at 70°C. The shoulders around 39.2Å and 41.4Å were not listed.

Temperature/°C	d-spacing (d001)/Å	d-spacing (d002)/Å	d-spacing (d003)/Å	Repeating ratios	Structure
20	40.2	20.1	13.4	1:1/2:1/3	Lamellar
30	40.2	20.1	13.4	1:1/2:1/3	Lamellar
40	40.2	20.1	13.4	1:1/2:1/3	Lamellar
50	40.2	20.1	13.4	1:1/2:1/3	Lamellar
60	40.2 41.4	20.1	13.4	1:1/2:1/3	Lamellar
70					

The SAXS patterns of the samples with 90% stearic acid and 10% perfume are similar with the samples contain 80% stearic acid as shown in figure 7-11a. The shoulders around 39.2Å and 41.4Å can still be observed with weak intensities as shown in figure 7-11b. The intensity of the peak at 40.2Å decreased 12.6% from 50°C to 60°C, whereas the peak decreased 22.6% in the samples with 80% stearic acid. Hence, the melting process started between 50°C to 60°C, which is below the melting point determined by DSC.

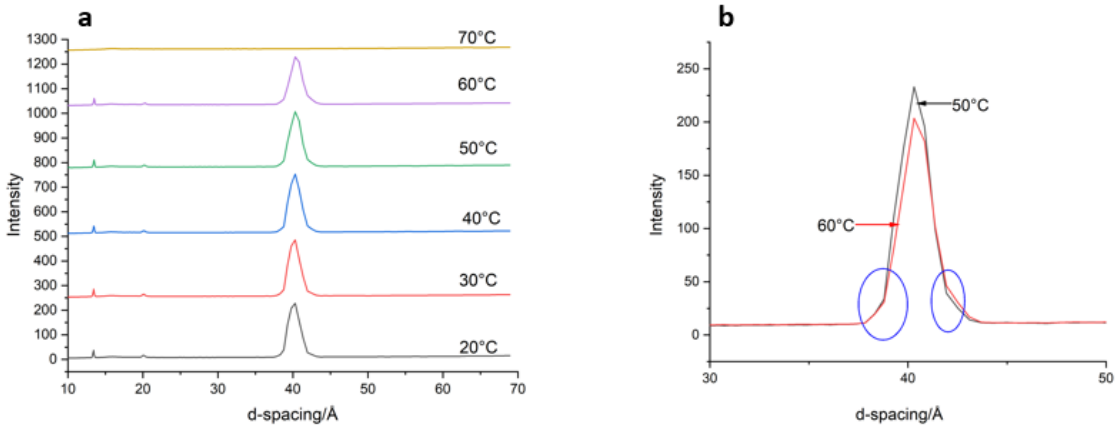

Figure 7-11 The SAXS patterns of the samples with 90% stearic acid and 10% perfume. a, the SAXS patterns from 20°C to 70°C. b, comparing the peak intensities at 50°C (black) and 60°C (red). The blue circles in b are the shoulders around 39.2Å and 41.4Å.

Table 7-10 The d-spacing of the crystals formed in the samples contain 90% stearic acid and 10% perfume. The repeating peaks indicated that the crystals are lamellar structure. The peaks were disappeared at 70°C. The shoulders around 39.2Å and 41.4Å were not listed.

Temperature/°C	d-spacing (d001)/Å	d-spacing (d002)/Å	d-spacing (d003)/Å	Repeating ratios	Structure
20	40.2	20.1	13.4	1:1/2:1/3	Lamellar
30	40.2	20.1	13.4	1:1/2:1/3	Lamellar
40	40.2	20.1	13.4	1:1/2:1/3	Lamellar
50	40.2	20.1	13.4	1:1/2:1/3	Lamellar
60	40.2 41.4	20.1	13.4	1:1/2:1/3	Lamellar
70					

In the mixtures of stearic acid and the perfume, there are three main peaks observed at 39.2Å, 40.2Å and 40.8Å. The peak at 40.2Å is corresponding with the stearic acid lamellar crystals. The d-spacing is larger than the theoretical d-spacing of stearic acid, which may because of the penetration of perfume. As the ingredient of the perfume are not reactive with the stearic acid, the lamellar crystals formed in the mixtures are corresponding with the stearic acid. Three polymorphs of stearic acid were published and the d-spacings are 39.84Å, 44.20Å and 44.68Å,[132] and these peaks were not observed in the mixtures. Hence, the crystal structure of stearic acid formed in the

mixtures was still form C. The d-spacing change is because of the molecules of the perfume penetrated into the lamellar crystals of stearic acid. The perfume has two influences on the stearic acid crystals: some ingredients expanded the intermolecular spacing and some ingredients shrunk the d-spacing. The hypothesis is some ingredients of the perfume are oil-like, and these molecules can dispersed in the alkyl chains of stearic acid, which can increase the flexibility of the alkyl chain and the d-spacing of the lamellar crystals are decreased. Some ingredients of the perfume cannot penetrate in the alkyl chain, and they formed liquid layers between the layers of stearic acid and expanded the intermolecular spacing of the lamellar crystals, which lead the d-spacing increased.

7.2.3 The cryo-SEM and hot-stage microscopy images

The samples contain 50% stearic acid and 50% perfume were measured by cryo-SEM and hot-stage microscopy to observe the crystal structures. The crystals formed in the mixtures are large lamellar crystals as shown in figure 7-12 a & b. Amorphous regions were observed in the samples as shown in the figure 7-12 c & d: no crystal structures were observed in the regions circled with red lines. The amorphous regions indicated that the existence of free perfume in the mixture. The stearic acid crystals were well structured. However, small amount crystals were surrounded by free perfume as shown in figure 7-12 e & f, the lamellar structures were disrupted by the perfume. This conformed with the SAXS results that the samples with 50% stearic acid has two kind of lamellar structures with d-spacing at 39.2Å and 40.4Å and the intensity of the peak at 40.4Å is stronger. Hence, the well-structured lamellar crystals correspond with the crystals with d-spacing of 40.4Å, and the crystals surrounded by perfume correspond with the crystals with d-spacing of 39.2Å. This also confirmed that the crystals with d-spacing of 39.2Å are also lamellar crystals.

In order to observe the crystallisation process of stearic acid in perfume, the samples were cooled from 70°C to 20°C. It's not easy to observe the crystals during melting process because the stearic acid crystals stacked together. No birefringence was observed in the samples with 50% stearic acid and 50% perfume at 70°C and 60°C, which suggested that the samples were liquid and no crystals/micelles formed. The ribbon-like crystals appeared at 50°C, whilst the melting point determined by DSC was at 45.4°C. There're no obvious transitions observed from 50°C to 20°C.

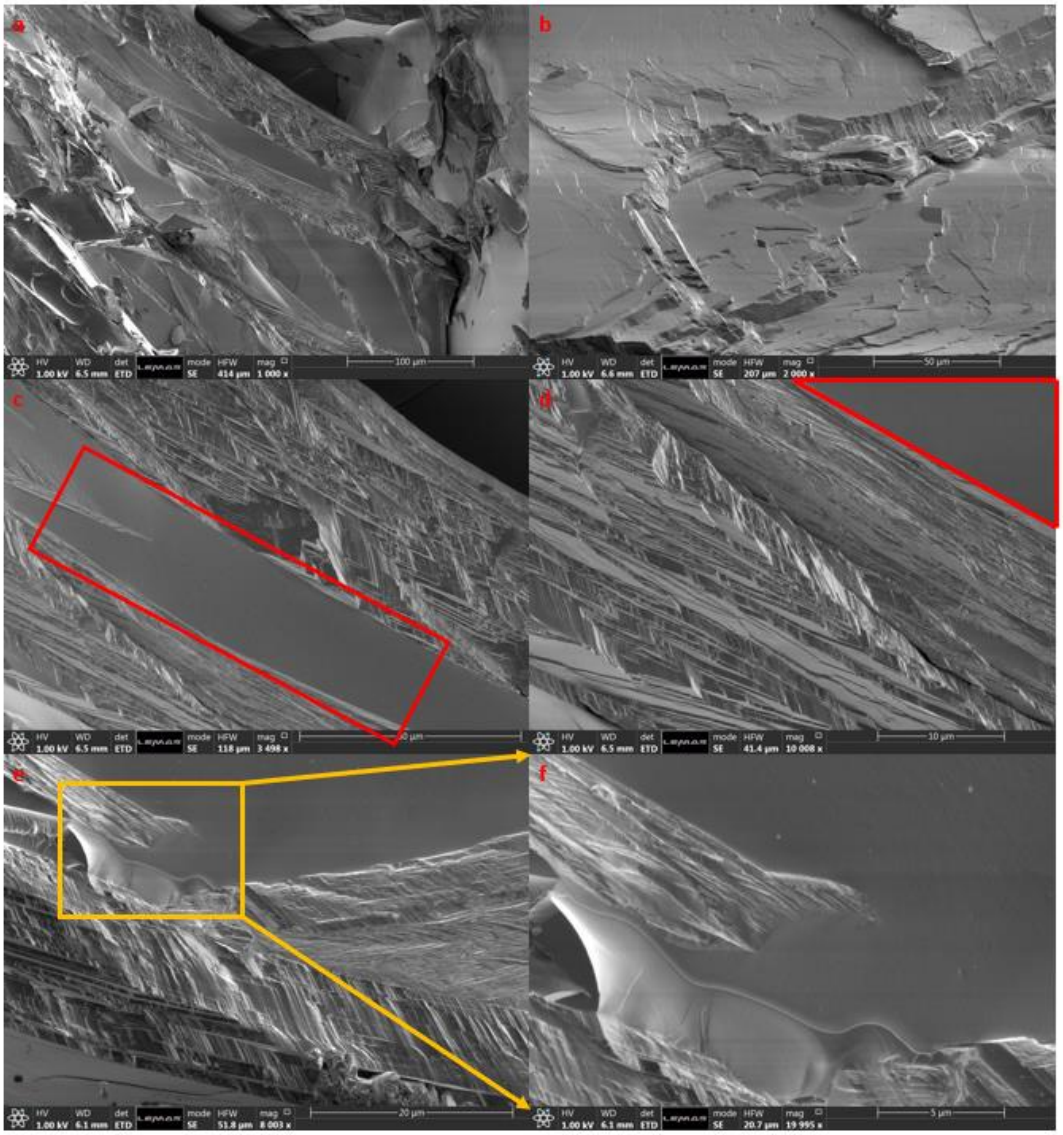

Figure 7-12 The cryo-SEM images of the sample with 50% stearic acid and 50% perfume. The circled region (red) in c and d are the amorphous regions correspond with free perfume. f is the enlarged region in e (yellow circle), the lamellar crystals were surrounded by the perfume and the lamellar structure was not well arranged compare with other regions.

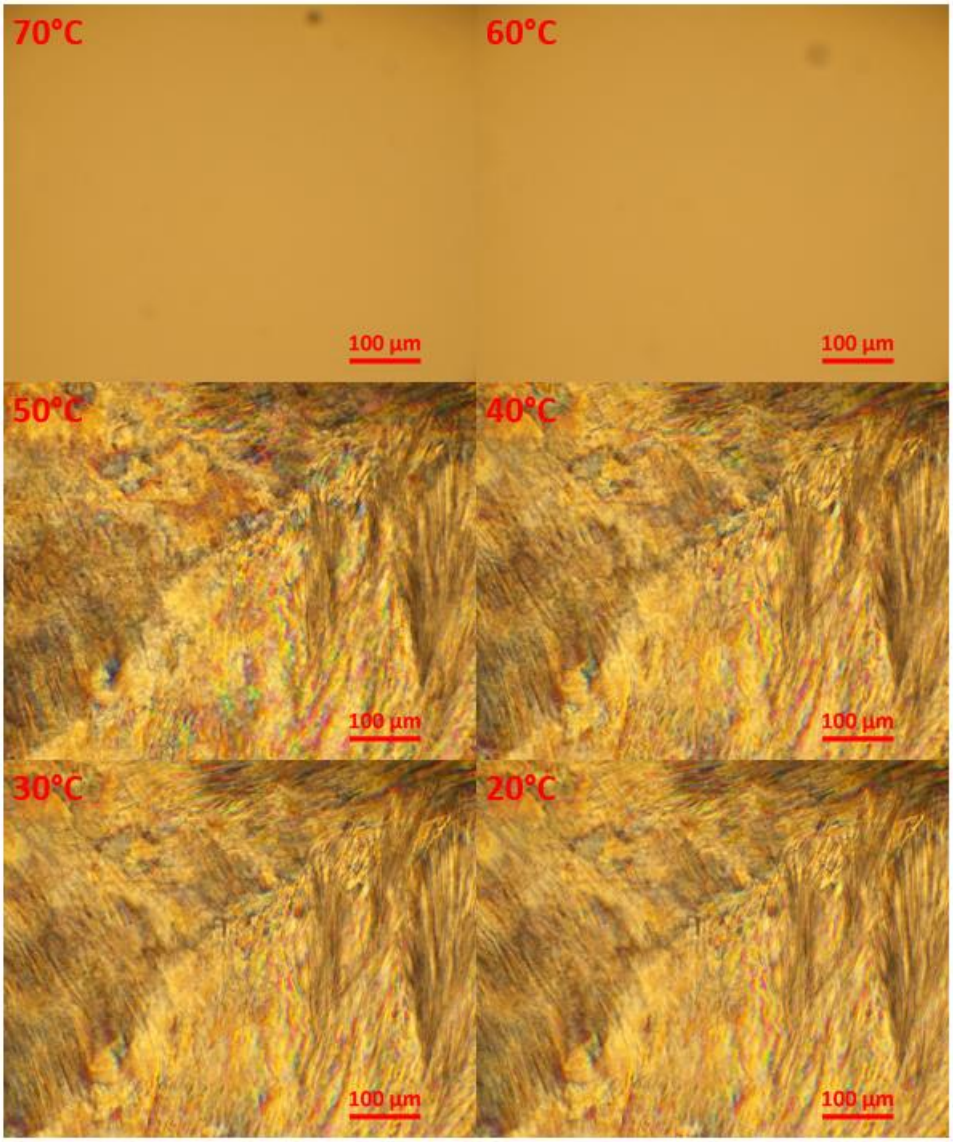

Figure 7-13 The hot-stage microscopy images of the samples with 50% stearic acid and 50% perfume. The ribbon-like crystals correspond with stearic acid appeared at 50°C and no further transition observed below 50°C.

7.3 The influence of perfume on AES liquid crystals.

The SAXS patterns change were observed during the heating process to investigate the influence of perfume on the liquid crystal structure of AES. The AES liquid crystals were observed in chapter 6.3 and the SAXS patterns indicated that the liquid crystals are lamellar structured. The SAXS patterns of the mixtures of stearic acid and perfume indicated that some ingredients of the perfume can expand the lamellar structure and some ingredients can shrink the d-spacing of the lamellar structure of stearic acid. In order to investigate the influence of the perfume on AES liquid crystal, the mixtures of AES and perfume were prepared with certain ratios as listed in table 7-11.

Table 7-11 The compositions of AES/perfume mixtures.

AES/Perfume	9/1	4/1	3/1	2.5/1
AES/%	90	80	75	71.4
Perfume/%	10	20	25	28.6

The SAXS patterns of samples with 10% perfume and 90% AES are shown in figure 7-14a. Only one peak at 40.9Å was observed at 20°C, and the repeating peaks correspond with this peak were at 20.5Å and 13.6Å. These peaks following the repeating ratio of $1:1/2:1/3$, which indicated that the liquid crystals formed in the samples are lamellar structure. The peak migrated to smaller d-spacing as the temperature increasing as shown in figure 7-14c. This conformed with the d-spacing change of the liquid crystals of AES, whereas the d-spacing observed in the samples contain perfume is smaller than the AES only. The SAXS patterns of AES is shown in figure 7-14b, and the d-spacing of the liquid crystals at 20°C was at 41.17Å. This is because the perfume increased the flexibility of the molecules of AES, which has similar effect of the temperature change on the AES molecules. The peak positions of d001, d002 and d003 are listed in table 7-12, the repeating ratios of the liquid crystals at different temperatures indicated that the liquid crystals formed are lamellar structure.

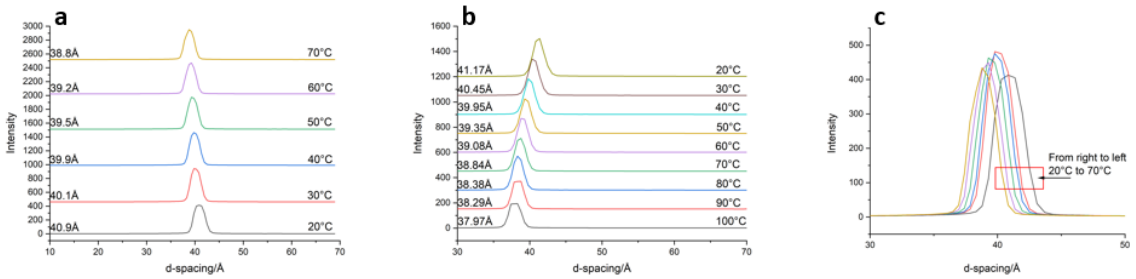

Figure 7-14 the SAXS patterns of the AES/perfume (9/1) as function of temperature. b, the SAXS patterns of AES as function of temperature (cooling ramp). c, the peak migration from 20°C to 70°C.

Table 7-12 The d-spacing of the liquid crystals formed in the AES/perfume (9/1) from 20°C to 70°C. The repeating ratios indicated that the crystals are lamellar structure.

Temperature/°C	d-spacing (d001)/Å	d-spacing (d002)/Å	d-spacing (d003)/Å	R epeating ratios	Structure
20	40.9	20.5	13.6	$1:1/2:1/3$	Lamellar
30	40.1	20.0	13.4	$1:1/2:1/3$	Lamellar
40	39.9	20.0	13.3	$1:1/2:1/3$	Lamellar
50	39.5	19.8	13.2	$1:1/2:1/3$	Lamellar
60	39.2		13.1	$1:1/3$	Lamellar
70	38.8		12.9	$1:1/3$	Lamellar

The samples with 80% AES and 20% perfume (4/1) have the same trend with the samples with 10% perfume. Limited changes in SAXS patterns were observed as shown in figure 7-14a. The d-spacing of the liquid crystals of AES was 40.2Å at 20°C and the repeating peaks indicated that the liquid crystals are lamellar structure. The d-spacing shrunk as temperature raising and the d-spacing at 70°C was 39.1Å. It is more clear that the peak migrated to smaller d-spacing as temperature raising as shown in figure 7-14b. The d-spacings of the liquid crystal at different temperatures are listed in table 7-13, the repeating peaks are following the repeating ratio of $1:1/2:1/3$, which indicated that the liquid crystals are still lamellar structure.

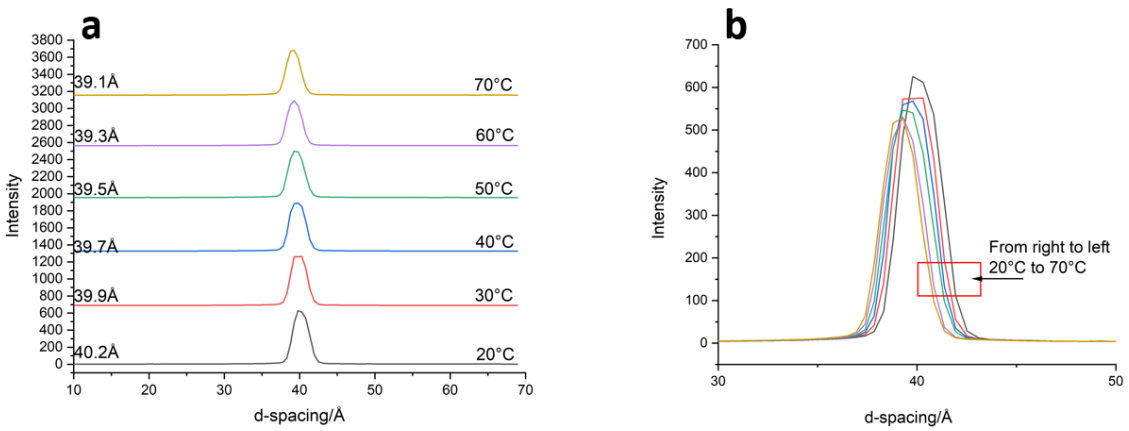

Figure 7-15 a, the SAXS patterns of the AES/perfume (4/1) as function of temperature. b, the peak migration from 20°C to 70°C, and it's clear that the peak migrated to smaller d-spacing as temperature raising.

Table 7-13 The d-spacing of the liquid crystals formed in the AES/perfume (4/1) from 20°C to 70°C.

Temperature/°C	d-spacing (d001)/Å	d-spacing (d002)/Å	d-spacing (d003)/Å	Repeating ratios	Structure
20	40.2	20.1	13.4	$1:1/2:1/3$	Lamellar
30	39.9	19.9	13.3	$1:1/2:1/3$	Lamellar
40	39.7	19.8	13.2	$1:1/2:1/3$	Lamellar
50	39.5	19.7	13.2	$1:1/2:1/3$	Lamellar
60	39.3	19.6	13.1	$1:1/2:1/3$	Lamellar
70	39.1	19.6	13.0	$1:1/2:1/3$	Lamellar

The SAXS patterns of the 3/1 samples are shown in figure 7-16. Comparing with the 4/1 samples, the d-spacing of the liquid crystals in 3/1 are smaller. And the peak migrated to smaller d-spacing as temperature raising, which is similar with the samples with lower concentration of perfume. However, the d-spacing of the liquid crystals were same at 60°C and 70°C as shown in figure 7-16b, and the d002 confirmed that the d-spacing of the liquid crystals are the same as shown in the enlarged figure. The d003 was not observed in the SAXS patterns because of the weak intensities, and the d-spacings are listed in table 8-14. The ratios of d001:d002 are $1:1/2$, as the d-spacing are similar with the samples with low concentration of perfume, the liquid crystals formed in 3/1 were lamellar structure.

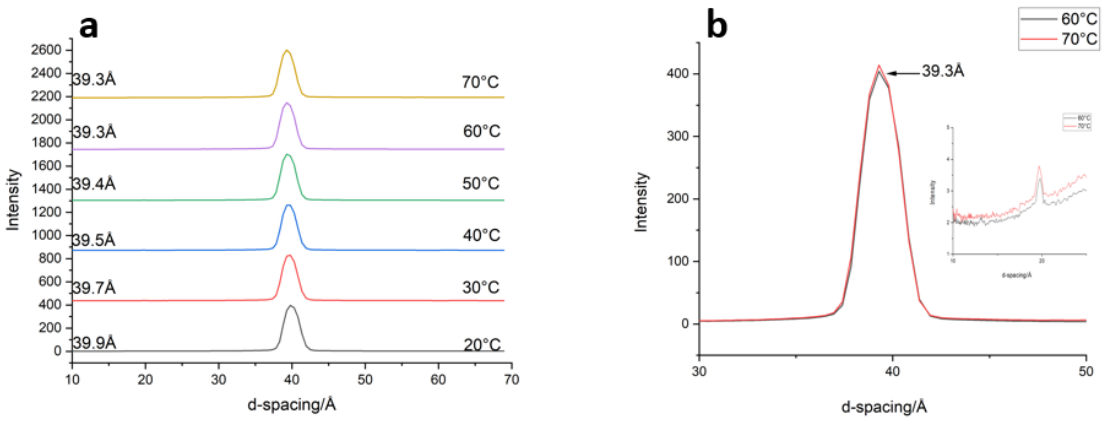

Figure 7-16 a, the SAXS patterns of the AES/perfume (3/1) as function of temperature. b, The peak position at 60°C and 70°C and the small figure is the enlarged d002 corresponding with the peak at 39.3Å.

Table 7-14 The d-spacing of the liquid crystals formed in the AES/perfume (3/1) from 20°C to 70°C.

Temperature/°C	d-spacing (d001)/Å	d-spacing (d002)/Å	Repeating ratios	Structure
20	39.9	19.9	1:1/2	Lamellar
30	39.7	19.8	1:1/2	Lamellar
40	39.5	19.8	1:1/2	Lamellar
50	39.4	19.7	1:1/2	Lamellar
60	39.3	19.7	1:1/2	Lamellar
70	39.3	19.7	1:1/2	Lamellar

Similar trend was found in the samples with 28.6% perfume (2.5/1), whereas the d-spacing of AES liquid crystals at 20°C decreased to 39.7Å. The d-spacing of the liquid crystals decreased as temperature raising until the d-spacing reached 39.3Å, which should be the stable state of the liquid crystal. The repeating peaks listed in table 8-15 indicated that the liquid crystals were lamellar structure. The SAXS pattern of the sample at 70°C is shown on the log-log plot (figure 7-17b) and the slope in intermediate q region was -1.19, which indicated that the liquid crystals at high temperature has rod-like behaviour. Hence, the liquid crystals with d-spacing of 39.3Å have rod-like bilayers structure.

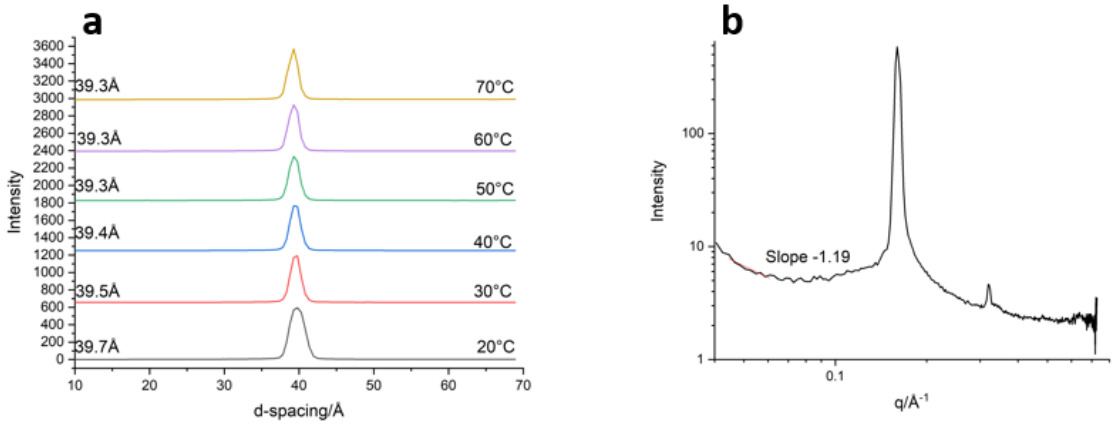

Figure 7-17 The SAXS patterns of 2.5/1 (28.6% perfume) as function of temperature. b, the SAXS pattern of the sample at 70°C on log-log plot. The slope in intermediate q was -1.19, which is close to -1.

Table 7-15 The d-spacing of the liquid crystals formed in the AES/perfume (2.5/1) from 20°C to 70°C.

Temperature/°C	d-spacing (d001)/Å	d-spacing (d002)/Å	Repeating ratios	Structure
20	39.7	19.9	1:1/2	Lamellar
30	39.5	19.8	1:1/2	Lamellar
40	39.4	19.7	1:1/2	Lamellar
50	39.3	19.65	1:1/2	Lamellar
60	39.3	19.66	1:1/2	Lamellar
70	39.3	19.65	1:1/2	Lamellar

The samples with 75% AES and 25% perfume (3/1) were observed by hot-stage microscopy as shown in figure 7-18. There's no significant transition observed between 20°C and 40°C. The birefringence observed in the samples confirmed the existence of liquid crystals. The enlarged figure at 20°C is the oil droplet, which indicated the existence of free perfume. When the temperature raised to 50°C, a large air bubble appeared in the visual field and the liquid crystals rearranged at the edge of the air bubble. The small oil droplets aggregated and formed larger droplets as shown in the enlarged zone of the sample at 50°C. When the temperature raised to 60°C, some spherical liquid crystals were observed and the size were around 17μm. And the size of the droplets decreased in the samples at 70°C.

As the sizes of the droplet are much larger than the AES molecules length and the SAXS patterns indicated that the liquid crystals were lamellar structure, the droplets form in the samples were not micelles. As the d-spacing of the liquid crystals formed in the 2.5/1 samples were same with the 3.0/1, the structure of these two samples should be the same at 70°C. The slope of the q in intermediate region indicated that the liquid crystals have rod-like property, so the droplets observed in hot-stage microscopy should be the cross section of the rod-like liquid crystals.

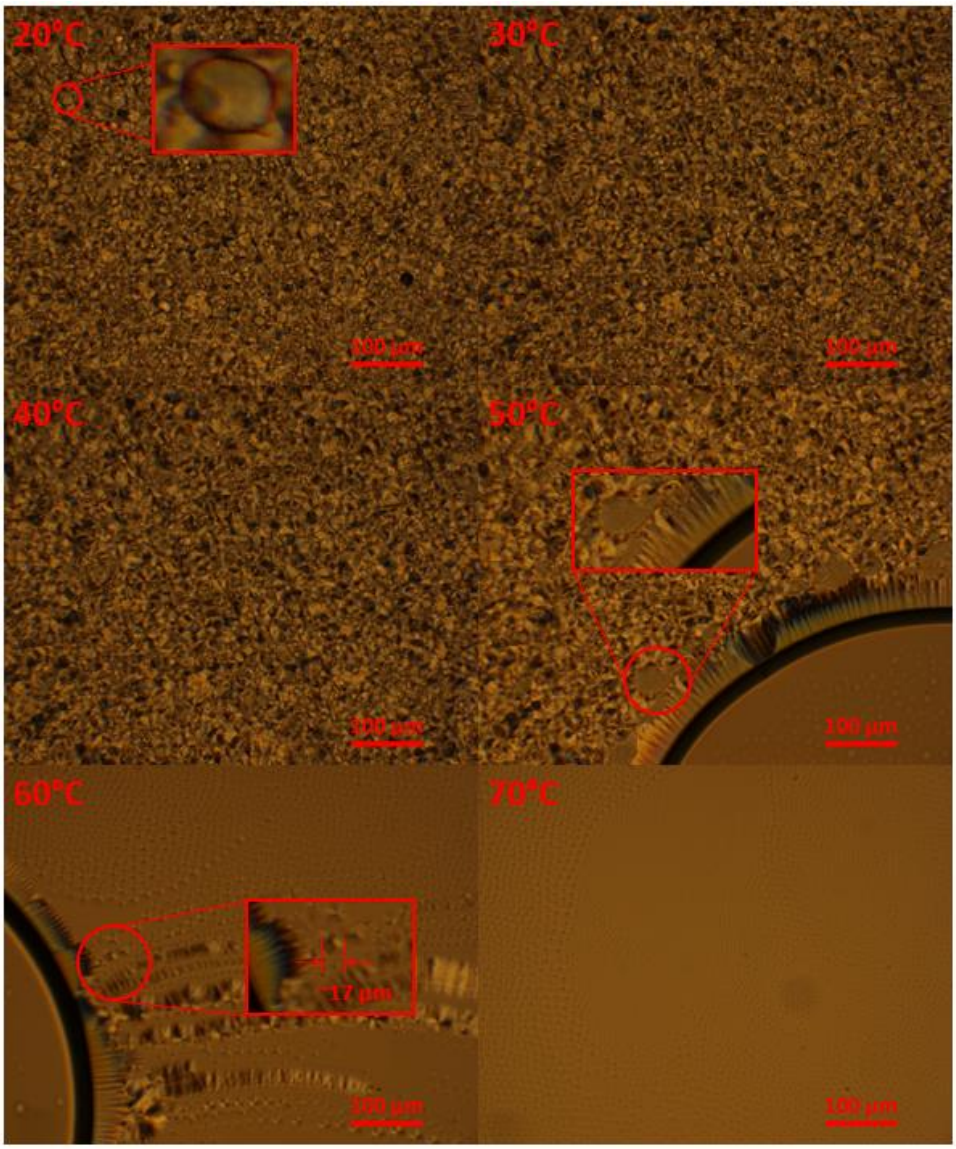

Figure 7-18 The polarized hot-stage microscopy images at different temperatures. The enlarged image at 20°C is the oil droplets of free perfume. The birefringence corresponds with liquid crystals can also be observed. No obvious transitions were observed from 20°C to 40°C. An air bubble appeared at 50°C and the liquid crystals rearranged at the edge of air bubble. The enlarged image was the aggregated oil droplet. Some round liquid crystals appeared at 60°C.

The cryo-SEM images of the samples with 75% AES and 25% perfume (3/1) are shown in figure 7-19. The dark area (red circle) in figure 8-19a is the free perfume corresponds with the oil droplets observed by hot-stage microscopy. The layers correspond with the AES liquid crystals was observed in the continuous phase. The round liquid crystals was also observed in the cryo-SEM images as shown in figure 7-19b, the diameter of the round circle is around 8.8μm and lamellar structure can be observed in it. The circled area in figure 7-19c confirmed that the round area is the cross section of rod-like crystals. The possible structure of the rod-like crystals is shown in figure 7-20.

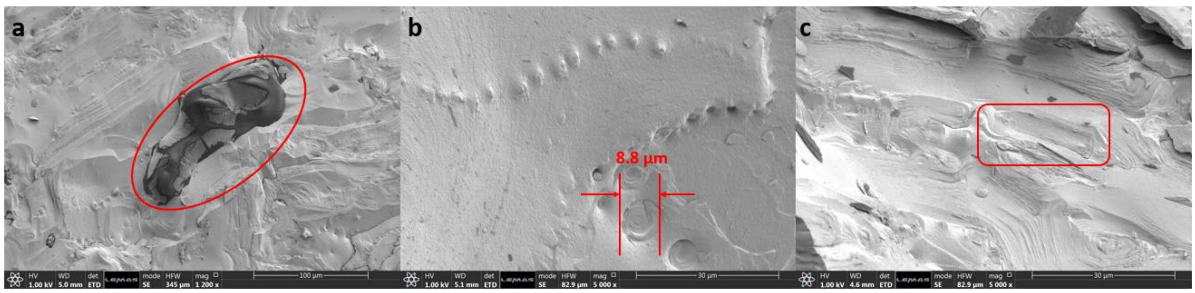

Figure 7-19 The cryo-SEM images of 3/1 (25% perfume) samples. a, the circled dark area was the free perfume. b, the round cross-section of rod-like crystal was observed, and the diameter was aruond 8.8 micros. c, the circled area confirmed the existence of rod-like crystals.

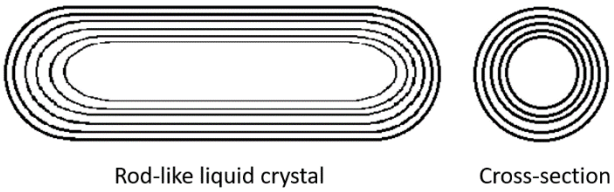

Figure 7-20 The possible structure of rod-like crystals.

The mixtures of AES and perfume confirmed that some ingredients of the perfume can penetrate into the liquid crystal of AES and some ingredients of the perfume are not miscible with the AES and formed oil droplets in the mixtures. This conformed with the results of the mixture of stearic acid and perfume. The perfume penetrated into the lamellar liquid crystals can increase the flexibility of AES molecules, which is similar

with the influence of temperature illustrated in chapter 6.3.1. The tilt angle decreased as the increasing flexibility of the AES molecules, which caused the shrunk of the d-spacing of liquid crystals. As temperature increasing, part of the AES was dissolved in the perfume and this was confirmed by the SAXS patterns that the peak intensities dropped from 50°C to 60°C, and this was also observed in the hot-stage microscopy images. The rod-like liquid crystals were observed in the cryo-SEM images, and the spherical liquid crystals observed in hot-stage microscopy are the cross-sections of the rod-like crystals. This can also explain that the slope of SAXS pattern at 70°C was close to -1, which is corresponding with the rod-like behaviour.

7.4 The influence of perfume on the AES/HSt mixture.

In order to investigate the influence of perfume on the liquid crystal structure of AES and the acid-soap formation, the samples with 60% AES, 20% stearic acid and 20% perfume were prepared. The composition of the samples was based on the industrial formula. The samples were cooled down from 70°C to 20°C with 10°C interval. By comparing the SAXS patterns before and after heating, the peak positions didn't change and the intensities increased significantly after heating as shown in figure 7-21. As the crystal structures in the samples did not change before and after heating, the crystallisation process was studied from 70°C to 20°C.

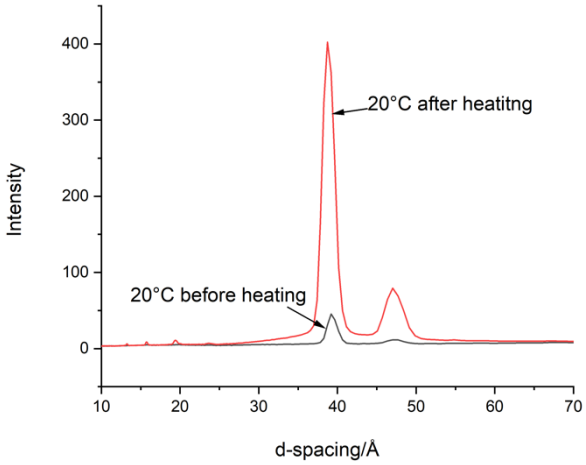

Figure 7-21 The comparison of SAXS patterns before and after heating. The peak positions did not change and the intensities of the sample after heating were stronger than the sample before heating.

The SAXS patterns of the AES/HSt/perfume is shown in figure 7-22 and the peak positions are listed in table 7-16. A broad peak around 37.2Å was observed at 70°C, and the intensity of this peak decreased as the appearance of the peak at 47.1Å and 38.3Å at 50°C. The SAXS pattern of the sample at 40°C is shown on log-log plot in figure 7-22b, the repeating peaks indicated that the peak at 38.4Å consists two peaks at 38.4Å and 39.8Å, similar phenomenon was found in the samples at lower temperature.

The structures of the crystals formed in the AES/HSt/perfume mixtures can be confirmed by combining with the SAXS patterns of AES/HSt (70/30), HSt/perfume (50/50) and AES/perfume (3/1) mixtures. The peak at 37.1Å was also found in the AES/HSt (70/30) at 70°C, and the repeating peaks indicated that the liquid crystal with d-spacing of 37.1Å are lamellar structure. And this peak migrated to higher d-spacing at 38.3Å, which was also found in this sample. The d-spacing of the AES liquid crystals migrated to 42Å in the AES/HSt mixtures, whereas the peak at 38.8Å was found in the AES/HSt/perfume at 20°C. The d-spacing of the crystals corresponds with stearic acid in the AES/HSt mixtures are around 40Å, whereas the d-spacing found in AES/HSt/perfume are at 39.8Å. The d-spacing of 2:1 stearate acid-soap is 47.4Å and the d-spacing of 2:1 acid-soap in AES/HSt was expanded to 47.7Å, whereas the d-spacing corresponding with 2:1 acid-soap in AES/HSt/perfume decreased to 47.1Å. So the perfume can increase the flexibility of the AES and HSt molecules, which caused the shrunk of the d-spacing of the crystals.

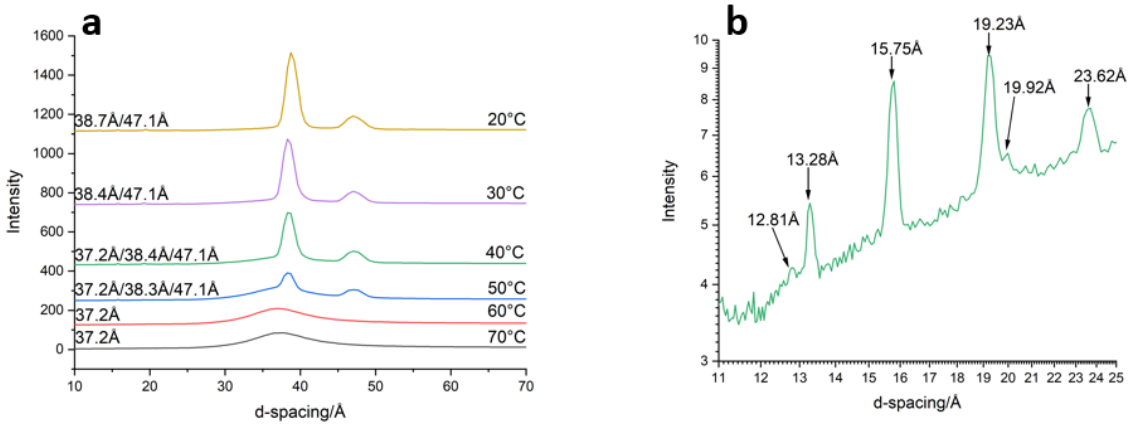

Figure 7-22 a, the SAXS patterns of AES/HSt/perfume (60/20/20) as function of temperature. b, the repeating peaks at 40°C on log-log plot, the appearance of the peak at 19.92Å/13.28Å and 19.23Å/12.81Å indicated that the peak at 38.3Å consists two peaks at 38.4Å and 39.8Å.

Table 7-16 The d-spacing of the crystals formed in the AES/HSt/perfume (60/20/20) from 70°C to 20°C.

Temperature/°C	d-spacing (d001)/Å	d-spacing (d002)/Å	d-spacing (d003)/Å	Repeating ratios	Structure
70	37.2				Lamellar
60	37.2				Lamellar
50	37.2				Lamellar
	38.3	19.23		1:1/2	Lamellar
		19.85			Lamellar
	47.1	23.62	15.75	1:1/2:1/3	Lamellar
40	37.2				Lamellar
	38.3	19.23	12.81	1:1/2:1/3	Lamellar
		19.92	13.28	1/2:1/3	Lamellar
	47.1	23.62	15.75	1:1/2:1/3	Lamellar
30	38.4	19.22	12.80	1:1/2:1/3	Lamellar
		19.94	13.26	1/2:1/3	Lamellar
	47.1	23.63	15.75	1:1/2:1/3	Lamellar
20	38.7	19.40 (with shoulder)		1:1/2	Lamellar
			13.26		Lamellar
	47.1	23.63	15.75	1:1/2:1/3	Lamellar

The hot-stage microscopy images are shown in figure 7-23. The rod-like crystals found in the AES/perfume mixtures were also found in the AES/HSt/perfume. The diameter of the cross-section of road-like crystals was around 20μm, which is similar with the crystals found in AES/perfume. Needle-like crystals were appeared at 60°C, and the size and amount of the needle-like crystals increased significantly from 60°C to 50°C. However, no transitions were observed in SAXS from 70°C to 60°C, and the appearance of the crystals with d-spacing of 47.1Å and 39.8Å correspond with the needle/ribbon-like crystals appeared at 50°C. This may because that the evaporation of the perfume. The solidification of AES was observed between 50°C and 40°C, and this transition corresponds with the d-spacing change from 37.1Å to 38.3Å observed in SAXS. Although the peak at 38.3Å was appeared in SAXS at 50°C, the peak intensity was weak. The peak migration from 38.3Å to 38.7Å was not observed in hot-stage microscopy.

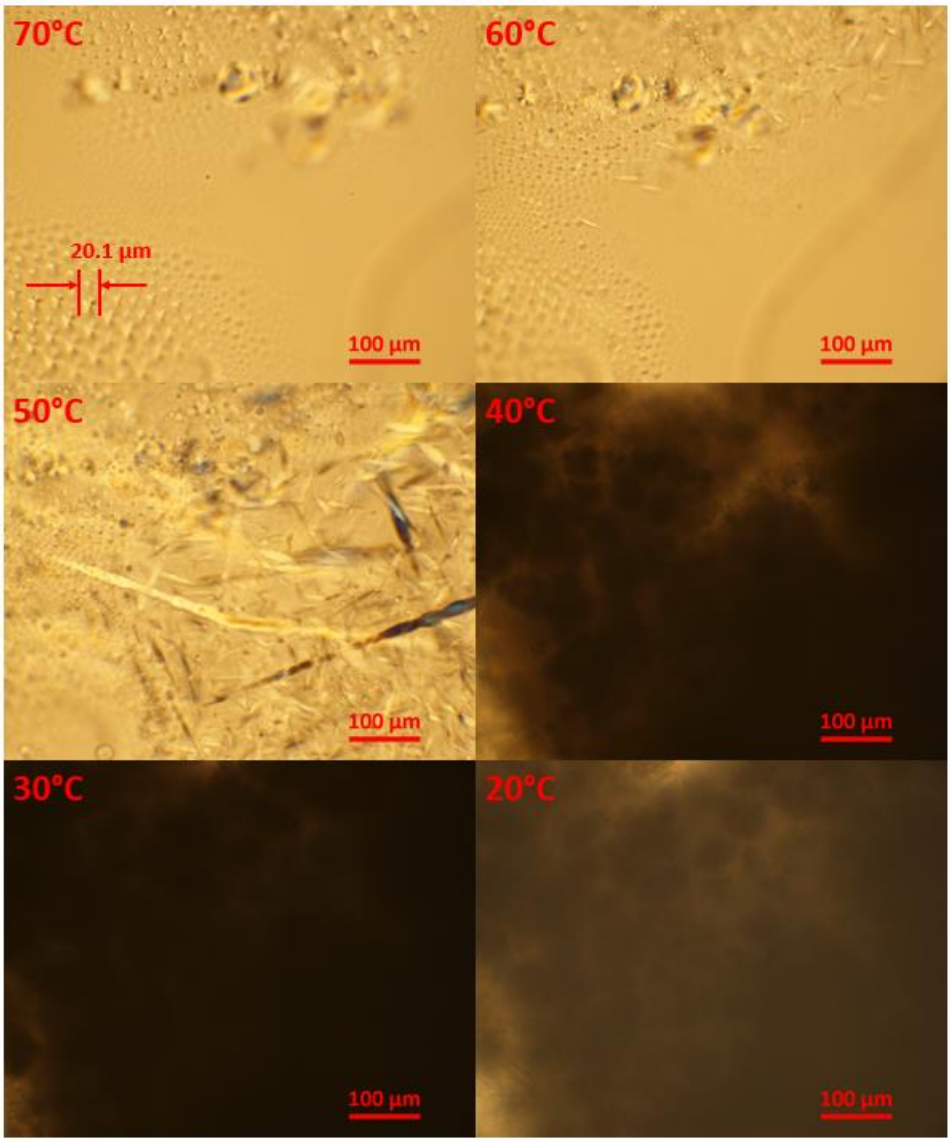

Figure 7-23 The hot-stage microscopy images of the AES/HSt/perfume (60/20/20). The samples were cooled from 70°C to 20°C. The rod-like liquid crystals was observed. The needle-like crystals appeared at 60°C. The visual field became dark at 40°C.

The cryo-SEM images of the AES/HSt/perfume (60/20/20) are shown in figure 7-24. The rod-like liquid crystals of AES were observed in figure 7-24a. Comparing with the AES/perfume mixtures, the size of the rod-like crystal in AES/perfume was 21.9µm, whereas the size in AES/HSt/perfume was around 1µm. This is because of the appearance of stearic acid/acid-soap crystals restricted the movement of the AES. The layers correspond with the AES liquid crystals were observed in 7-24b. Well-structured lamellar crystals were found in figure 7-24c, and these crystals correspond

with the stearic acid or acid-soaps. The lamellar crystals of stearic acid/acid-soap were also observed in 7-24d, and the thickness of one layer was roughly 22Å, which is close to the half of the d-spacing of stearic acid/acid-soap crystals. In figure 7-24 d & e, some porous materials were found between the lamellar crystals and these structures were not found in other mixtures. The hypothesis is that the perfumes come out from the AES liquid crystals and formed oil droplets, the stearic acid/acid-soap crystals restricted the movement of AES and the liquid crystals formed the porous structure. The oil droplets (free perfume) were observed in hot-stage microscopy images and the figure 7-24 f. The smooth region in red circle (7-24f) is the perfume droplet.

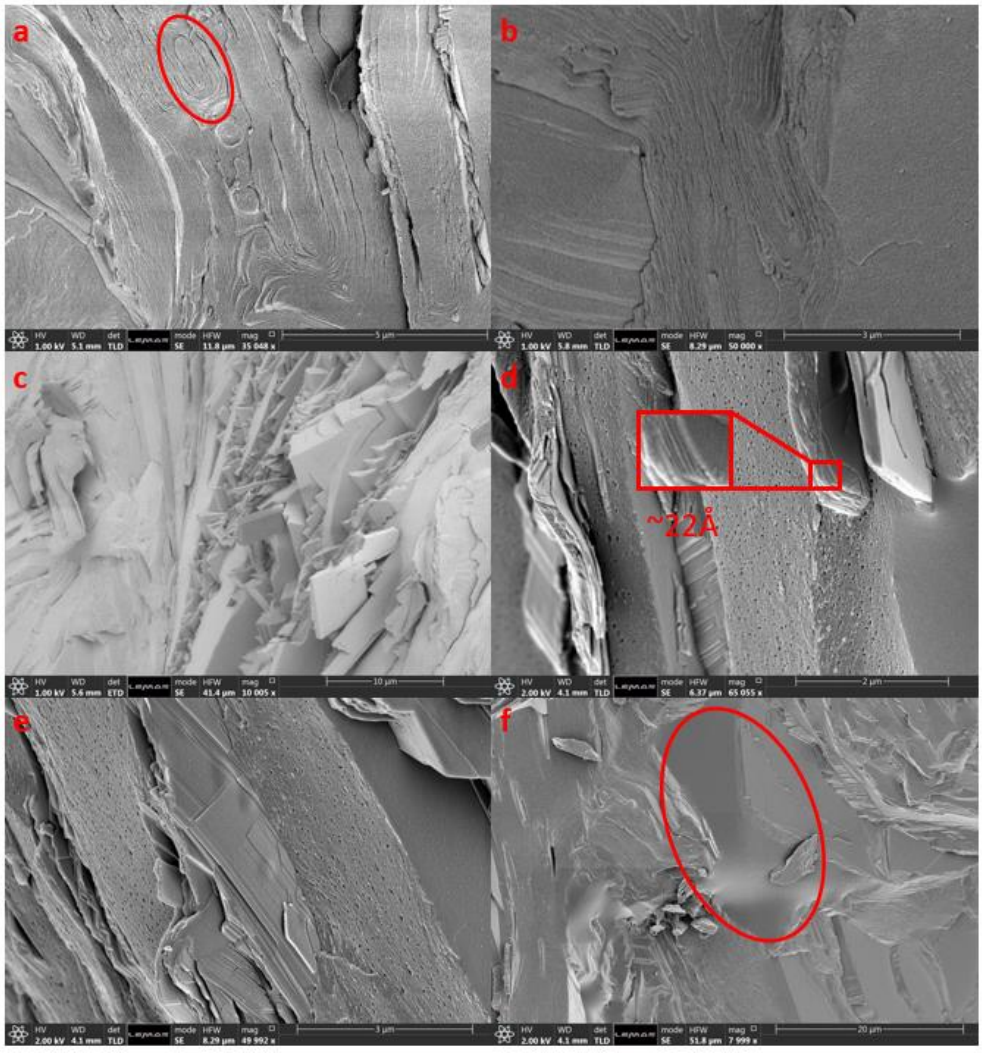

Figure 7-24 The cryo-SEM images of AES/HSt/perfume (60/20/20). A,The rod-like liquid crystals was observed in red circle. b, the lamellar liquid crystals of AES. c, well-structured lamellar crystals of stearic acid/acid-soap. d & e, the porous AES liquid crystals dispersed between the stearic acid/acid-soap crystals. f, the smooth area in red circle was the oil droplet of perfume.

7.5 Conclusions

The ingredients of the perfume used in this chapter are unknown as the formula is classified. The SAXS results of the mixtures of HSt/perfume indicated that the perfume has two effects on the stearic acid crystals: part of the molecules can penetrate into the bilayer and increase the flexibility of alkyl chain; part of the molecules form solvent layers in the lamellar crystals to expand the d-spacing. The cryo-SEM images confirmed that there's free perfume appeared in the mixtures and the crystal structures surrounded by perfume was disrupted.

The cryo-SEM images and polarised light microscopy (PLM) images of AES/perfume mixtures confirmed that the perfume has two groups molecules. The water-poor perfume molecules formed oil droplets in the mixtures. And another group molecules penetrated into the lamellar liquid crystals of AES and the d-spacing becomes smaller. At high temperature, some spherical droplets were observed by PLM. The birefringence pattern indicated that the droplets are liquid crystals. These spherical droplets were also observed by cryo-SEM, and the droplets are "rod-like" lamellar crystals, which could be induced by shear.

Similar phenomenon was observed in the AES/HSt/perfume mixtures. The industrial purpose is encapsulating the perfume in AES lamellar liquid crystals to slow down the evaporation rate, and the stearic acid was added to solidify the gel-like AES. However, this cannot be achieved because of the formulation of perfume.

Chapter 8 Conclusions and future work

8.1 Conclusions

The stearate acid-soaps structures were determined by powder-XRD and the diffraction patterns indicated that the acid-soaps are lamellar structured. Two types acid-soap crystals were formed at room temperature with stoichiometric ratios (acid:soap) of 2:1 and 1:1, which is contradicted with previous publications. The characteristic long-range d-spacings associate with these two types acid-soaps are 47.4Å and 49.8Å respectively. Assuming the alkyl chain is fully extended, the chain length of stearic acid can be calculated. The d-spacing is smaller than 2 times of chain length of stearic acid, so the crystals of 2:1 and 1:1 acid-soaps are bilayer lamellar crystals. The tilt angles of these two types acid-soaps are 66° and 73.7° respectively. The acid-soaps formed spontaneously in the mixtures and have tendency to form the type with higher soap ratio, which indicated that the stability of 1:1 acid-soap crystals is better than 2:1 acid-soap and stearic acid crystals.

The phase behaviours of acid-soaps were studied by DSC and SAXS/WAXS with temperature stage. The 2:1 acid-soap exhibits two transitions: dissolve in stearic acid melt and form micelles, transform to 1:1 acid-soap around 80°C. The 2:1 acid-soap has three polymorphs: form I, form II and form III. The previous publications indicated that the 1:1 acid-soap transform to 1:2 acid-soap at certain temperature. However, the 1:2 acid-soap was not found in stearate system. And the phase transformation temperature of 2:1 to 1:1 acid-soap is close to 1:1 acid-soap form I to form II. The form III is hexagonal liquid crystal, which is not lamellar crystals.

The morphologies of acid-soaps were observed by SEM, rhombus crystals were found in 50% and 70% neutralised samples, and this kind crystals is associating with 1:1 acid-soaps. However, the amount of this kind crystals are small. This may be another polymorphs of 1:1 acid-soap and can only form under slow evaporation.

The phase behaviour and crystal structures were studied by SAXS/WAXS with temperature stage. The characteristic peak of 1:1 acid-soap at 49.8Å was observed in the mixtures, which confirmed the formation of acid-soaps in environment of non-ionic surfactants. The phase transition temperatures were lowered in the mixtures, which suggested that the non-ionic surfactants still have interactions with acid-soaps. The characteristic peak associate with 2:1 acid-soap migrated to higher d-spacing in the

mixtures of AES and stearic acid. The calculated d-spacing of 1:1 AES-HSt cocrystals is 48.31Å, which is close to the experimental results. Hence, the AES can form cocrystals with stearic acid with stoichiometric ratio of 1:1. This could be side evidence for the interactions in acid-soaps are hydrogen bonds. The hydrophilic head group of non-ionic surfactants cannot be ionised, so they cannot form the cocrystals with stearic acid.

The morphologies of the acid-soap crystals form in environment of surfactants were observed by polarized light microscopy and SEM/cryo-SEM. The ribbon like crystals were observed in SEM in the NI/HSt mixtures, and no rhombus crystal was found in the mixtures. Lamellar crystals were found in AES/HSt mixtures. However, the shape of the crystals was not observed.

The ingredients in perfume can be divided into two groups: saturated and unsaturated. The unsaturated perfume molecules are polarisable, it can penetrate through the bilayers and form free perfume disperse in the mixtures. The saturated molecules are dispersed in the hydrophobic tails, which can increase the flexibility of alkyl chain and lead the peak migrate to smaller d-spacing. The existence of free perfume was confirmed by polarised light microscopy and cryo-SEM.

8.2 Review of thesis aims

The research made significant progress in characterising the stearate acid-soap types and the phase behaviour. Phase diagram of sodium stearate/stearic acid system was generated. The crystals of acid-soaps formation process were monitored during cooling ramps. The appearance of acid-soap crystals in non-ionic surfactant can significantly accelerate the solidification process. Proctor & Gamble has applied this method in Rakona, and the anti-caking property of washing powder has improved significantly.

However, the thesis objectives were not fully met. The encapsulating of perfume in AES/HSt was un-achievable. This is because of the formula of perfume: the unsaturated perfume molecules are mobile in AES liquid crystals.

8.3 Suggestions for future work

The dynamic transition from monomer to acid-soap crystals could be monitored by synchrotron SAXS and SANS. The AES has tendency to form acid-soap like cocrystals with stearic acid. This process was quite slow, and the aggregation was not well structure during measuring. It is possible to slow down the aggregation process further by choosing proper ionic surfactant to control the viscosity to restrain the movement of molecules. The SAXS can be used to monitor the aggregation process. And SANS can provide more information in the initial stage of aggregation. FTIR can be used for investigating the C=O stretch shifting associate with the hydrogen bonds formation.

References

1. Rosen, M. J.; Kunjappu, J. T., *Surfactants and interfacial phenomena*. John Wiley & Sons: 2012.

2. Edser, C., Status of global surfactant markets. *Focus on Surfactants* **2008,** *2008* (11), 1-2.

3. Global Surfactants Market By Type, By Application, By Geographic Scope And Forecast To 2026. https://www.verifiedmarketresearch.com/product/surfactants-market/.

4. Rico-Lattes, I.; Lattes, A., Synthesis of new sugar-based surfactants having biological applications: key role of their self-association. *Colloids and Surfaces A: Physicochemical and Engineering Aspects* **1997,** *123*, 37-48.

5. Folmer, B. M.; Svensson, M.; Holmberg, K.; Brown, W., The physicochemical behavior of phytosterol ethoxylates. *Journal of colloid and interface science* **1999,** *213* (1), 112-120.

6. Folmer, B. M.; Holmberg, K.; Klingskog, E. G.; Bergström, K., Fatty amide ethoxylates: synthesis and self-assembly. *Journal of Surfactants and Detergents* **2001,** *4* (2), 175-183.

7. Hattiangdi, G. S., Characterization of Some Commercial Soaps By X-Ray Diffraction. *Journal of research of the National Bureau of Standards* **1949,** *42* (4), 331-341.

8. Conway, J. U.S. Cleaning Products Industry - Statistics & Facts. https://www.statista.com/topics/1277/cleaning-products-industry-in-the-us/.

9. Hoof, G. V.; Schowanek, D.; Feijtel, T., Comparative Life-Cycle Assessment of laundry detergent formulations in the UK: part I: environmental fingerprint of five detergent formulations in 2001. *Tenside, surfactants, detergents* **2003**, 266-275.

10. Bittner, L.; Schönbichler, S.; Schmutzler, M.; Lutz, O.; Huck, C., Vibrational spectroscopic methods for the overall quality analysis of washing powders. *Talanta* **2016,** *148*, 329-335.

11. Myers, D., *Surfactant science and technology*. John Wiley & Sons: 2005.

12. Small, D. M., A classification of biologic lipids based upon their interaction in aqueous systems. *Journal of the American Oil Chemists Society* **1968,** *45* (3), 108.

13. Cistola, D. P.; Atkinson, D.; Hamilton, J. A.; Small, D. M., Phase behavior and bilayer properties of fatty acids: hydrated 1: 1 acid-soaps. *Biochemistry* **1986,** *25* (10), 2804-2812.

14. Chevreul, M. E., *Recherches chimiques sur les corps gras d'origine animale*. FG Levrault: 1823.

15. Ekwall, P.; Mylius, W., On acid sodium salts of palmitic acid. *Ber Dtsch Chem Ges* **1929,** *62*, 1080-1084.

16. McBain, J. W.; Field, M. C., 216. Phase-rule equilibria of acid soaps. Part II. Anhydrous acid sodium palmitates. *Journal of the Chemical Society (Resumed)* **1933**, 920-924.

17. Mcbain, J. W.; Field, M. C., Phase Rule Equilibria of Acid Soaps. I. Anhydrous Acid Potassium Laurate. *The Journal of Physical Chemistry* **1933,** *37* (6), 675-684.

18. Porter, M. R., *Handbook of surfactants*. Springer: 2013.

19. Doan, C. D.; Tavernier, I.; Okuro, P. K.; Dewettinck, K., Internal and external factors affecting the crystallization, gelation and applicability of wax-based oleogels in food industry. *Innovative Food Science & Emerging Technologies* **2018,** *45*, 42-52.

20. Ryer, F., Acid sodium stearates. *Oil & Soap* **1946,** *23* (10), 310-313.

21. Andreeva, E.; Boyarchuk, Y. M.; Shul'gin, E., Transitions between symmetrical and unsymmetrical hydrogen bonds in phase transformations in acid soaps. *Journal of Structural Chemistry* **1978,** *19* (1), 149-150.

22. Lynch, M. L., Acid-soaps. *Current opinion in colloid & interface science* **1997,** *2* (5), 495-500.

23. Brouwer, H.; Skoda, W., Calorimetric, dilatometric and microscopic investigations of the system sodium stearate-stearic acid. *Kolloid-Zeitschrift und Zeitschrift für Polymere* **1969,** *234* (2), 1138-1147.

24. Lynch, M. L.; Wireko, F.; Tarek, M.; Klein, M., Intermolecular interactions and the structure of fatty acid− soap crystals. *The Journal of Physical Chemistry B* **2001,** *105* (2), 552-561.

25. Piispanen, P. Synthesis and characterization of surfactants based on natural products. Kemi, 2002.

26. Mersmann, A., *Crystallization technology handbook*. CRC Press: 2001.

27. Volmer, M., Kinetik der phasenbildung. **1939**.

28. Pan, W.; Galkin, O.; Filobelo, L.; Nagel, R. L.; Vekilov, P. G., Metastable mesoscopic clusters in solutions of sickle-cell hemoglobin. *Biophysical journal* **2007,** *92* (1), 267-277.

29. Sauter, A.; Roosen-Runge, F.; Zhang, F.; Lotze, G.; Jacobs, R. M.; Schreiber, F., Real-time observation of nonclassical protein crystallization kinetics. *Journal of the American Chemical Society* **2015,** *137* (4), 1485-1491.

30. Borchardt-Ott, W., *Crystallography: an introduction*. Springer Science & Business Media: 2011.

31. Mullin, J. W., *Crystallization*. Butterworth-Heinemann: 2001.

32. Bernstein, J.; Bernstein, J. M., *Polymorphism in molecular crystals*. Oxford University Press: 2002; Vol. 14.

33. Brittain, H. G.; Grant, D. J.; Myrdal, P. B., Effects of polymorphism and solid-state solvation on solubility and dissolution rate. *Polymorphism in pharmaceutical solids* **1999,** *95*, 279-330.

34. Giordano, F., Polymorphism in pharmaceutical solids-Edited by Harry G. Brittain, Marcel Dekker, New York, 1999, 427 pp. *Journal of Controlled Release* **2001,** *3* (71), 354-355.

35. Pamplin, B. R., *Crystal growth*. Pergamon: Oxford, 1980; Vol. 6.

36. Kadam, S. S.; Kulkarni, S. A.; Ribera, R. C.; Stankiewicz, A. I.; ter Horst, J. H.; Kramer, H. J., A new view on the metastable zone width during cooling crystallization. *Chemical engineering science* **2012,** *72*, 10-19.

37. McCabe, W. L.; Smith, J. C.; Harriott, P., *Unit operations of chemical engineering*. McGraw-Hill New York: 1993; Vol. 5.

38. Sear, R. P., Nucleation: theory and applications to protein solutions and colloidal suspensions. *Journal of Physics: Condensed Matter* **2007,** *19* (3), 033101.

39. Oxtoby, D. W., Homogeneous nucleation: theory and experiment. *Journal of Physics: Condensed Matter* **1992,** *4* (38), 7627.

40. Oxtoby, D. W., Nucleation of first-order phase transitions. *Accounts of chemical research* **1998,** *31* (2), 91-97.

41. Kwon, S. G.; Hyeon, T., Formation mechanisms of uniform nanocrystals via hot-injection and heat-up methods. *Small* **2011,** *7* (19), 2685-2702.

42. Thanh, N. T.; Maclean, N.; Mahiddine, S., Mechanisms of nucleation and growth of nanoparticles in solution. *Chemical reviews* **2014,** *114* (15), 7610-7630.

43. Myerson, A., *Handbook of industrial crystallization*. Butterworth-Heinemann: 2002.

44. Agrawal, S.; Paterson, A., Secondary nucleation: mechanisms and models. *Chemical Engineering Communications* **2015,** *202* (5), 698-706.

45. Erdemir, D.; Lee, A. Y.; Myerson, A. S., Nucleation of crystals from solution: classical and two-step models. *Accounts of chemical research* **2009,** *42* (5), 621-629.

46. Vekilov, P. G., Nucleation. *Crystal growth & design* **2010,** *10* (12), 5007-5019.

47. ten Wolde, P. R.; Frenkel, D., Enhancement of protein crystal nucleation by critical density fluctuations. *Science* **1997,** *277* (5334), 1975-1978.

48. Bahrig, L.; Hickey, S. G.; Eychmuller, A., Mesocrystalline materials and the involvement of oriented attachment - a review. *CrystEngComm* **2014,** *16* (40), 9408-9424.

49. Zhang, J.-H.; Zhang, Y.; Wen, Y.-H.; Zhu, Z.-Z., Comparative study of Cu 13 and Co 13 clusters deposition and diffusion on the Cu (001) surface. *Computational Materials Science* **2010,** *48* (2), 250-257.

50. Shilova, A. Development of serial protein crystallography with synchrotron radiation. Grenoble Alpes, 2016.

51. water cooled X-ray tube. https://en.wikipedia.org/wiki/X-ray_tube.

52. Cullity, B.; Stock, S.; Stock, S., Elements of X-ray Diffraction, 3rd editionPrentice Hall. *New Jersey* **2001**.

53. Ladd, M.; Palmer, R., I Optical and X-ray Examination of Crystals. In *Structure Determination by X-ray Crystallography*, Springer: 2003; pp 213-287.

54. Instrument X-ray Optics. http://pd.chem.ucl.ac.uk/pdnn/inst1/optics1.htm.

55. Taguchi, T., A new position sensitive area detector for high-speed and high-sensitivity X-ray diffraction analysis. *Powder diffraction* **2006,** *21* (2), 97-101.

56. Glatter, O.; Kratky, O., *Small angle X-ray scattering*. Academic press: 1982.

57. Giannini, C.; Ladisa, M.; Altamura, D.; Siliqi, D.; Sibillano, T.; De Caro, L., X-ray diffraction: a powerful technique for the multiple-length-scale structural analysis of nanomaterials. *Crystals* **2016,** *6* (8), 87.

58. Lifshin, E., *X-ray Characterization of Materials*. John Wiley & Sons: 2008.

59. Singh, A. K., *Advanced x-ray techniques in research and industry*. IOS press: 2005.

60. Guinier, A.; Fournet, G.; Yudowitch, K. L., Small-angle scattering of X-rays. **1955**.

61. Stribeck, N., *X-ray scattering of soft matter*. Springer Science & Business Media: 2007.

62. Svergun, D. I.; Koch, M. H., Small-angle scattering studies of biological macromolecules in solution. *Reports on Progress in Physics* **2003,** *66* (10), 1735.

63. Boerefijn, R.; Dontula, P.-R.; Kohlus, R., Detergent granulation. *Handbook of powder technology* **2007,** *11*, 673-703.

64. Martín, M.; Martínez, A., A methodology for simultaneous process and product design in the formulated consumer products industry: The case study of the detergent business. *Chemical Engineering Research and Design* **2013,** *91* (5), 795-809.

65. Wang, G. D.; Mallet, F. P.; Ricard, F.; Heng, J. Y., Pharmaceutical nanocrystals. *Current Opinion in Chemical Engineering* **2012,** *1* (2), 102-107.

66. Zhang, N.; Nguyen, A. V.; Zhou, C., A review of the surface features and properties, surfactant adsorption and floatability of four key minerals of diasporic bauxite resources. *Advances in colloid and interface science* **2018,** *254*, 56-75.

67. Raffa, P.; Broekhuis, A. A.; Picchioni, F., Polymeric surfactants for enhanced oil recovery: A review. *Journal of Petroleum Science and Engineering* **2016,** *145*, 723-733.

68. Wolf, R.; Wolf, D.; Tüzün, B.; Tüzün, Y., Soaps, shampoos, and detergents. *Clinics in dermatology* **2001,** *19* (4), 393-397.

69. Carroll, B., Physical aspects of detergency. *Colloids and Surfaces A: Physicochemical and Engineering Aspects* **1993,** *74* (2-3), 131-167.

70. Minguet, M.; Subirats, N.; Castan, P.; Sakai, T., Behenamidopropyl dimethylamine: Unique behaviour in solution and in hair care formulations. *International journal of cosmetic science* **2010,** *32* (4), 246-257.

71. Griffin, W. C., Classification of surface-active agents by" HLB". *J. Soc. Cosmet. Chem.* **1949,** *1*, 311-326.

72. Griffin, W. C., Calculation of HLB values of non-ionic surfactants. *J. Soc. Cosmet. Chem.* **1954,** *5*, 249-256.

73. Griffin, W., Calculation of HLB values of non-ionic surfactants. *Am Perfumer Essent Oil Rev* **1955,** *65*, 26-29.

74. Bergström, L. M.; Aratono, M., Synergistic effects in mixtures of two identically charged ionic surfactants with different critical micelle concentrations. *Soft Matter* **2011,** *7* (19), 8870-8879.

75. Dave, N.; Joshi, T., A Concise Review on Surfactants and Its Significance. *International Jurnal of Applied Chemistry* **2017,** *13* (3), 663672.

76. Stuart, M. C.; Boekema, E. J., Two distinct mechanisms of vesicle-to-micelle and micelle-to-vesicle transition are mediated by the packing parameter of phospholipid–detergent systems. *Biochimica et Biophysica Acta (BBA)-Biomembranes* **2007,** *1768* (11), 2681-2689.

77. Anachkov, S. E.; Kralchevsky, P. A.; Danov, K. D.; Georgieva, G. S.; Ananthapadmanabhan, K. P., Disclike vs. cylindrical micelles: generalized model of micelle growth and data interpretation. *Journal of colloid and interface science* **2014,** *416*, 258-273.

78. Rusanov, A., The wonderful world of micelles. *Colloid Journal* **2014,** *76* (2), 121-126.

79. Rusanov, A.; Kuni, F.; Shchekin, A., Thermodynamic and kinetic foundations of the theory of micellization: 1. General aspects. *Colloid Journal-Official English Translation of Kolloidnyi Zhurnal* **2000,** *62* (2), 167-171.

80. Nyrkova, I. A.; Semenov, A. N., On the theory of micellization kinetics. *Macromolecular theory and simulations* **2005,** *14* (9), 569-585.

81. Starov, V.; Zhdanov, V.; Kovalchuk, N., Kinetic models of micelles formation. *Colloids and Surfaces A: Physicochemical and Engineering Aspects* **2010,** *354* (1-3), 268-278.

82. Daful, A. G.; Avalos, J. B.; Mackie, A. D., Model shape transitions of micelles: spheres to cylinders and disks. *Langmuir* **2012,** *28* (8), 3730-3743.

83. Halle, B.; Landgren, M.; Jönsson, B., The shape of ionic micelles. *Journal de Physique* **1988,** *49* (7), 1235-1259.

84. Kosswig, K., Surfactants. *Ullmann's encyclopedia of industrial chemistry* **2000**.

85. Soldi, V.; Keiper, J.; Romsted, L. S.; Cuccovia, I. M.; Chaimovich, H., Arenediazonium salts: new probes of the interfacial compositions of association colloids. 6. Relationships between interfacial

counterion and water concentrations and surfactant headgroup size, sphere-to-rod transitions, and chemical reactivity in cationic micelles. *Langmuir* **2000,** *16* (1), 59-71.

86. Thévenot, C.; Grassl, B.; Bastiat, G.; Binana, W., Aggregation number and critical micellar concentration of surfactant determined by time-dependent static light scattering (TDSLS) and conductivity. *Colloids and Surfaces A: Physicochemical and Engineering Aspects* **2005,** *252* (2-3), 105-111.

87. Šegota, S., Spontaneous formation of vesicles. *Advances in colloid and interface science* **2006,** *121* (1-3), 51-75.

88. Davies, T. S.; Ketner, A. M.; Raghavan, S. R., Self-assembly of surfactant vesicles that transform into viscoelastic wormlike micelles upon heating. *Journal of the American Chemical Society* **2006,** *128* (20), 6669-6675.

89. Lin, Z.; Cai, J.; Scriven, L.; Davis, H., Spherical-to-wormlike micelle transition in CTAB solutions. *The Journal of Physical Chemistry* **1994,** *98* (23), 5984-5993.

90. Rajak, P.; Nath, L.; Bhuyan, B., Liquid Crystals: An Approach in Drug Delivery. *Indian Journal of Pharmaceutical Sciences* **2019,** *81* (1), 11-21.

91. Blunk, D.; Bierganns, P.; Bongartz, N.; Tessendorf, R.; Stubenrauch, C., New speciality surfactants with natural structural motifs. *New Journal of Chemistry* **2006,** *30* (12), 1705-1717.

92. Latypova, L.; Góźdź, W.; Pieranski, P., Facets of lyotropic liquid crystals. *Langmuir* **2014,** *30* (2), 488-495.

93. Shah, D., *Micelles: Microemulsions, and Monolayers: Science and Technology*. Routledge: 2017.

94. Hoffmann, H.; Thunig, C.; Munkert, U.; Meyer, H.; Richter, W., From vesicles to the L3 (sponge) phase in alkyldimethylamine oxide/heptanol systems. *Langmuir* **1992,** *8* (11), 2629-2638.

95. Singh, S.; Dunmur, D. A., *Liquid crystals: fundamentals*. World Scientific: 2002.

96. Frankel, D. A.; O'Brien, D. F., Supramolecular assemblies of diacetylenic aldonamides. *Journal of the American Chemical Society* **1994,** *116* (22), 10057-10069.

97. Tiddy, G. J., Surfactant-water liquid crystal phases. *Physics reports* **1980,** *57* (1), 1-46.

98. Hyde, S. T., Identification of lyotropic liquid crystalline mesophases. *Handbook of applied surface and colloid chemistry* **2001,** *2*, 299-332.

99. Shah, D. O., *Surface phenomena in enhanced oil recovery*. Springer: 1981.

100. Gang, O. Small Angle X-Ray Scattering (SAXS) from Bulks and Surfaces. https://www.bnl.gov/ps/userguide/lectures/Lecture-7-Gang.pdf.

101. Ekwall, P.; Mylius, W., Acidic sodium salts of lauric acid. *Ber Dtsch Chem Ges* **1929,** *62*, 2687-2690.

102. Ekwall, P., System of palmitin acid–sodium palmitate. *Z Anorg Allg Chem* **1933,** *210*, 337-349.

103. McBain, J. W.; Peaker, C. R.; King, A. M., ABSOLUTE MEASUREMENTS OF THE SURFACE CONDUCTIVITY NEAR THE BOUNDARY OF OPTICALLY POLISHED GLASS AND SOLUTIONS OF POTASSIUM CHLORIDE. *Journal of the American Chemical Society* **1929,** *51* (11), 3294-3312.

104. Tandon, P.; Raudenkolb, S.; Neubert, R. H.; Rettig, W.; Wartewig, S., X-ray diffraction and spectroscopic studies of oleic acid–sodium oleate. *Chemistry and physics of lipids* **2001,** *109* (1), 37-45.

105. Wen, X.; Lauterbach, J.; Franses, E. I., Surface densities of adsorbed layers of aqueous sodium myristate inferred from surface tension and infrared reflection absorption spectroscopy. *Langmuir* **2000,** *16* (17), 6987-6994.

106. Buerger, M., Soap crystals. *American Mineralogist: Journal of Earth and Planetary Materials* **1945,** *30* (9-10), 551-571.

107. Lynch, M. L.; Pan, Y.; Laughlin, R. G., Spectroscopic and thermal characterization of 1: 2 sodium soap/fatty acid acid− soap crystals. *The Journal of Physical Chemistry* **1996,** *100* (1), 357-361.

108. Zhu, S.; Heppenstall-Butler, M.; Butler, M.; Pudney, P.; Ferdinando, D.; Mutch, K., Acid soap and phase behavior of stearic acid and triethanolamine stearate. *The Journal of Physical Chemistry B* **2005,** *109* (23), 11753-11761.

109. Bian, J.; Weng, S.; Wu, J., Vibrational Spectroscopic Studies on the Acid Salts of Capric Acid and Lauric Acid. *ACTA SCIENTIARUM NATURALIUM-UNIVERSITATIS PEKINENSIS* **1995,** *31*, 711-717.

110. Mantsch, H.; Weng, S.; Yang, P.; Eysel, H., Structure and thermotropic phase behavior of sodium and potassium carboxylate ionomers. *Journal of molecular structure* **1994,** *324* (1-2), 133-141.

111. Dumbleton, J., The unit-cell dimensions of potassium myristate and 1: 1 acid potassium myristate. *Acta Crystallographica* **1965,** *19* (2), 279-280.

112. Heppenstall-Butler, M.; Butler, M. F., Nonequilibrium behavior in the three-component system stearic acid− sodium stearate− water. *Langmuir* **2003,** *19* (24), 10061-10072.

113. Wärnheim, T.; Jönsson, A., Phase behavior of alkanolammonium carboxylates. In *Advances in Colloid Structures*, Springer: 1992; pp 18-22.

114. Jansson, M.; Jönsson, A.; Li, P.; Stilbs, P., Aggregation in tetraalkylammonium dodecanoate systems. *Colloids and surfaces* **1991,** *59*, 387-397.

115. McBain, J. W.; de Bretteville Jr, A.; Ross, S., Diffraction of X-Rays by Sodium Stearate at Room Temperature. *The Journal of Chemical Physics* **1943,** *11* (4), 179-183.

116. Stokes, R. J.; Evans, D. F., *Fundamentals of interfacial engineering*. John Wiley & Sons: 1996.

117. Liang, J.; Ma, Y.; Zheng, Y.; Davis, H. T.; Chang, H.-T.; Binder, D.; Abbas, S.; Hsu, F.-L., Solvent-induced crystal morphology transformation in a ternary soap system: sodium stearate crystalline fibers and platelets. *Langmuir* **2001,** *17* (21), 6447-6454.

118. Ai, Y. F.; Hasjim, J.; Jane, J. L., Effects of lipids on enzymatic hydrolysis and physical properties of starch. *Carbohydrate Polymers* **2013,** *92* (1), 120-127.

119. Lai, H.-M.; Padua, G. W.; Wei, L. S., Properties and microstructure of zein sheets plasticized with palmitic and stearic acids. *Cereal chemistry* **1997,** *74* (1), 83-90.

120. Ripmeester, J.; Dunell, B., A Differential Scanning Calorimeter Study of Phase Transitions in Alkali Metal Stearates. *Canadian Journal of Chemistry* **1971,** *49* (17), 2906-2909.

121. Brouwer, H.; Spier, H., Acid-soap formation in various anhydrous sodium soaps. In *Thermal Analysis*, Springer: 1972; pp 131-144.

122. Klein, R.; Tiddy, G. J.; Maurer, E.; Touraud, D.; Esquena, J.; Tache, O.; Kunz, W., Aqueous phase behaviour of choline carboxylate surfactants—exceptional variety and extent of cubic phases. *Soft Matter* **2011,** *7* (15), 6973-6983.

123. Ananthapadmanabhan, K.; Somasundaran, P., Acid-soap formation in aqueous oleate solutions. *Journal of colloid and interface science* **1988,** *122* (1), 104-109.

124. Ekwall, P., Solutions of alkali soaps and water in fatty acids IX. The location of theL_2-phase in three-component systems of sodium soap—fatty acid—water, in view of the occurrence of acid soaps. *Colloid and Polymer Science* **1988,** *266* (3), 279-282.

125. Morigaki, K.; Walde, P., Fatty acid vesicles. *Current Opinion in Colloid & Interface Science* **2007,** *12* (2), 75-80.

126. Eagland, D.; Franks, F., Association equilibria in dilute aqueous solutions of carboxylic acid soaps. *Transactions of the Faraday Society* **1965,** *61*, 2468-2477.

127. Kanicky, J.; Shah, D., Effect of premicellar aggregation on the p K a of fatty acid soap solutions. *Langmuir* **2003,** *19* (6), 2034-2038.

128. Craig, S.; Hastie, G.; Roberts, K., Chain length dependent polymorphism in even number n-alkanes: line profile analysis of synchrotron powder X-ray diffraction data. *Journal of materials science letters* **1996,** *15* (14), 1193-1196.

129. Van Sprang, H.; Aartsen, R., The temperature dependence of liquid-crystal tilt angles. *Journal of applied physics* **1984,** *56* (2), 251-262.

130. Dreiss, C. A., Wormlike micelles: where do we stand? Recent developments, linear rheology and scattering techniques. *Soft Matter* **2007,** *3* (8), 956-970.

131. Steltenkamp, R. J., The chemistry of detergent perfumery. *Journal of the American Oil Chemists' Society* **1968,** *45* (6), 429-432.

132. Moreno, E.; Cordobilla, R.; Calvet, T.; Cuevas-Diarte, M.; Gbabode, G.; Negrier, P.; Mondieig, D.; Oonk, H. A., Polymorphism of even saturated carboxylic acids from n-decanoic to n-eicosanoic acid. *New Journal of Chemistry* **2007,** *31* (6), 947-957.